Università degli Studi di Padova

Dipartimento di Tecnica e Gestione dei Sistemi Industriali

CORSO DI DOTTORATO DI RICERCA IN INGEGNERIA MECCATRONICA E DELL'INNOVAZIONE MECCANICA DEL PRODOTTO

CURRICULO: MECCATRONICA

CICLO XXIX

Unintentional Islanding in Distribution Networks with Large Penetration of Power Electronics and Renewable Energy Systems

Coordinatore: Ch.mo Prof. Roberto Caracciolo
Supervisore: Ch.mo Prof. Paolo Mattavelli
Co-Supervisore: Ch.mo Prof. Roberto Turri

Dottorando: Riccardo Sgarbossa

Contents

Chapter 1

Introduction

The worldwide mix of primary fuels used to generate electricity has changed over the past several decades. Generation from nuclear power increased rapidly from the 1970s through the 1980s, and natural gas-fired generation increased considerably after the 1980s. The use of oil for generation declined after the late 1970s, when sharp increases in oil prices encouraged power generators to substitute other energy sources for oil.

At the beginning in the early 2000s, concerns about the environmental consequences of greenhouse gas emissions intensified interest in the development of renewable energy sources that emits significantly less CO2 than either oil or coal per kWh generated. In the international energy outlook 2016 (IEO2016) [1], presented by the U.S. energy information administration (EIA), the long-term global prospects continue to improve the power generation from natural gas, nuclear, and renewable energies are the fastest-growing source of energy for electricity generation.

1.1 Renewable Energy Source Development

Renewable energies have experienced one of the largest growth areas in percentage of over 30% per year. The goal of the European community (the EU) is to reach 20% of energy consumption from renewables in 2020. The US has adopted similar goals under the pressure of public opinion concerned by environmental problems. However, the policies of Asia and Pacific countries, with 35% of world energy share, will probably be more important in the future energy scenario.

Since the end of 2004, worldwide renewable energy capacity grew at rates of 10 - 60% annually for many technologies. Wind energy has rapidly reached 4% of worldwide electricity production and 11.4% in the EU [2, 3]. However, grid-connected photovoltaics (PV) increased at the fastest rate among of all renewable technologies, with a 60% annual average growth rate. According to the 2011 projection by the international energy agency

(IEA) [4], solar power generators may produce most of the world's electricity within 50 years, reducing the emissions of greenhouse gases that harm the environment.

Cedric Philibert, senior analyst in the renewable energy division at the IEA said: "Photovoltaic and solar-thermal plants may meet most of the world's demand for electricity by 2060 – and half of all energy needs – with wind, hydro power and biomass plants supplying much of the remaining generation.

The year 2015 witnessed several developments in the renewable energy scenario, including the lowest-ever prices for renewable power long-term contracts and an increase in attention to energy storage. Furthermore, a climate agreement brought together the global community in December at the United Nations Framework Convention on Climate Change's (UNFCCC) 21st Conference of the Parties (COP21) in Paris, where 195 countries agreed to limit global warming to well below 2 degrees Celsius. A majority of countries committed to scaling up renewable energy and energy efficiency.

Renewable technologies are now established around the world as mainstream sources of energy. Consequently, new markets for both centralized and distributed renewable energy are emerging in all regions, providing an estimated 19.2% of global final energy consumption by the end of 2014, as shown in Fig. 1.1. Out of this total share, traditional biomass, used primarily for cooking and heating in remote and rural areas of developing countries, accounted for about 8.9%, and modern renewables (not including traditional biomass) increased their share slightly over 2013 to approximately 10.3%. In 2014, hydro power accounted for an estimated 3.9% of final energy consumption, other renewable power sources comprised 1.4%, renewable heat energy accounted for approximately 4.2% and transport bio-fuels provided about 0.8% [5].

Global investment also has been increased to a new record level and for the sixth consecutive year, renewable energy sources outpaced fossil fuels for net investment in electric power capacity additions.

Based on 2016 REN21 (Renewable Energy Policy Network for the 21st Century) report, renewable electric power generation capacity saw its largest annual increase in 2015, with an estimated 147 GW of renewable capacity added, where 77% is from wind and solar PV together and 19% from hydroelectric reaching an estimated 1064 GW. Fig. 1.2 reports the electricity production by the end of 2015, where the renewable energy sources represent an estimated 23.7% of global electricity production and the hydroelectric sources are providing about 16.6% [4].

Renewable energies achieved high penetration levels in several countries. For example: wind power met 42% of electricity demand in Denmark, 23.2% in Portugal and 15.5% in Uruguay, while the solar power accounted for 7.8% of electricity demand in Italy, 6.5% in

Greece and 6.4% in Germany.

The Italian electricity market is changed along the global electricity production transformation. In Fig. 1.4 is reported the transformation of electricity production share in Italy from 2005 to 2015, in which the renewable production share increased from the 14% to the 29%.

The diffusion of renewable energy sources is due to technological improvements that have reduced the production and installation costs. However, the economic competitiveness of renewable technologies still depends on regulatory framework and market design [7].

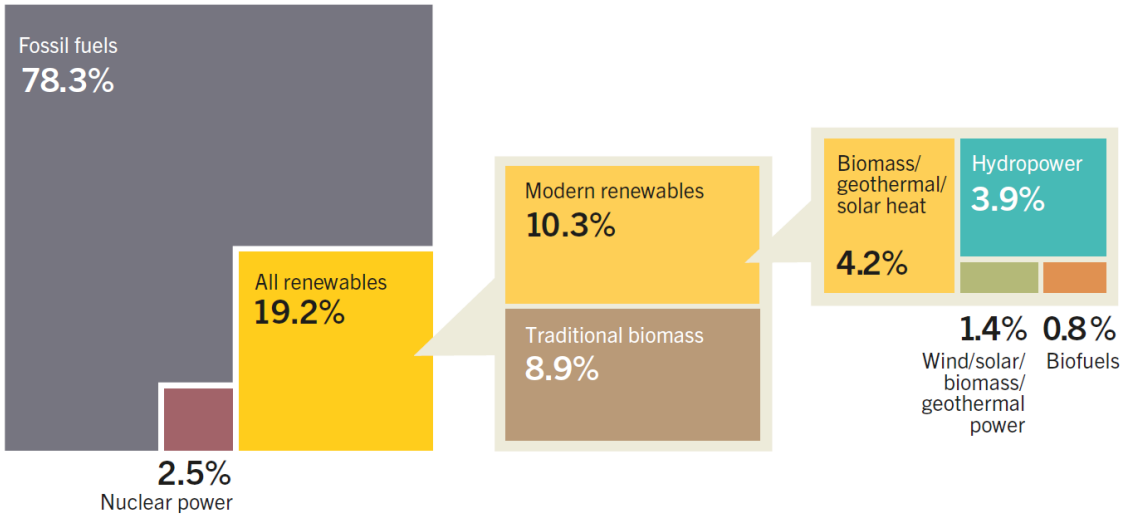

Figure 1.1: Estimated renewable energy share of global final energy consumption in 2014 [5].

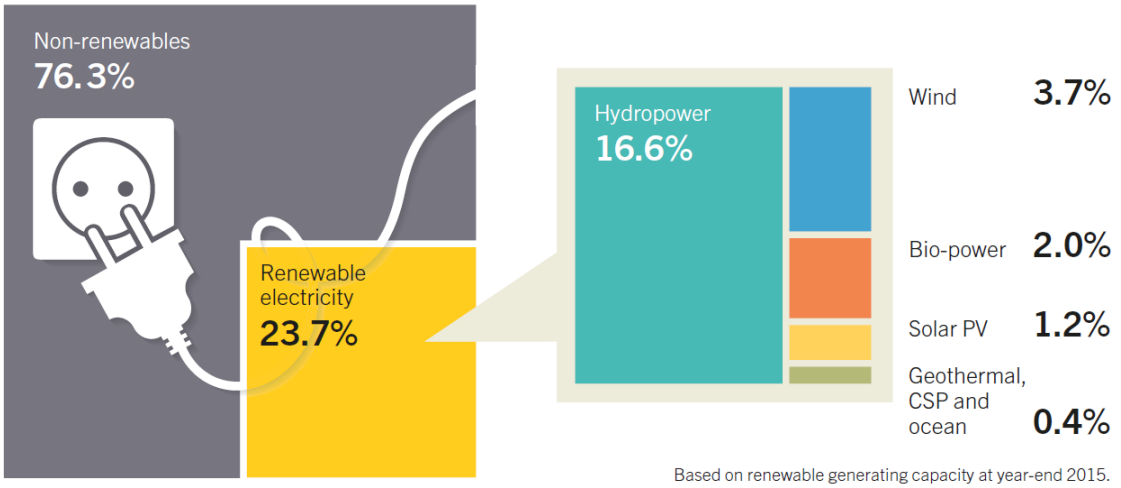

Figure 1.2: Estimated renewable energy share of global electricity production at the end of 2015 [5].

	Global	EU-28	BRICS[1]	China	United States	Germany	Japan	India	Italy	Spain
TECHNOLOGY	GW			GW						
Bio-power	106	36	31	10.3	16.7	7.1	4.8	5.6	4.1	1
Geothermal power	13.2	1	0.1	~0	3.6	~0	0.5	0	0.9	0
Hydropower	1,064	126	484	296	80	5.6	22	47	18	17
Ocean power	0.5	0.3	~0	~0	0	0	0	0	0	~0
Solar PV	227	95	50	44	26	40	34	5.2	18.9	5.4
Concentrating solar thermal power (CSP)	4.8	2.3	0.4	~0	1.7	~0	0	0.2	~0	2.3
Wind power	433	142	180	145	74	45	3	25	9	23
Total renewable power capacity including hydropower	**1,849**	**402**	**746**	**496**	**202**	**97**	**65**	**83**	**51**	**49**

Figure 1.3: Renewable electric power global capacity in the top countries in 2015 [5].

1.2 Integration Challenge

Around the world, technical, economic and market transformation of the electric power sector continued to accelerate in 2015, creating both challenges and opportunities. Renewable energy is increasingly displacing existing generation system and interfering with traditional energy markets and business models. Several factors, as technological advances, social changes and policy goals, are driving a transformation from centralized systems to more-complex systems that comprise a growing number of decentralized generating units. The factors which supported the integration of renewable energy are the technology and efficiency improvements, the increasing use of smart grid technologies and the significant

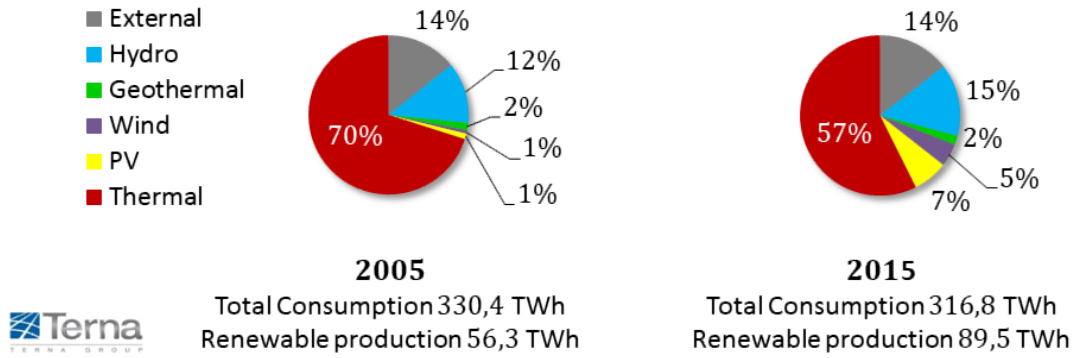

Figure 1.4: Ten years evolution of the Italian electricity share of production [6].

progress in hardware and software design. The key challenge is adapting the power grid to integrate rising shares of renewable generation, developing more-flexible systems to balance variable resources (on both the supply and demand sides), while minimizing the costs [8]. Many developed countries and some developing countries have begun to respond to the challenge of grid integration, included various combinations of: increased flexibility on the demand side and on the supply side (e.g., innovations in flexible fossil power plants; energy storage, particularly pumped storage; active power controls at wind and solar power plants); construction of new transmission networks; development of smarter grids; interconnection and co-ordination with neighboring grids; advanced resource forecasting; integrated heating and cooling systems; and innovative market designs [8, 9]. Utility-scale storage in the power sector, not including pumped storage and lead-acid batteries, increased by a record 250 MW in 2015 (compared with an estimated 160 MW in 2014) [10]. An example of the integration issue is the innovative hybrid systems of the Longyangxia station in China, where a 1280 MW of hydro power is linked to an 850 MW solar PV plant [11].

Globally, renewable electric power production in 2015 continued to be dominated by large generators (>4 MW) that are owned by utilities or large investors [12]. At the same time, a number of distributed, small-scale generation has started to rise and developed countries and regions, like Australia, Europe, Japan and North America, have witnessed a significant growth in numbers of residential electricity customers that produce their own electric power. Hence, the diffusion of renewable energy resources is continuously changing the structure and operation of the medium and low voltage (MV and LV) distribution networks, where these generators are connected. In particular the residential environments have experienced one of the most relevant growth of distributed-generation power systems [13–15]. Most of the low-power distributed energy resources (DER) units consist of power electronic converters with limited number of sensors and communication capabilities [16], increasing the complexity of the network management and operation for the distribution system operator (DSO) [17].

In a growing number of regions and countries, the increasing distributed renewable energies penetration requires changes to the grid system, regulations and market design. The main goal to increase the flexibility of electricity and to facilitate the growth and integration of variable renewable energy is to develop innovative business models, regulations and technical rules. To address such challenges in the EU, several initiatives are under way to advance grid integration [18]. Furthermore, advancements in inverter technologies are enabling solar and wind power to provide a range of crucial balancing services in order to secure the stability of the electric power system.

This complex scenario has influenced the latest grid code requirements for DER units [19, 20]. In fact, European standards state the reference technical rules for the DER connection in order to ensure the power quality and stability of distribution and transmission electric systems. Standards state DER requirements for grid connection under normal and transient conditions of the electric system. Furthermore, many standard bodies require that distributed generators have to play an active role in the system stability by participating to the ancillary services of active and reactive power regulation.

1.3 Grid Integration - Power Electronic Converters

Power electronic converter technology is the link between energy sources (renewable energy generation, energy storage ...) and the electric power system enabling an efficient and flexible interconnection. Hence, the power converters play a key role in the future decentralized power system based on smart grid technologies, as in the traditional centralized power system the synchronous machines play a central role. Power generation based on power electronics is changing the electric power system transient behavior: while the electromagnetic field has a major role in the synchronous machine, the grid converter is based mainly on semiconductor technology, signal processing and its connection filter. The increase in the power that needs to be managed by the distributed generation systems leads to the use of more voltage levels, leading to more complex structures based on a single-cell converter or a multi-cell converter and the use lower switching frequency to manage a higher power level as well as to the availability of a more powerful computational device [21].

In the design and control of the grid converter, challenges and opportunities are related to the need of grid synchronization and integration. All DER units interfaced by inverters deal with issues related to synchronization with the grid, control and stability at the system level in order to detect and manage islanding conditions for PV power systems and control under grid faults for wind turbine power systems.

1.4 Thesis Motivation and Objectives

The proliferation of distributed renewable energy resources, such as PV systems combined with the new technical rules, has led to an increasing concern about the problem of *unintentional islanding* (also referred as undesired or uncontrolled) in the medium and low voltage distribution electric networks. The islanding condition is defined as a portion of the utility system containing both loads and DER units that remain energized while it is

isolated from the main grid. Many studies and research activities address the intentional islanding topic, which will be of growing importance in the future. These studies deal with control strategies, protections improvements, etc. However, the intentional islanding is still not diffused in the existing distribution network. Hence, this thesis is focused on the actual islanding issues related to the DERs units connected to the electric distribution networks. In existing distribution lines, islanding, even for very short time, is undesirable, as the voltage on the islanded portion can drift respect to the one of the main grid, with a risk of damage in the electric equipment during the automatic grid reconnection. Therefore, islanding detection methods are essential in the design of the inverter control strategy, with the role of recognizing the islanding conditions and disconnecting the islanded DER unit.

The integration of distributed renewable energy resources in medium and low voltage distribution electric network is the ultimate challenge that Italian legislation and standard bodies are facing (similarly to many other developed countries). Therefore, the Italian regulatory authority for electricity gas and water AEEGSI (*autorità per l'energia elettrica, il gas e il sistema idrico*) asked one of the major DSO, called *e-distribuzione SpA* to conduct specific studies about unintentional islanding.Part of the research activity of this thesis has been pursued in collaboration with *e-distribuzione SpA*. This study concerns the analysis of distribution electric networks with large penetration of distributed renewable energy resources based on power electronic converters, with respect to the new connection rules required by standard bodies. Particular focus has been addressed to the possible interaction between DERs, protection systems and connection rules, in order to analyze the causes and the influencing factors of unintentional islanding in MV and LV distribution network. The unintentional islanding issue has interested many studies and publications over the last decades [13, 16, 22–24]. However, the literature seems to be lacking of considering the lately introduced European standards and technical specifications for DERs.

This thesis describes the novel aspects of how requirements and ancillary services influence the unintentional islanding operations and highlights new relevant factors, such as the role of the loads characteristics, the influence of the frequency measure and the inverter regulation speed. Therefore, the major scientific contributions of this thesis are:

- The effects of the regulating droop functions (P/f and Q/V), required by recent standards, on the unintentional islanding operations and anti-islanding protection, while in literature DERs units are often considered as mere current source inverters (CSIs) with constant power generation and unity power factor, as reported in several publications [25–27];

- Analysis of the DERs grid synchronization systems (phase locked loops) during islanding conditions of low power single-phase and three-phase current controlled voltage source inverters, where a specific single-phase phase locked loop (PLL) structure increases the islanding risks [28];
- Temporary islanding analysis in presence of automatic re-closure procedures adopted in several countries, which is described under several aspects in [29–31];
- Crucial role of the settling time of the power regulating droop functions, i.e. the power regulation speed of a DER unit influence may affect the possibility of islanding events even in presence of active anti-islanding techniques, as presented in [29,32,33];
- Analysis and experimental research of residential type loads (typical of the electric distribution networks) for unintentional islanding studies instead of the paralleled RLC resonant load introduced in literature studies, which is considered the worst case scenario in terms of islanding detection, but do not represent the possible islanding events in distribution networks, as presented in [34, 35].

Moreover, these results enable the distribution system operators (DSOs) to predict how the large diffusion of DERs would affect the unintentional islanding and they describe possible solutions and corrective actions for upcoming guidelines and international standards.

In the following paragraph, the structure of this thesis is briefly summarized. The second chapter describes the unintentional islanding events and presents an overview of the actual islanding detection methods and test-bench conditions on which the majority of the literature works is based on. Furthermore, the new requirements introduced by standard bodies are reported, describing the new rules for the connection of DERs units (i.e. inverter capability and power regulating droop functions). In particular, the Italian case is described, where the automatic maneuver procedures influence the temporary islanding operations. The analysis of the loads typical of the electric distribution networks is presented in the third chapter, since the load characterization plays an important role on the islanding phenomena. The introduction of different power dependences on voltage amplitude and frequency presents new islanding behavior that was not considered in the actual anti-islanding requirements and test-benches stated by international standards. Then, the thesis describes the models and the tools, that allowed the islanding operation investigations and validations. The description of the power converter modeling is reported in the fourth chapter, while the experimental setup and hardware in the loop configuration (HIL) are proposed in the fifth chapter. The sixth chapter describes the unintentional islanding non detection zone (NDZ), which reveals the particular conditions when the protection

system may fail to detect the islanding operations. In chapter six, the novel influence of the power regulating droop functions is also described. Moreover, the inverter speed regulation plays an important role on the definition of the NDZ, introducing a new player in the unintentional islanding operations not evaluated by anti-islanding requirements. The role of the phase locked loop (PLL) grid synchronization system is investigated in the seventh chapter. The description of the temporary unintentional islanding is presented in chapter eight, where the automatic re-closure procedure is considered. These results show the lack of integration of DERs in the grid automation procedures in case of unintentional islanding. This chapter confirms the dangerousness of the islanding events and the need of improvements on anti-islanding requirements. The ninth chapter introduces the active anti-islanding technique Sandia frequency shift (SFS). In the literature, such active methods have a negligible NDZ. However, here the SFS is presented in combination with the power regulating droop functions and with different inverter regulation speed, describing potentially dangerous effects of high regulation speed on the NDZ size. The regulation speed influences the behavior of the active anti-islanding protection and it may reduce its effectiveness. Then, in chapter ten the multiple inverter case is presented. Here, the analysis of the power regulation speed is proposed in a more complex scenario, where different percentage of power is regulated by different regulation speed. This concept was not presented in the literature and here is described as a key player in the unintentional islanding operations. Finally, chapter eleven draws the thesis conclusions highlighting the lack of standards requirements and proposing corrective actions in order to prevent the unintentional islanding.

Chapter 2

Unintentional Islanding

2.1 Introduction

The high penetration of distributed renewable resources (DERs) in the electric distribution network system, generally integrated by power electronic converters, is changing the electric power system structure and behavior. This complex scenario, shown in Fig. 2.1, is regulated by different technical requirements of the DER units depending on their size and level of integration in the power system. Thus, monitoring of the grid conditions is always a crucial feature for the DERs units at any level, where the detection of a possible unintentional (i.e. uncontrolled) islanding condition is always important.

For DERs units, such as residential PV systems, the distribution system operator (DSO) defines an anti-islanding requirement if the main electric grid should cease to energize the down stream distribution lines. Furthermore, DERs are regulated by requirements that contribute to the stability of the grid, such as low-voltage ride-through capability, which avoids the disconnection from the grid during faults.However, the power system is evolving and a future scenario may consider the presence of smart micro-grid with the capability of automatically managing the stand-alone operation and the grid reconnection. Furthermore, since the new grid codes are facing a continuous growth of the integrated low power DERs units into the distribution system, the recent requirements have introduced also local power control strategies, called droop functions.Hence, the typical low power DER anti-islanding requirements may not be effective and the detection of islanding can be considered as an important feature.

Unintentional islanding operations occur when a section of the distribution network system is isolated from the main grid due to a certain fault as an example, but local DERs continue to supply its loads without any protection intervention. The electrical model shown in Fig. 2.2 may be considered in order to simplify the definition of unintentional

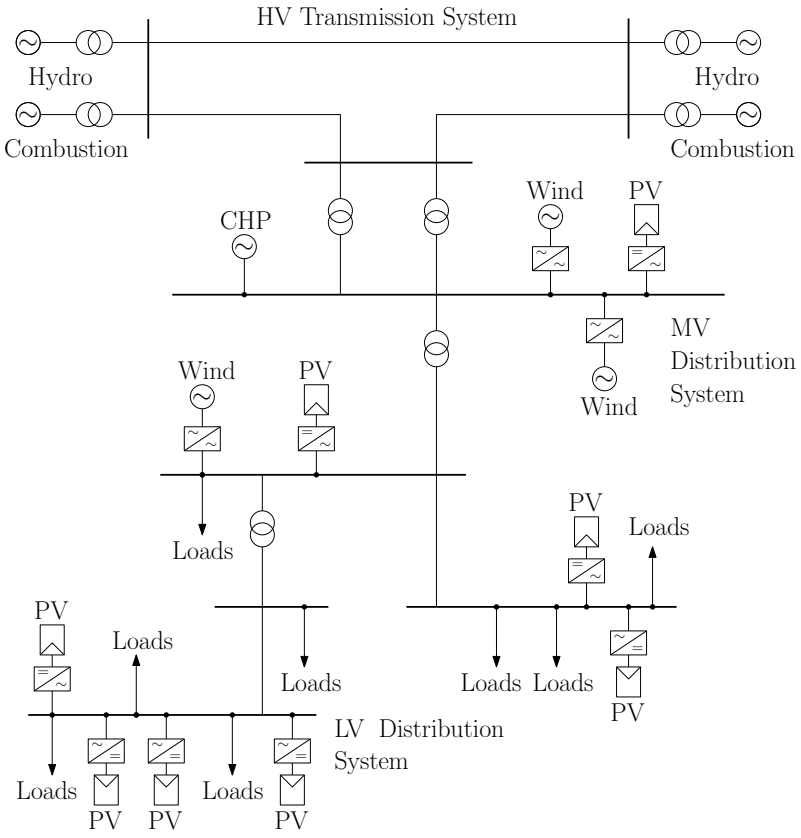

Figure 2.1: Electric diagram of a LV network connected to a MV distribution grid, characterized by the presence of local generation, for example: photovoltaic (PV) energy sources.

islanding operation. This model consists of a three-phase PV inverter paralleled with a local load and both are connected to the main grid through a utility breaker.

According to the power flows defined in Fig. 2.2, consider a case in which $P_L = P_{PV}$ and $Q_L = Q_{PV}$, where P_L is the load active power, P_{PV} is the PV inverter active power, Q_L is the load reactive power and Q_{PV} is the PV inverter reactive power. Under this condition, there is no current flowing through the utility breaker and $\Delta P = \Delta Q = 0$, where ΔP and ΔQ are defined in 2.2. Hence, if the utility breaker is opened, the PV DER continues to supply the parallel load without any variations in the system parameters, such as voltage amplitude and frequency. In this case, it is not possible to prevent the islanding operation and the isolated system continues to operate.

Unintentional islanding operations are undesirable for several reasons, where the most important reason is that the utility personnel may not be aware that a portion of the utility system is still energized by equipment at the customer's side. Thus, they are exposed to an electric shock hazard. Another important reason is that if the PV system drifts slightly out of phase with the utility voltage source during islanding, large surge

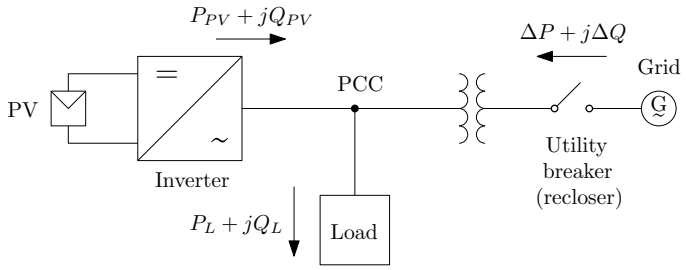

Figure 2.2: Unintentional islanding operation in a basic LV system, which comprises PV unit, local load and main grid that provides the power mismatch of $\Delta P + j\Delta Q$ between the PV generated power ($P_{PV} + jQ_{PV}$) and the load power ($P_L + jQ_L$).

currents can flow upon reconnection, damaging the PV system, customer loads, or other utility equipment. In particular, in some countries, like Italy, the utility operator has implemented an automatic reclosing procedure that allows short time disconnections in case of temporary faults along the distribution networks, minimizing the electric outages. Hence, islanding events, even for very short time, risk to damage the electric equipments during the automatic grid reconnection [31, 34].

Due to the severity of these risks, utilities and standard bodies require from the different DERs units to be equipped with specific islanding detection and prevention schemes in order to disconnect the PV system, when an islanding is detected. This aspect is regulated by different country-level standards, which require different control strategies and protection systems.

So far, different anti-islanding techniques have been proposed and implemented in the power converters based applications. These techniques have been reviewed in [21, 36, 37] and they are usually classified into active and passive inverter-resident and utility level or communication based techniques. Each of these techniques has different performance in terms of reliability (i.e. detecting all the existing islanding conditions), selectivity (i.e. distinguishing between islanding and grid disturbances) and minimum perturbation capabilities [21]. However, when there is a large number of DERs, the behavior of such provisions, being different from each manufacturer and not specified by standards, is unpredictable and in some cases these techniques can fail to detect the islanding operation mode and the disconnection of the inverter may not happen [24].

Fig. 2.3 and 2.4 present the unintentional islanding even that took place during May 2009 in Iberdola distribution network in Spain, where the frequency and the voltage amplitude are reported respectively.

In this case, Iberdrola electric distribution network was disconnected from the main grid due to maintenance work, but the system continued an uncontrolled operation with-

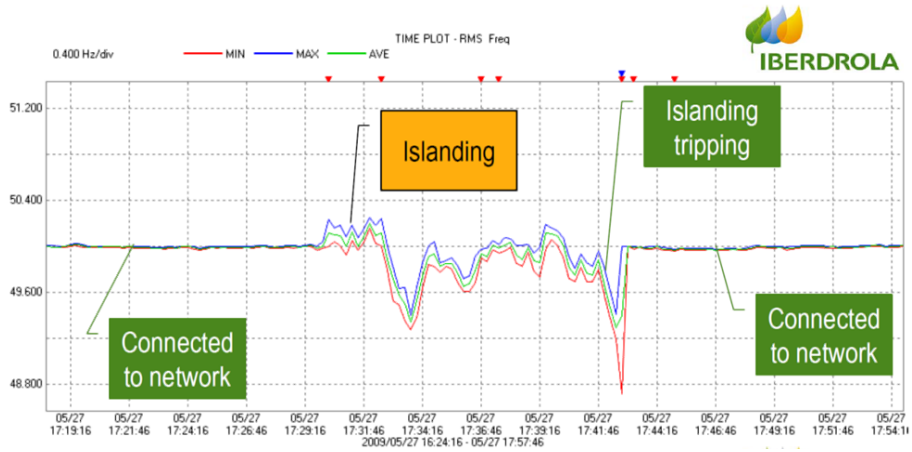

Figure 2.3: Measured minimum, maximum, and average frequency values during the unintentional islanding event in the Iberdrola distribution network in Spain [38].

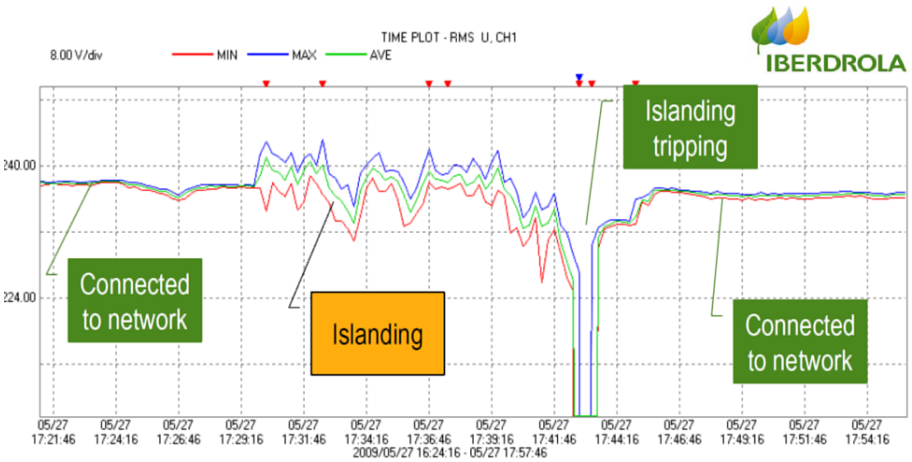

Figure 2.4: Measured minimum, maximum, and average line-to-ground voltage values measured during the unintentional islanding event in the Iberdrola distribution network in Spain [38].

out the protections intervention. During the unintentional islanding event, the 2.5 MW PV plants connected to the network continued to supply the local loads for 13 minutes. The achieved generation-load balance did not change the values of voltage frequency and amplitude, which were inside the protections thresholds during the islanding operation. Therefore, technical personnel had to manually disconnect the system and interrupt the unintentional islanding operation before reconnecting the islanded distribution network to the main grid.

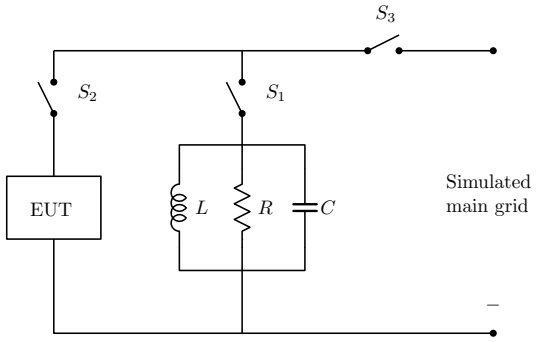

Figure 2.5: Test-setup for the anti-islanding requirement of DER system in IEEE 1547.1 [39].

2.2 Anti-Islanding Requirements

The anti-islanding requirements are considered as one of the most challenging technical features in the grid integration of the different DERs units. In order to avoid unintentional islanding events with possible sever consequences, safety anti-islanding (AI) requirements have been issued in several international standards. Recently, they made a great effort to revise the technical requirements due to the challenge of DERs integration with the existing legislation and technical rules of the electric distribution system. Adopted AI requirements all over the world, differs from a country to another, where each one is using its own local regulations. In the following are reported the international standards IEEE 1547 [39] and IEC 62116 [40], which describe the AI test-bench requirements. Furthermore, the German standard VDE 0126-1-1 is presented as an example of national standard.

2.2.1 Anti-Islanding Requirements According to IEEE Std 1547

According to IEEE Std 1574, the AI requirements impose that, after an unintentional islanding, the DER shall detect the islanding condition and disconnect within 2 seconds [39]. The test-setup, shown in Fig. 2.5, represents the used DER system according to [39], where adjustable RLC load is connected in parallel with the equipment under test (EUT) and the grid.

The resonant LC circuit should be adjusted to resonate at the rated grid frequency f and to have a quality factor $Q_f = 1$, because it represents the most difficult condition for

islanding detection. Thus, the values of the local RLC load are calculated by:

$$\begin{cases} R = \dfrac{V^2}{P} \\ L = \dfrac{V^2}{2\pi f P Q_f} \\ C = \dfrac{P Q_f}{2\pi f V^2}, \end{cases} \tag{2.1}$$

where P is the DER active power. The R, L and C parameters values are selected in order to balance the active power of the DER system under test. In this balanced condition, S_3 should be opened and the time before disconnection should be less than 2 seconds.

2.2.2 Anti-Islanding Requirements According to IEC 62116

The IEC 62116 presents AI requirements similar to IEEE 1547. Moreover, the test-setup is the same as the one used in the IEEE 1547.1 shown in Fig. 2.5 and a power balance is required before the islanding detection test. The requirements for passing the test and confirming island detection includes different steps, where the inverter is tested at three power levels (A: 100–105 %, B: 50–66 % and C: 25–33 % of its rated power) [40]. The maximum trip time is the same as in IEEE 1547.1 Std, which is 2 seconds.

2.2.3 Anti-Islanding Requirements According to VDE 0126-1-1

The VDE 0126-1-1 standard allows the compliance for AI requirements using one of the following methods:

1. impedance measurement, whose test-setup is depicted in Fig. 2.6. In this method, the procedure is based on local balancing of the active and reactive power using the variable RLC circuit and the switch S is opened in order to increase the grid impedance by 1 Ω. The disconnection required time for the inverter should be within 5 seconds. The test should be repeated for different values of the simulated grid impedance (R_2, L_2).

2. disconnection detection with RLC resonant load, whose test-setup is the same as for IEEE 1547.1, shown in Fig. 2.5, in which the RLC load is in balanced power condition with the inverter, but with the difference that the RLC resonant circuit parameters should be calculated for a $Q_f > 2$ as presented in (2.1). In islanding conditions, the inverter should disconnect within 5 seconds as before, considering for the following power levels: 25 %, 50 % and 100 %.

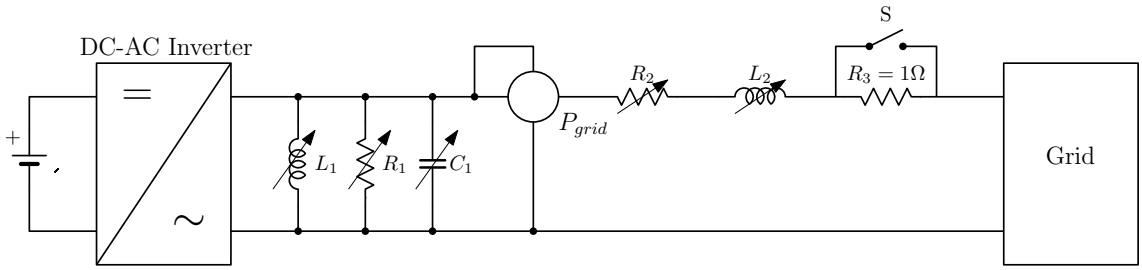

Figure 2.6: Test setup for the anti-islanding requirement of DER system in VDE 0126-1-1.

2.3 Islanding Detection Methods

Developing an effective islanding detection method has been seen as a challenging task, resulting in a large number of research works and publications. Two main approaches have been adopted for islanding detection: the first one is called grid-resident detection, which is based on the communication between the grid and DER inverters. A transmitter is installed near the line protection switch and a receiver is positioned at the point of common coupling (PCC) in the proximity of the inverter [41]. The communication signal is based on power line communication PLC technology and, during normal operating conditions, it is sent to the inverter receiver. In case of grid disconnection, the communication signal is absent and the islanding is detected. The same goal can be achieved with a dedicated line of communication.The grid-resident methods have not been commercialized yet because of the high installation cost, but they are the ultimate islanding detection methods, also working perfectly in case of multiple inverters operating in parallel, one of the hardest goals to achieve by all other methods. The second approach is called inverter-resident detection and relies on software implementation inside the inverter control platform. Over the years, several anti-islanding algorithms have been proposed and they can be classified into passive and active methods [42]. Passive methods verify changes of grid parameters at the DER PCC due to the power mismatch after the disconnection, such as over/under voltage (OUV), over/under frequency (OUF) [43], detection of the voltage/current harmonics [21, 44] and phase variations [16]. Active methods introduce disturbances at the PCC, such as active frequency drift (AFD), slip mode frequency shift and active/reactive power variations [21, 45, 46]. The active methods are claimed more efficient in islanding detection, but they present a set of fundamental drawbacks: they are not regulated by standards, they are not mandatory in all countries and they are different from each manufacturer. Moreover, the different perturbations generated by each inverter may be compensated by each other in a large distribution network and, last but not least, they have the potential to affect power quality and to generate instability in the grid, especially if more inverters are connected in parallel.

Standard bodies required islanding detection methods to be complaint with the AI test requirements as IEEE Std 1547, IEC 62116 and VDE 0126-1-1. This load condition is assumed to be the worst case in terms of unintentional islanding detection. However, the loads connected at the distribution level present different characteristics in active and reactive power dependency on voltage frequency and amplitude. Moreover, the dynamic behavior of the load on a distribution system varies depending on the load type, being residential, commercial or industrial, as well as the season and the climate conditions [47, 48]. More details on load frequency dependence and composition employed in this work are reported in Chapter 3.

2.4 Passive Islanding Detection Methods

The passive methods rely on monitoring grid parameters that typically change during islanding. In literature different passive islanding detection methods are described and the most relevant one are reported in the following sections.

2.4.1 OUF-OUV Protections

All grid-connected DER inverters are required by standard bodies to have an over/under frequency (OUF) and over/under voltage (OUV) protections. The inverter should be disconnected if the voltage or the frequency value is out of the imposed thresholds. Voltage and frequency during islanding conditions differs from their rated values due to the power balance conditions before the disconnection from the main grid. Therefore, monitoring these two parameters is typically used in order to trip the inverter in case of OUV or OUF and thus, islanding detection is achieved. However, when the amount of power mismatch is small, this method may fail to detect islanding as voltage and frequency variations might be negligible to hit OUF or OUV limits.

2.4.2 Phase Jump Detection Method

This method observes the phase difference between the inverter terminal voltage and its output current. Typically, during islanding the phase between voltage and current changes due to the power mismatch. Compared to the OUF/OUV method, the phase jump detection (PJD) can theoretically detect much faster the islanding condition, because a phase change may be detected faster than a frequency variation. A typical implementation of this method is to use the zero-cross detection synchronization methods, where the phase of the current is updated once every zero-crossing of the voltage and thus it is possible to detect the phase jump. Another implementation is done by using the phase-locked

loop (PLL) synchronization system, but it is necessary to use two PLLs, one with a fast synchronization dynamics (e.g. with a settling time of 100 ms) and the second one is very slow for islanding detection (e.g. with a settling time of 1–2 s). Thus, by comparing the calculated two phases, it is possible to detect the jump of phase. However, choosing the correct threshold for a reliable islanding detection is the most difficult part. In fact, during reactive loads switching (capacitors banks, inductive motors, etc.) or for inverters working with non-unity power factor, the nuisance trips are the main drawback of this method.

2.4.3 Harmonic Detection Method

The voltage harmonic detection method monitors the total harmonic distortion (THD) of the voltage at the PCC and it detects the islanding events in case the THD exceeds the threshold. DER inverters, even if perfectly controlled to work as an ideal current source, produce high order harmonics due to switching, dead-time and semiconductor voltage drop or ripple of the DC link voltage. A typical standard requirement for a grid-connected inverter is to maintain the THD index below 5% [39]. Thus, manufactures introduce hardware solutions (typically filters) or compensation techniques embedded in the control algorithm. The amount of voltage harmonics depends on the level of the grid impedance, which is usually low, so during grid-connected operations, the THD is maintained low and difficult to detect. In case of islanding event, the grid impedance is replaced by the load impedance, which is higher. Therefore, the voltage THD will be increased and can be used as an indicator for islanding detection. The main difficulties related to the application of this method are in the choice of the parameters that should be evaluated (harmonics or indexes that combines some of them) for islanding detection and in the choice of the thresholds. In fact, it is not easy to discriminate between the harmonic pollution created by the grid, by the loads and by islanded DERs units, hence, false trips are possible. Also, transient voltage disturbances, such as those related to the switching of capacitor banks, could be interpreted by DER system as a momentary increase in THD, depending on the used measurement technique [49]. The challenge is to make the method selective and reliable for islanding detection, avoiding nuisance trips. In literature, many studies are described, which are related to the choice of the indicators, with the aim to increase the robustness of the THD method, and other studies that give guidelines for selecting the right thresholds by analyzing the relation between various harmonics causes. Many possible solutions have been studied to overcome this problem, but these techniques cannot be implemented cost-effectively in small DER. For this reason, the harmonic distortion method had a limited diffusion.

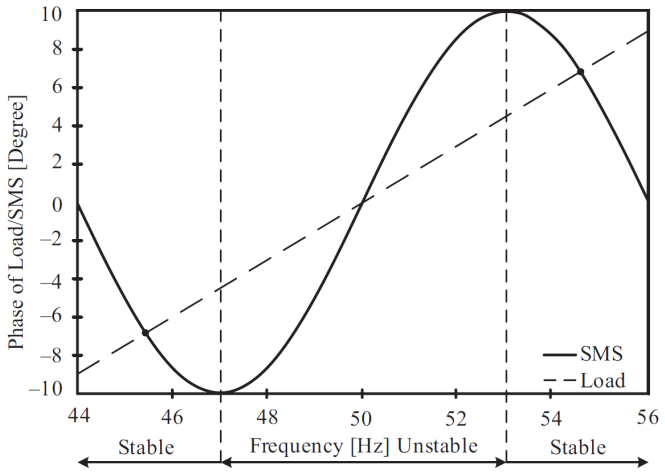

Figure 2.7: Inverter output current phase-frequency dependence using slip-mode frequency shift (SMS) anti-islanding method [21].

2.5 Active Islanding Detection Methods

Active AI methods involve the injection of small perturbations at the inverter output, generating variations of a parameter of the islanded system as frequency, phase, harmonics, active and reactive power. There are several possible techniques implementations in the literature [22, 42].

It is worth mentioning, that active AI methods are not mandatory in all countries. The compliance with the anti-islanding requirements is a task developed by the manufacturers, that decide the active AI algorithm to implement in the embedded control of the DER inverters.

In the following subsections the most popular active AI methods are reported.

2.5.1 Slip-Mode Frequency Shift

In this scheme, a positive feedback is applied to the phase of PCC voltage to destabilize the inverter by changing the short-term frequency. The phase angle of the inverter is made a function of the frequency, as depicted in Fig. 2.7, and the reference injected current is:

$$i^* = \sqrt{2} I \sin\left[2\pi f t + \Phi_{SMS}(f)\right], \tag{2.2}$$

where f is the frequency of the PCC voltage and the $\Phi_{SMS}(f)$ represents the current phase, which is a function of the frequency.

The phase response curve of the inverter is designed such that the phase of the inverter increases faster than the phase of the (RLC) load with a unity-power factor in the region near the utility frequency.

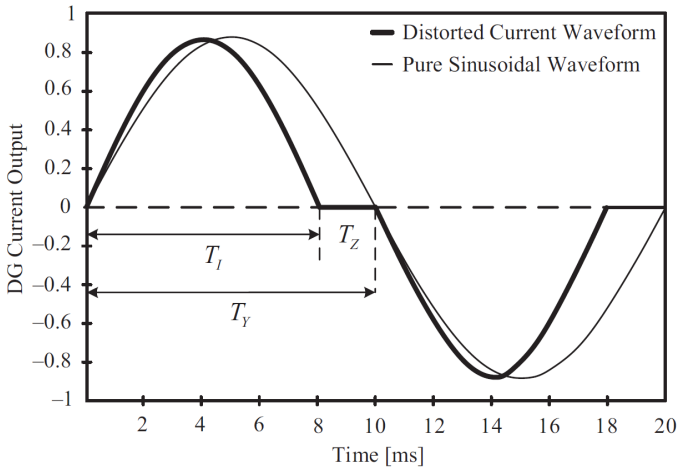

Figure 2.8: Inverter output current waveform using active frequency drift AFS anti-islanding method [21].

The design of the phase-frequency dependence makes the nominal frequency an unstable operating point for the DER system. If the utility is disconnected, the phase-frequency operating point of the load and DER can be at an intersection of the load line and DER phase response curve. If there is any small perturbation in the voltage frequency, the inverter phase response curve increases the phase error and, hence, causes instability in the frequency. This instability further amplifies the perturbation of the frequency of PCC voltage and drive the system to a new stable operating point designed to be out of the OUF protection thresholds. The possible implementation of this method is in the design of the synchronization control system of the inverter.

The drawback of this AI method is the influence of the loads. In particular if the loads have phase response curves that increase faster than the phase of the slip-mode frequency shift (SMS), the nominal frequency becomes a stable operating point and renders SMS ineffective.

2.5.2 Active Frequency Drift Method

This method perturbs the frequency reference with a positive feedback. As long as the grid is present, the frequency can not be drifted, but when the grid is disconnected, the disturbance will be able to drift the frequency until it hits OUF limits. The inverter output current is slightly distorted, presenting a zero current segment for a drift-up operation [50].

As reported in Fig 2.8, the implementation of the active frequency drift (AFD) method is based on the use of a zero-current segment per semi-cycle for a time T_z, defined by

$$T_z = \frac{1}{2}[(1/f) - (1/(f + \delta f))], \tag{2.3}$$

where f is the measured grid voltage frequency and δf is the difference between f and the current frequency during the positive semi-cycle. The ratio between T_z and half of the grid voltage period T_Y is referred as the chopping fraction cf, defined by

$$cf = \frac{2 \cdot t_z}{T_Y} = 2 \cdot f \cdot t_z. \tag{2.4}$$

The inverter reference and phase for this method in the steady state are

$$\begin{aligned} i^* &= \sqrt{2} I \sin\left[2\pi \left(f + \delta f\right)\right], \\ \theta_{AFD} &= \pi f T_z = \frac{\pi \delta f}{f + \delta f}. \end{aligned} \tag{2.5}$$

During the first portion of the first half-cycle, the PV system's current output is a sinusoidal wave with a frequency slightly higher than the one of the utility voltage. When the PV output current reaches zero, it remains at zero for time t_z before beginning the second half-cycle. For the first part of the second half-cycle, the PV output current is the negative half of the sine wave from the first half-cycle. When the PV current again reaches zero, it remains at zero until the rising zero crossing of the utility voltage. Thus, there is a continuous trend to change the frequency, but the grid presence will prevent this. In case of islanding operations, for example applying the current waveform in Fig. 2.8 to a resistive load, its voltage response will follow the output current of the inverter waveform. The PV system detects an increase in the voltage frequency and tends to increase its current reference frequency to attempt to maintain the relationships in (2.4). The resistive load again responds by advancing the negative to positive voltage zero crossing by T_z, which is again interpreted by the PV system as an increase in frequency. Therefore, the frequency will be drifted away with eventually tripping of the OUF protection. AFD is effective in detecting a wide range of islanding conditions. However, this method presents same drawbacks, especially if the local load has a high capacitive portion (e.g. insertion of capacitor banks). In fact, the presence of a capacitive load tends to increase the frequency of an islanded system in presence of a current source inverter. Therefore, if the T_z of the inverter output current is fixed, there is always a particular value of capacitance which can be added to a resistive load, resulting in a downward frequency drift that exactly cancels the upward frequency drift of the DER, and under this condition islanding can continue [51].

2.5.3 Sandia Frequency Shift Method

The Sandia frequency shift (SFS) method is an extension of the AFD. It presents an additional feature by applying a positive feedback to the voltage frequency of PCC. To implement the SFS, the chopping fraction cf is a function of the frequency as given by

$$cf = cf_0 + k(f - f_n), \tag{2.6}$$

where k is the acceleration gain, cf_0 is the chopping factor when there is no frequency error and $f - f_n$ is the difference between the estimated frequency and nominal value. When the DER is connected to the grid, no frequency changes are detected and the SFS follows the behavior of the AFD, which attempts to increase the frequency of the injected current, but the stiff grid prevents any change in the system frequency. However, during islanding operations the frequency error increases and the chopping fraction increases and the PV inverter also increases its frequency. The inverter, thus, acts to reinforce the frequency deviation, and this process continues until the frequency reaches the threshold of the OUF.

2.5.4 Reactive Power Variation Method

This AI method consists on a perturbation signal (typically with low frequency, i.e. 1 Hz) in the reference of the reactive current i_q^*. This perturbation on the reactive component attempts to modulate the frequency of the system due to the nature of the resonant RLC load. When the DER is connected to the grid, the stiff system does not allow any frequency change of the voltage. In the islanding situation, the voltage depends linearly on the injected current and the frequency variations can be detected. The periodical alteration of the reactive power component makes a phase difference between the output voltage and current of the system during islanding conditions. The phase difference induces an increase or decrease of the frequency of load voltage that eventually hits the OUF limits. In the literature, different implementation of this AI techniques are presented, differing in the detection time and the perturbation signal amplitude and frequency [45, 52, 53].

2.5.5 Harmonic Injection Grid Impedance Estimation

The concept is that a certain disturbance, such as harmonic injection (HI), is used to estimate the grid impedance based on the response of the grid. In other words, it is based on the injection of a harmonic current and measuring the resultant voltage harmonic. Thus, it is possible to estimate the grid impedance at that harmonic. A special attention is required on the selection of the harmonic injected, that shall not be a frequency present in the electric system, avoiding nuisance trips. Also, the non-characteristic frequencies are

chosen to avoid interaction with the current controller in the case when the proportional resonant current controller with harmonics compensation is used and they should not be near the output filter resonance frequency.

Many different implementations are presented in literature and they differ for the harmonic selection and numbers of injected harmonics (one or two harmonics) [54–56]. In the case of two harmonics, the grid parameters are calculated by

$$\begin{cases} Z_1^2 = R_g^2 + \omega_1^2 L_g^2 \\ Z_2^2 = R_g^2 + \omega_2^2 L_g^2, \end{cases} \tag{2.7}$$

$$\begin{cases} L_g = \sqrt{\dfrac{Z_1^2 - Z_2^2}{\omega_1^2 - \omega_2^2}} \\ R_g = \sqrt{\dfrac{\omega_1^2 Z_2^2 - \omega_2^2 Z_1^2}{\omega_1^2 - \omega_2^2}}, \end{cases} \tag{2.8}$$

$$Z_g = \sqrt{R_g^2 + \omega_g^2 L_g^2}, \tag{2.9}$$

where ω_1 and ω_2 are the injected harmonic frequencies, Z_1 and Z_2 are the impedances calculated at ω_1 and ω_2, and R_g and L_g are the resistive and inductive parts of the grid.

2.6 Grid Code Requirements

In the last few years, grid codes and standards requirements have been revisited in order to maintain the quality and stability of the electric power system. The Italian standards CEI 0-21 and CEI 0-16, which regulate DERs connections at the low voltage (LV) and medium voltage (MV) levels respectively, introduce some innovations on permissive thresholds of the interface protection system (IPS) and the power control strategies at the local level. Fig. 2.9 shows the permissive voltage and frequency thresholds based on a fault ride through (FRT) allowing the DER units to maintain the grid connection during temporary variations of the distribution networks parameters.

The new standards require ancillary services of the DER inverters with rated power above 6 kW, with the aim of improving the quality of the electric power system. These inverters are required to change their active and reactive power level with the droop regulating functions P/f and Q/V. The droop characteristics are reported in Fig. 2.10 and are based on a local logic, monitoring the voltage amplitude and frequency at the

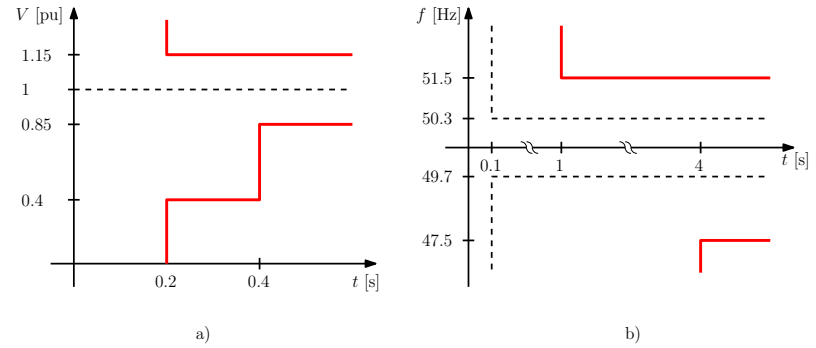

Figure 2.9: Over/under voltage and over/under frequency limits: a) voltage protection with low voltage fault ride through LVFRT philosophy; b) frequency protection, where the old restrictive thresholds (dashed lines) and the recent permissive thresholds (solid lines) are reported.

inverter terminals.

Voltage values (V_{1i}, V_{1s} and V_{2i}, V_{2s}) in Fig. 2.10 *b*) are defined by the distribution system operator (DSO) with default in per units level of $V_{1i} = 0.98$ p.u., $V_{1s} = 1.02$ p.u., $V_{2i} = 0.9$ p.u., and $V_{2s} = 1.1$ p.u. The reactive power limits Q_{max} and Q_{min} are based on the imposed capability in Fig. 2.11 as a power factor of 0.9 ($Q_{max,min} = \pm 0.483 \cdot P_N$), where only rectangular red zone is mandatory. In this work, only the rectangular capability has been considered. Therefore, the inverter nominal power (P_n) is P' and the active power production is not reduced in case of need of reactive power by the Q/V regulation.

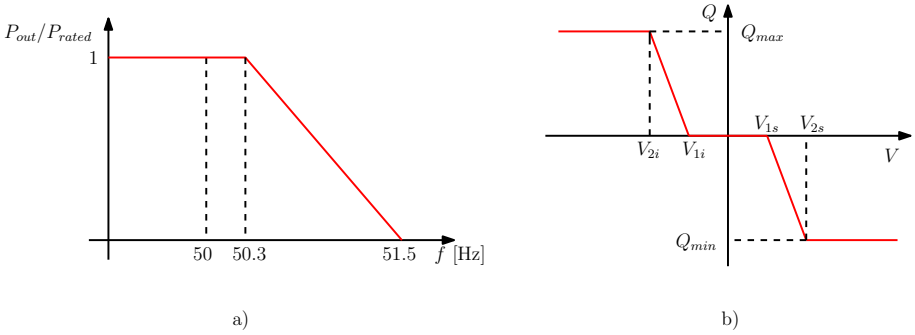

Figure 2.10: Droop characteristics based on local logic required by Italian standards [57, 58]. a) active power over frequency regulation function (P/f); b) reactive power over voltage amplitude regulation function (Q/V).

In this work, the droop P/f performs a continuous regulation during frequency variations as shown in Fig. 2.10a. This active power regulation is required at the European level with the technical specifications CENELEC TS 50549 [20, 59].

The Italian version of the P/f regulation presents a hysteresis behavior, i.e. the inverter reduces the active power in front of the first rise of the frequency f, and should maintain for the reduced level (P') for 300 s when f decreases to the nominal value, as

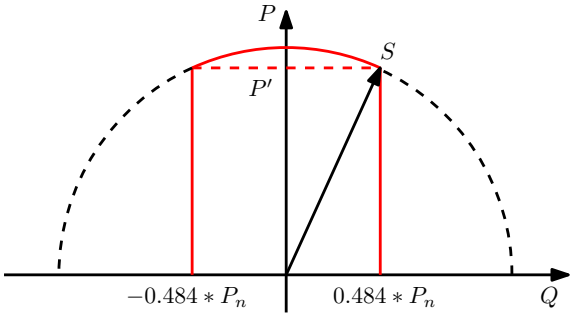

Figure 2.11: Capability of grid connected inverter with nominal power above 6 kW [57].

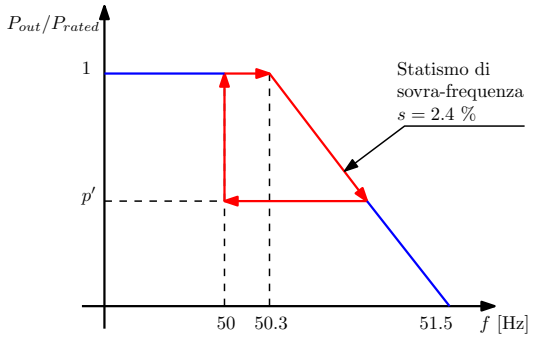

Figure 2.12: Active power regulation during over frequency events [57].

shown in Fig. 2.12.

The P/f regulation required by European technical specifications [20, 59] has been selected for this thesis work, as allowing a complete study of unintentional islanding operations in front of a possible future standard integration.

Moreover, the European grid code and technical specification require the DER inverter based units to perform the P/f and Q/V regulating droop characteristics as fast as technical feasible, in order to support the power electric system. Instead, the Italian standard fixes maximum settling times for the power regulations, which are 2 s for the P/f and 10 s for the Q/V.

2.6.1 Automatic Selection of Faulted Line Sections

The main purpose of the automatic selection procedure of faulted line sections in MV lines is the fast fault localization, the isolation of the faulted section and the reduction of the outages time due to temporary faults. In Italy, MV distribution networks are equipped with circuit breakers located in HV/MV (high voltage / medium voltage) primary substation, which operate with maximum current and directional earth-fault current relays.

The analysis of unintentional islanding operations due to the high penetration of DER systems, concerns also the temporary islanding due to fault events. In this case, the pri-

mary substation protections disconnect the faulty lines from the main grid. However, the DER units continue to energize the faulted section, causing serious issues especially when dealing with network automation procedures for fault selection and supply restoration, as it is the case in the Italian distribution networks. In that case, the automatic re-closure procedure may introduce risks associated with the possibility of out-of-synchronism reconnection of two separate systems due to the DERs temporary islanded operation.

Here are reported the automatic re-closure procedures that may increase the dangerousness associated to temporary islanding events. The breaker installed in the HV/MV primary substation performs a re-closures cycle when a faulty condition is detected. This procedure aims at minimizing the disconnection time with the main grid in case of temporary faults. The sequence maneuvers of the re-closure cycle depend on the distribution network type, neutral connection and possible presence of line automation. In Tab. 2.1, the number and the type (i.e. time of intervention) of automatic re-closures of the Italian distribution networks are reported, where two main procedures are adopted. In the case of simple automatic re-closure procedure, only the breaker in the primary substation (PS) is used to disconnect the downstream lines if faults happen. Instead in presence of automatic selection of faulted line section procedure, the downstream lines are equipped with specific devices for a more accurate selection of the fault position, combining the PS breaker re-closure cycle with the re-closure procedure of these devices. The distribution networks with the automatic selection of faulted line section procedure, present also one more last re-closure of the PS breaker in order to supply the safe lines sections, after the disconnection of the single faulted line section. This type of automatic procedure is described in the followings. Furthermore, in Tab. 2.1, the different number of re-closure are reported, depending on the line types, where lines are cables or a combination of cables and over-head lines.

In Fig. 2.13, is reported the sequence maneuvers of the re-closure cycle of the PS breaker for a MV distribution network with simple automatic re-closure procedure.The rapid re-closure time is T_{RR}=600 ms, which is enough to allow the extinction of a temporary fault condition.

The sequences maneuvers of the re-closure cycle for a MV distribution network consist of two parts:

- first series of automatic re-closures of the breaker installed in the primary substation, typically for temporary faults;
- a following series of re-closures (automatic or manual) in case of permanent faults.

The automation of an electric distribution network with automatic selection of faulted

Table 2.1: Automatic re-closure device (ARD) installed in the HV/MV primary substation (PS).

Automation	Line type	Number of re-closure	Re-closure type
Simple automatic re-closure procedure	cable	2	1°rapid 2°slow (30s)
	mixed	3	1°rapid 2°slow (30s) 3°slow (70s o 120s)
Automatic selection of faulted line section procedure	cable	3	1°rapid 2°slow (30s) 3°slow (70s o 120s)
	mixed	4	1°rapid 2°slow (30s) 3°slow (70s o 120s) 4°slow (70s o 120s)

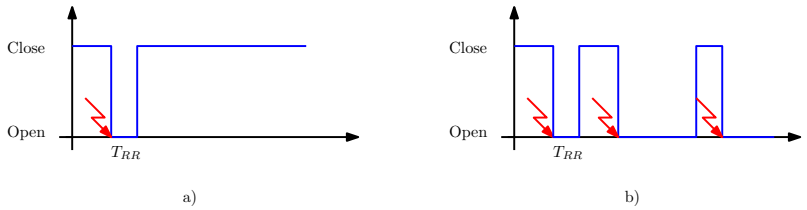

Figure 2.13: Primary substation breaker state during a re-closure cycle under two hypothesis. a) rapid re-closure succeeded; b) slow re-closure failed, with T_{RR} the rapid re-closure time.

line section procedure is possible using specific devices called fault passage indicators (FPI), whose Italian acronym is RGDAT, installed at the MV/LV secondary substations, which are able to elaborate the information of three phase over-current, directional earth fault current and presence/absence of downstream line voltage.

The numbers of line sections should be selected by the probability of faults and number of connected users. The sections number has to consider the following cases:

- a small number of sections reduces the re-closure maneuvers and dedicated devices, but increases the number of possible disconnected users;
- a high number of sections increases the re-closure maneuvers and dedicated devices, but reduces the number of possible disconnected users, allowing a more precise selection of faulted section.

The typical number of line sections for an Italian electric distribution network is 4 $\div$ 6, with 3 $\div$ 5 secondary substations. The line sections are called level and the level values starts from the end of the lines increasing going upstream. In Fig. 2.14, a 4 level distribution line is reported.

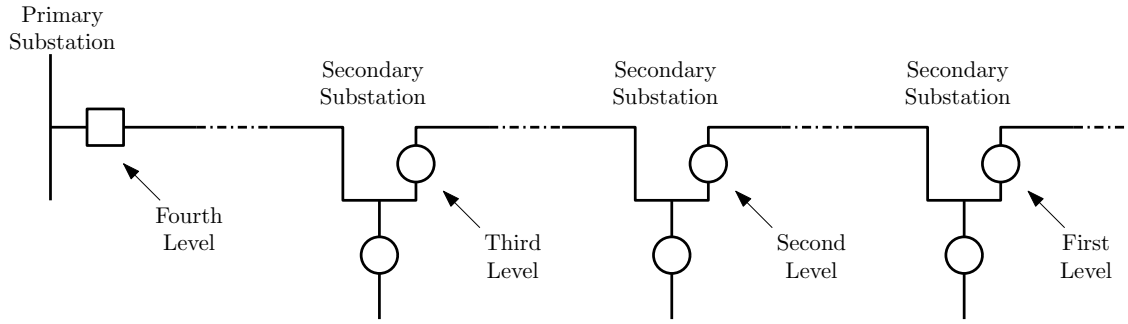

Figure 2.14: Level subdivision of automated distribution lines.

The automation is performed by a temporized procedure without any communication between the primary and secondary substations. The FPI, installed in the secondary substation, allow the disconnection of the downstream line by the local breaker, with a procedure, which depends on the neutral connection of the distribution network and the type of fault. The automatic selection of faulted line sections procedure are:

- FRG (Italian acronym for function based on fault indicators) procedure used for isolated neutral and any fault type or for compensated neutral and multi-phase faults;
- FNC (Italian acronym for function for neutral compensated) procedure for compensated neutral and single-phase to ground faults.

2.6.2 FRG Procedure

This technique is used in isolated or compensated neutral state. With this procedure only the FPI, that detects the fault current, allows the opening of the breaker at the secondary substation; the procedure is:

- the breakers of the secondary stations shall open if the relative FPI measures an under voltage (due to the first re-closure cycle of the primary substation breaker) and has measured the fault current;
- the closure of the open breakers of the secondary substations is after reading the nominal voltage level (due to primary substation re-closure) and with a specific order (starting from the nearest to the primary substation);
- the opening in a blocked state of the breaker whose FPI reads: under voltage within a selected time and the fault current;
- reconnection of the primary substation and the line section upstream the faulted one, whose breaker is open and blocked.

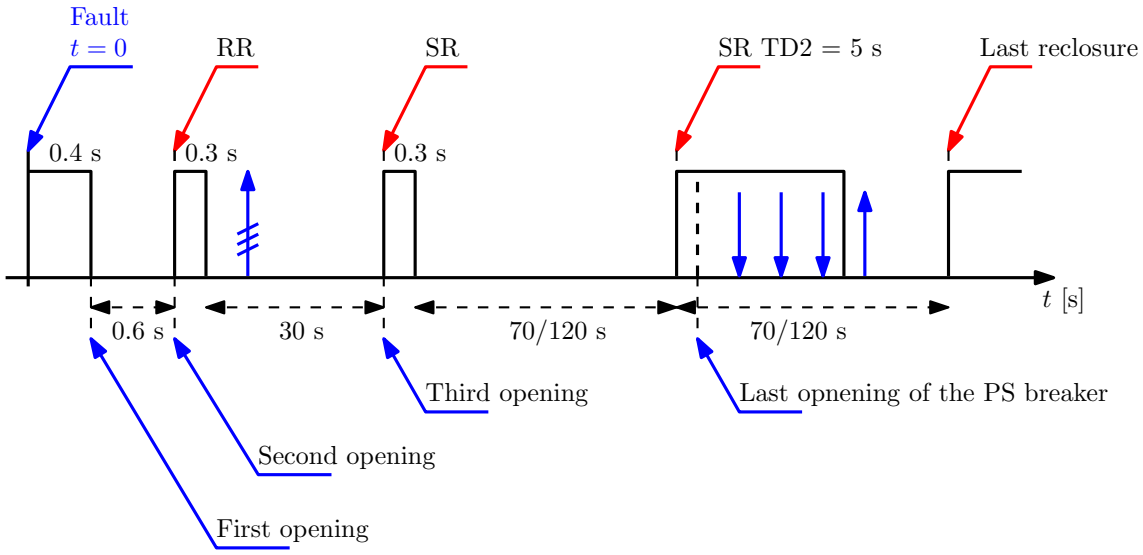

Figure 2.15: FRG procedure for the automatic selection of the faulted line section; with RR the rapid re-closure, SR the slow re-closure and TD is the discrimination time, which allows the opening on the PS breaker in presence of fault current during this time.

The FRG technique is reported in Fig. 2.15.

2.6.3 FNC Procedure

The FNC procedure is applied only for compensated neutral (with Petersen coil) and single-phase to ground faults, where in any other case the procedure switch to the FRG.

With this technique after the fault there is not the first automatic re-closing cycle of the primary sub station. Instead the breaker at the secondary substations opens with a specific time order in case of their FPI reads the single-phase to ground fault current. The PFIs, that detected the fault, allow to open the associated breaker starting from the end of the lines. During this procedure, the primary substation breaker remains closed. This allows the sections upstream the faulted one to be supplied by the main grid. In the case of fault located in the first section (last level), the primary substation starts the automatic procedure of re-closures. As for the FRG technique the breaker that detected the fault is open and blocked. In Fig. 2.16 the breaker state in the primary substation is shown.

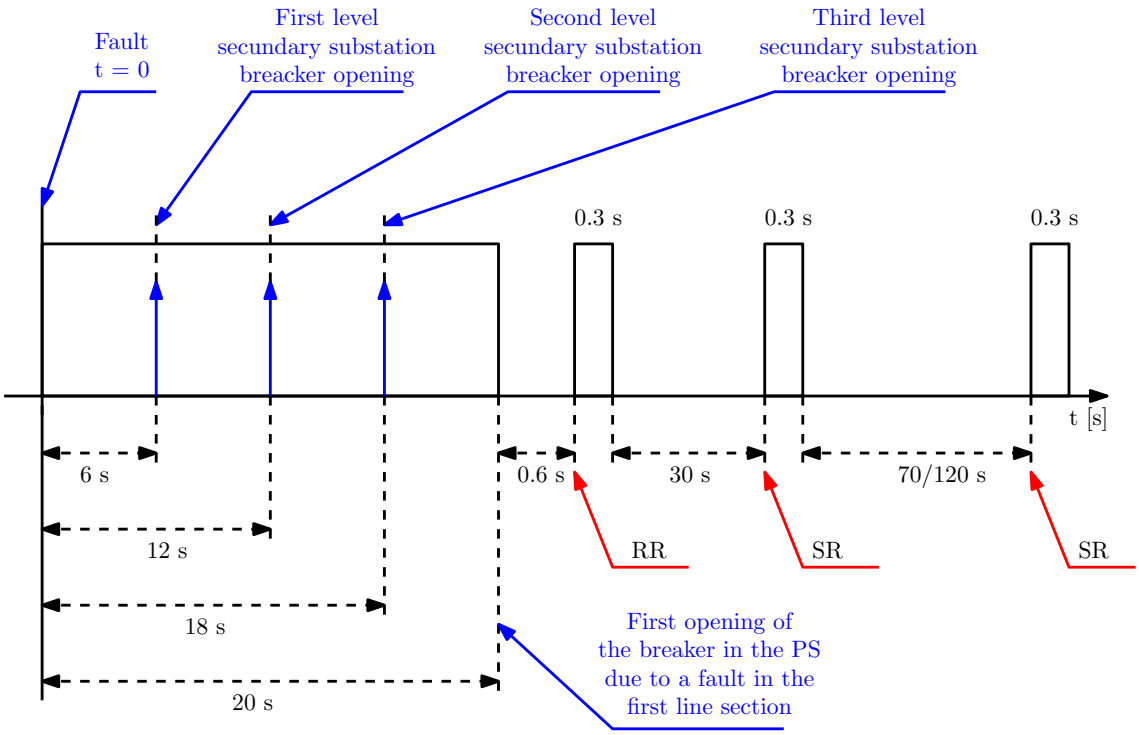

Figure 2.16: FNC procedure for the automatic selection of the faulted line section.

Chapter 3

Distribution Electric Network Load Modeling

This chapter deals with the analysis of typical distribution electric network loads, reporting the model for their characterization. The aim of load modeling is related to the study of islanding analysis, anti-islanding requirements and in general analysis of the distribution network behavior. In order to properly simulate the performance of the protection systems it is necessary to adopt accurate models of the electric network and loads. In fact, the condition of islanding mainly depends on network conditions before the grid disconnection (i.e. power balance condition between DERs and local loads) and the dynamic behavior of the loads, such as resistive, inductive, interfaced with power electronics, etc. Besides the characterization of the loads connected to the network, it is useful to predict and resolve instability situations of the electric system. In literature many different load models have proposed, depending on the type of the load and the field of application of the models:

- Model IEEE '93 [47];
- Linear model;
- Exponential model;
- Polynomial model.

In this analysis the more popular mathematical models are considered for each load and the representative model, which has the smaller error compared to the measured characteristic, is considered for the correct representation of the load.

3.1 Load Modeling Introduction

Load modeling is very useful, because by using these models it is possible to know the dynamics of very complex electrical systems, giving the possibility to prevent and avoid undesired and dangerous phenomena in the distribution networks. Hence, with different loads and the network models, it is possible to identify potential undesired situations and solve them. To analyze the loads and distribution network behavior, it is necessary to introduce some simplifications, which lead to a certain level of uncertainty on the results. The most used approach considers the worst operating conditions; however, it does not always manage to identify the worst case, and also risks to over-size for events with low probability to appear. On the other hand, the optimistic case may lead to a weak design in case of perturbations.

Distribution network load modeling identification and implementation are characterized by several issues:

- the electric system presents several different load types connected at the same time;
- loads composition varies during the day;
- a global load model is not suitable to represent all the load types, but it is necessary a combination of models;
- informations about the behavior and characteristics of different loads are required;
- some load types may introduce non-linear characteristics with problems related to the implementation of the model.

The introduction of power electronic changed the behavior of the loads and introduced the need of new load models.

3.2 Static Models

The static load models are implemented to study the variations of load active and reactive power absorbed due to alteration of the supply conditions, such as voltage amplitude and frequency. The accurate load representation is crucial for the unintentional islanding analysis presented in this work. In fact, the static models allow to evaluate the equilibrium point of the islanded system, where loads and DERs power characteristics match at specific voltage and frequency values, which are controlled by the over/under voltage (OUV) and over/under frequency (OUF) protections. Therefore, the loads static models allow to forecast the potential islanding risks or the intervention of the OUV and OUF protections.

Literature studies present the static models with the focus on steady-state solutions, without considering the transient behaviors, which, for residential loads connected to the electric low voltage distribution networks, present settling time typically $50 \div 100$ ms (i.e. the active and reactive load power reach the steady-state levels $50 \div 100$ ms after variation of the voltage or frequency values) [60]. For the purpose of this unintentional islanding analysis, these transient behaviors may be neglected, because the islanded systems, which are considered low voltage distribution networks in particular at the residential level, present slower dynamics. Loads active and reactive power are function of the network parameters amplitude and frequency of the voltage waveform:

$$\begin{cases} P = f_P(U, f) \\ Q = f_Q(U, f), \end{cases} \tag{3.1}$$

where P and Q are, respectively, the load active and reactive power and the f_P and f_Q are the different active and reactive power functions, which depend on the voltage amplitude (U) and frequency (f). The static models are typically useful to represent resistive loads, lights, residential type loads, and other with the exclusion of electric rotating machines.

3.2.1 Exponential Model

The exponential model is the most popular in literature; the equations of this model are derived from 3.2 and 3.3:

$$P = P_n \left(\frac{U}{U_n}\right)^{k_{pu}} \left(\frac{f}{f_n}\right)^{k_{pf}} \tag{3.2}$$

$$Q = Q_n \left(\frac{U}{U_n}\right)^{k_{qu}} \left(\frac{f}{f_n}\right)^{k_{qf}} \tag{3.3}$$

where P and Q represent respectively the active and reactive power at the voltage U and frequency f, P_n and Q_n are the active and reactive power at the nominal value of voltage U_n and frequency f_n, while k_{pu}, k_{pf}, k_{qu} and k_{qf} are the parameters that characterize each load type [61].

Usually in a distribution network the frequency variation are not frequent and a typical simplification is to consider the voltage variation. Therefore, the (3.2) and (3.3) are simplified as

$$P = P_n \left(\frac{U}{U_n}\right)^{k_{pu}} \tag{3.4}$$

$$Q = Q_n \left(\frac{U}{U_n}\right)^{k_{qu}}. \tag{3.5}$$

However, the (3.4) and (3.5) are not suitable for:

- load analysis with uncontrolled perturbations;
- low rated power systems, which present small inertia.

The model represented by the (3.4) and (3.5) can be a constant power load if k_{pu} and k_{qu} are equal to 0; a constant current load if k_{pu} and k_{qu} are equal to 1 and a constant impedance load if k_{pu} and k_{qu} are equal to 2. In some studies the frequency dependency in (3.2) and (3.3) is modified using the Taylor series due to the limited variation of frequency compared to the voltage variation. Thus, the Taylor simplified model is:

$$P = P_n \left(\frac{U}{U_n}\right)^{k_{pu}} (1 + k_{pf}\Delta f) \tag{3.6}$$

$$Q = Q_n \left(\frac{U}{U_n}\right)^{k_{qu}} (1 + k_{qf}\Delta f), \tag{3.7}$$

where $\Delta f = (f - f_n)/f_n$ represents the variation from the nominal value.

3.2.2 Polynomial Model

The polynomial model is also diffused in literature, in particular the second order model. The expression of this model, that does not consider any variation of frequency, is:

$$P = P_n \left[p_2 \left(\frac{U}{U_n}\right)^2 + p_1 \left(\frac{U}{U_n}\right) + p_0\right] \tag{3.8}$$

$$Q = Q_n \left[q_2 \left(\frac{U}{U_n}\right)^2 + q_1 \left(\frac{U}{U_n}\right) + q_0\right] \tag{3.9}$$

This model is also called ZIP, because it represents the load as sum of three constant factors: impedance (Z), current (I) and power (P). The parameters p_1 and q_1 are related to the constant impedance part, the p_2 and q_2 are related to the constant current part, and p_3 and q_3 are related to the constant power part. Moreover, the sums of $p_{1,2,3}$ and $q_{1,2,3}$ are both equal to 1. The relationships that consider the variation of the frequency are reported:

$$P = P_n \left[p_1 \left(\frac{U}{U_n}\right)^2 + p_2 \left(\frac{U}{U_n}\right) + p_3\right] (1 + k_{pf}\Delta f), \qquad \sum_{i=1}^{3} p_i = 1 \tag{3.10}$$

$$Q = Q_n \left[q_1 \left(\frac{U}{U_n}\right)^2 + q_2 \left(\frac{U}{U_n}\right) + q_3\right] (1 + k_{qf}\Delta f), \qquad \sum_{i=1}^{3} q_i = 1. \tag{3.11}$$

These equation are similar to (3.2) and (3.3), where a frequency dependency is added.

3.2.3 Linear Model

The linear model is typical in the analysis where the voltage variation is near the nominal value. Therefore, it introduces errors in case of wider voltage ranges.

The proposed linear model presents the a_0 and a_1 parameters for the active power and the b_0 and b_1 parameters for the reactive power [62], as described by

$$P = P_n \left(a_0 + a_1 \frac{U}{U_n} \right), \tag{3.12}$$

$$Q = Q_n \left(b_0 + b_1 \frac{U}{U_n} \right). \quad . \tag{3.13}$$

In the literature, it is also specified to use the linear model only for the active power and the polynomial model for the reactive power [63]. However, it is possible to describe the frequency dependency also with the linear model:

$$P = P_n \left(a_0 + a_1 \frac{U}{U_n} \right) (1 + k_{pf} \Delta f), \tag{3.14}$$

$$Q = Q_n \left(b_0 + b_1 \frac{U}{U_n} \right) (1 + k_{qf} \Delta f), \tag{3.15}$$

The relation between active and reactive power and the frequency is similar two polynomial model with the Taylor simplification.

3.2.4 Comprehensive Static Model

The static comprehensive model has been introduced for low voltage loads [64]. It is called comprehensive because the model includes loads with static and dynamic characteristics. This model is based on a polynomial model combined with two different exponential models:

$$P = P_n [P_{ZIP} + P_{EX_1} + P_{EX_2}], \tag{3.16}$$

where:

$$P_{ZIP} = p_2 \left(\frac{U}{U_n} \right)^2 + p_1 \left(\frac{U}{U_n} \right) + p_0 \tag{3.17}$$

$$P_{EX_1} = p_4 \left(\frac{U}{U_n} \right)^{a_1} (1 + k_{pf_1} \Delta f) \tag{3.18}$$

$$P_{EX_2} = p_5 \left(\frac{U}{U_n} \right)^{a_2} (1 + k_{pf_2} \Delta f) \tag{3.19}$$

The same procedure is adopted for the formulation of the reactive power equations.

3.2.5 IEEE Task Force 1993 Load Model

IEEE task force has studied the behavior of loads formulating a load model. The model coefficients are calculated basing on the typology of typical 1993 loads.

$$P = P_n \cdot (\frac{U}{U_n})^{k_{pu}} \cdot (1 + k_{pf} \cdot (f - f_n)) \tag{3.20}$$

$$Q = Q_n \cdot (\frac{U}{U_n})^{k_{qu}} \cdot (1 + k_{qf} \cdot (f - f_n)) \tag{3.21}$$

It represents the load voltage dependency with an exponential part and frequency dependency with a linear element, which is the same as the linear model. The coefficients depends on the load type and seasoning. The dynamic response of the model allows a rising time of 100 ms [65], with a first order dynamic for voltage and frequency variations.

3.3 Load Modeling - Experimental setup

In order to characterize the load models a measurement setup has been implemented, so that the load under test can be supplied by different voltage amplitude and frequency values. Further measurement and sensing devices combined with protection system have been introduced in the setup configuration to guarantee accurate representative models and to avoid the damaging of equipments. Two similar setups have been implemented depending on the load type. The first one is dedicated to single-phase load with rated power under 2 kVA, as typically present in domestic loads.

The second one is a three-phase setup for loads up to 30 kVA, as typically present in commercial or industrial loads.

The control, acquisition and preliminary data elaboration is performed by the National Instruments (NI) PXI, which is a real-time operative system device used for data acquisition/generation. The NI PXI controls the amplifier (single/three-phase) output voltage applied to the load under test, in terms of amplitude and frequency. At the same time, this device acquires the measured parameters as load voltage and current, and sends the acquisition to the PC for the final elaboration process. The single-phase amplifier has a maximum output power of 2 kVA, while the three-phase amplifier has a maximum output power of 30 kVA, with a 5 kHz bandwidth. In Fig. 3.3, the experimental setup for the single-phase low power loads is presented, where the LabVIEW code for generating the reference voltage source of the tests is running in the real-time system of the NI PXI. The current and voltage measurements are sampled by the NI PXI and then elaborated

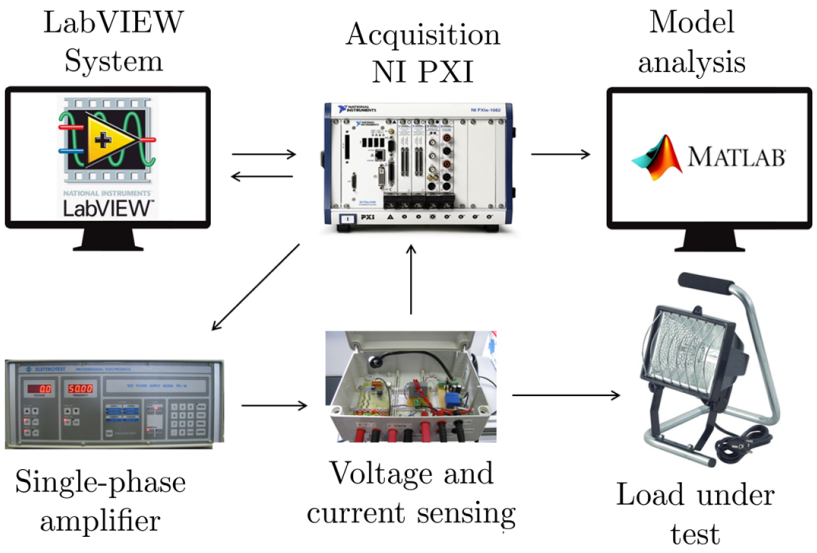

Figure 3.1: Single-phase setup for load under 2kVA.

with Matlab in order to calculate the load power characteristics and models. The same principle is applied to the experimental setup for high power three-phase loads, shown in Fig. 3.4, where the NI PXI signals are sent via LAN to the NI CompactRIO, which sends these signals to the three-phase amplifier.

These amplifiers generate a stable output voltage controlled by an analogical signal of the PXI. As presented in Fig. 3.2 and 3.1, the LabVIEW system implements program files that are performed in the PXI, and saves the acquired data by the PXI. The code used on the real-time system of the PXI allows the generation of the output voltage required for the tests as changing the voltage amplitude or frequency.

During the testing procedure, after the variations of the voltage level or frequency value, the acquisition system waits the end of the initial transient in order to measure the steady-state conditions. The acquired voltage and frequency are sent to the PC for the model elaboration. This is an automatic procedure replicated for each voltage and frequency level.

3.3.1 Acquisition Parameters

The load static characterizations are used for all the tested loads. The ranges of testing conditions are based on the thresholds of over/under voltage and over/under frequency protections for connection to the low voltage networks. Therefore, the tests are performed in the range of ±15% of the nominal voltage level ($195V_{rms}$ - $265V_{rms}$), with steps of $5V_{rms}$, and from 47.5 Hz to 51.5 Hz for the frequency variations, with a step of 0.2 Hz. The time between two consecutive variations depends on the specific load under test, e.g.

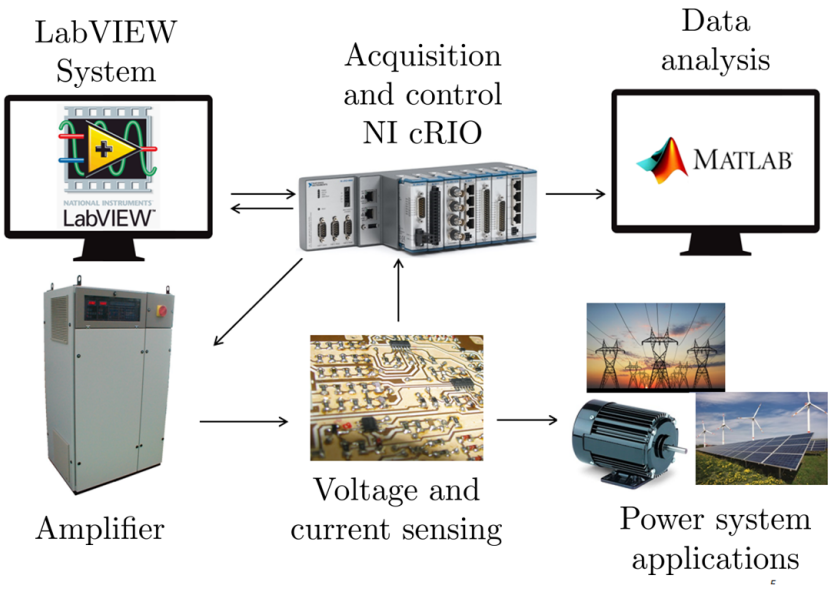

Figure 3.2: Three-phase setup for load up to 30kVA.

under 50 ms for LED lamps and 100ms for metal halide lamps.

During the voltage characterization the voltage frequency is stable at 50 Hz and each measure lasts 1 second. While during the frequency characterization the minimum time to guarantee 0.2 Hz precision is 5 seconds. The characteristics of the data acquisition system are:

- sampling of 100kSample/s;
- voltage variation tests: 1 second of data acquisition (100000 samples);
- frequency variation tests: 5 seconds of data acquisition (500000 samples);
- time for the test of voltage variation: 10 minutes;
- time for the test of frequency variation: 20 minutes.

Each test has been repeated three times and the model has been characterized with the average of the three results. In general terms, the variations of the results among the three tests were small.

3.3.2 Model Identification Tests

This subsection reports the active and reactive power calculation procedure.

The setup configuration has been compared with the wattmeter results, and after software compensations, the error introduced by the sensing devices, is under the 1.5%

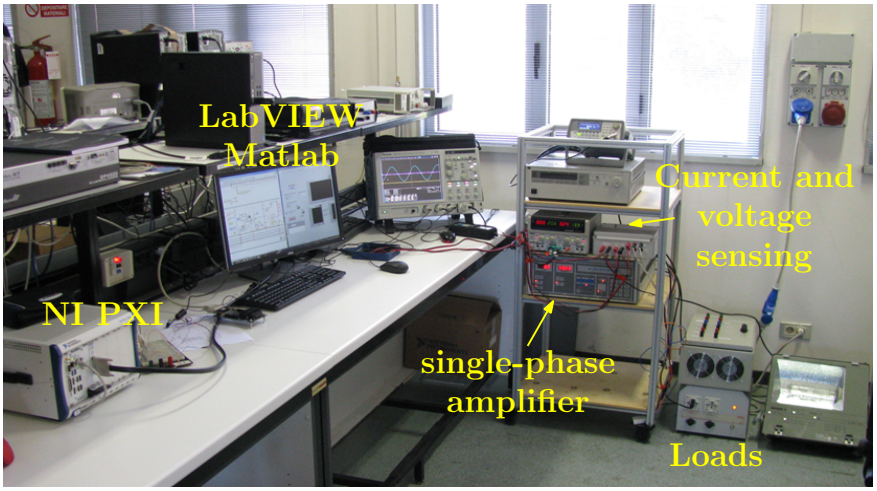

Figure 3.3: Single-phase experimental setup for load below 2kVA.

respect to the wattmeter. In order to understand the model identification procedures, the load characteristic curve of $P_L f(f, v)$ and $Q_L f(f, v)$ during only voltage variations is described in the following sections. The aim is to calculate the active and reactive load power from the current and voltage PXI acquisitions at each voltage level of the tests. After the PXI sample acquisitions, the signals are scaled (i.e. the signals are scaled to the real values after the sensing), the fast fourier transforms (*fft*) of the current and voltage samples of each testing voltage level (100000 samples in case of voltage variations tests) are performed in order to evaluate the fundamental harmonic of the signals.

The *fft* calculates the amplitude and phase values of the voltage and current, allowing the calculation of active and reactive power since the amplitude of voltage and current and the phase difference are known. In Fig. 3.5, this procedure is presented.

Using the *fft* analysis, it is possible to compensate voltage and current phase errors due to the sensing, comparing the results with the wattmeter.

The procedure is then similar for the frequency variation tests. The difference is the length of the acquisition signals, which in case of frequency variation tests depends on the frequency values, since the accuracy for each test is 0.2 Hz. Therefore, in this case the voltage and current signals are composed by 500000 samples.

The two model identification procedures (i.e. voltage amplitude and frequency variation tests) may be performed also for different voltage and frequency values used in the tests, by changing them in the front panel of the LabVIEW code.

After the power characterization tests, it is possible to evaluate the coefficients of the various load model presented and to select which load model better describes the load under test. This model identification procedure is done using a specific Matlab function (*fsolve*) for continuous non-linear systems. For each test of voltage and frequency

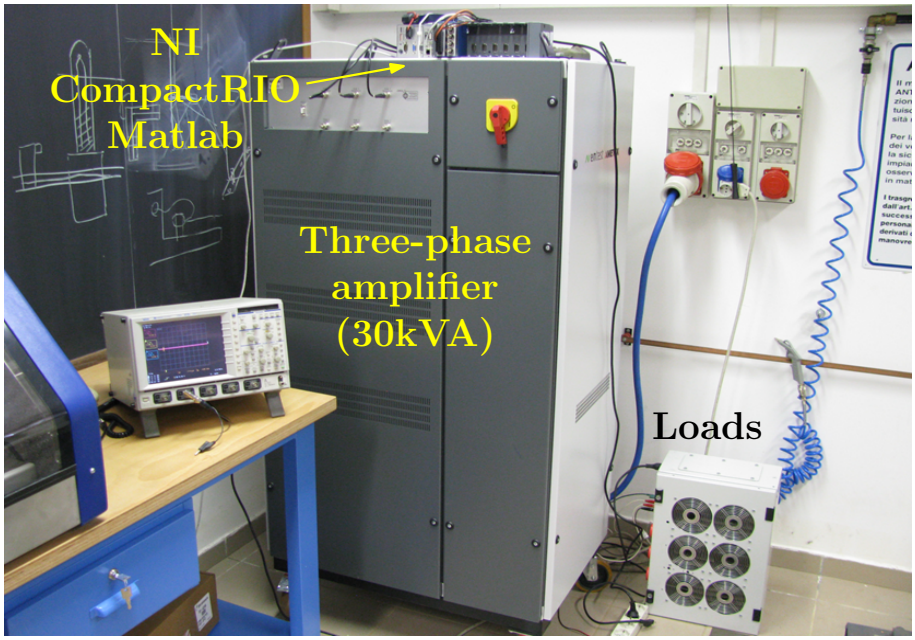

Figure 3.4: Three-phase experimental setup for load up to 30kVA.

variations, the active and reactive calculated power are used by the *fsolve* function to derive the coefficients of the model under consideration. Thus, the final model coefficients are the average values of all tests performed for each coefficient.

3.3.3 Load Considered For Tests

Different load types have been considered for the characterization of a typical residential environment. The residential type loads tested with the experimental setup are presented in Fig. 3.6. For all the loads, the representative models have been evaluated, i.e. the models that present the lower error in the $P_Lf(V)$, $P_Lf(f)$, $Q_Lf(V)$ and $Q_Lf(f)$ characteristic curves. Therefore, an equivalent load for a residential and domestic system can be created by the combination of the different load connected to the system. In Fig. 3.7, the potential beneficial of this load modeling analysis is shown. Further studies may use the combined model load as the more accurate representation of loads connected to the electric distribution networks not only for unintentional islanding.

- **IEEE 1993 model**

$$P(v,f) = P_n \cdot (\frac{U}{U_n})^{k_{pv}} \cdot (1 + k_{pf} \cdot (f - f_n))$$

$$Q(v,f) = Q_n \cdot (\frac{U}{U_n})^{k_{qv}} \cdot (1 + k_{qf} \cdot (f - f_n))$$

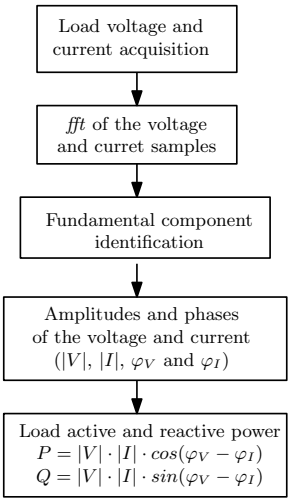

Figure 3.5: Static characterization procedure for active and reactive curves.

- **Linear model**

$$P(v,f) = P_n \cdot (a_1 \cdot \frac{U}{U_n} + a_0) \cdot (1 + k_{pf} \cdot (f - f_n))$$

$$Q(v,f) = Q_n \cdot (b_1 \cdot \frac{U}{U_n} + b_0) \cdot (1 + k_{qf} \cdot (f - f_n))$$

  where $a_0 + a_1 = 1$ e $b_0 + b_1 = 1$

- **Exponential model**

$$P(v,f) = P_n \cdot (\frac{U}{U_n})^{k_{pv}} \cdot (\frac{f}{f_n})^{k_{pf}}$$

$$Q(v,f) = Q_n \cdot (\frac{U}{U_n})^{k_{qv}} \cdot (\frac{f}{f_n})^{k_{qf}}$$

- **ZIP model**

$$P(v,f) = P_n \cdot [p_2 \cdot (\frac{U}{U_n})^2 + p_1 \cdot (\frac{U}{U_n}) + p_0] \cdot (1 + k_{pf} \cdot (f - f_n))$$

$$Q(v,f) = Q_n \cdot [q_2 \cdot (\frac{U}{U_n})^2 + q_1 \cdot (\frac{U}{U_n}) + q_0] \cdot (1 + k_{qf} \cdot (f - f_n))$$

  dove $p_1 + p_2 + p_3 = 1$ e $q_1 + q_2 + q_3 = 1$

The experimental results identify the coefficients to represent the behavior of the loads using the static models. An example is reported in Tab. 3.1, where the loads coefficients are calculated according to the IEEE task force load model. Tab. 3.1 reports the 1993

Table 3.1: Experimental results of the model identification of the loads reported in 3.6. Coefficients calculated according to the IEEE 1993 model.

IEEE 1993 model coefficients

Load	kpv	kqv	kpf	kqf
IEEE 1993 residential	1.3	2.7	0.8	-2
IEEE 1993 industrial	0.1	0.6	2.6	1.6
IEEE 1993 agricultural	1.4	1.4	5.6	4.2
Fluorescent lamp	1.016	0.555	0.0027	-0.0071
Halogen lamp	1.478	1.973	0.0006	-0.0312
LED lamp	0.098	-0.996	-0.0036	-0.0213
Neon lamp inductive reactor	1.817	3.179	-0.0247	-0.0293
Neon lamp electronic reactor	1.39	-0.011	0.0012	-0.0039
Sodium-vapor lamp	2.27	3.30	-0.0378	-0.3130
Metal halide lamps	1.806	8.337	-0.0219	-0.2260
Notebook	0.089	0.372	0.0017	-0.0013
Monitor	-0.049	0.928	-0.0015	0.0065
PC desktop	0.095	-4.607	-0.0001	0.0057
Motor with auxiliary pole	2.442	2.603	-0.0214	-0.0190
Compressor	1.031	7.234	0.0112	-0.1653
Electric pump	2.149	4.937	-0.0133	-0.0971
Washing machine	3.104	4.255	-0.0417	-0.0719

loads (i.e. IEEE 1993 residential, IEEE 1993 industrial and IEEE 1993 agricultural) and the measured loads coefficients. It is worth noting that the dependence on the frequency is strongly reduced mainly due to the introduction of new technologies. Thus, the load analysis is crucial to understand the behavior of the current electric distribution networks not only for islanding operations. For completeness, the calculated THD indexes introduced by the loads under investigation are reported in Tab. 3.2, where the presence of high THD index represents the effect of power electronic devices in the low power applications, especially at the domestic level.

Fig. 3.8 describes an example of active and reactive power characteristic curves during variations of voltage amplitude and frequency of an electro pump. Furthermore, the errors introduced by the use of a static load model are reported in Fig. 3.9, where the polynomial or ZIP model represents the best fit comparing the average errors values.

In this work, the loads modeling analysis reported the active and reactive characteristic curves and the coefficients of the static loads models, which represent the behavior of the typical loads connected to the electric distribution networks. These calculated models differ obviously from the specific paralleled RLC resonant load, used in the literature analysis of unintentional islanding and in the AI requirements presented in standard.

Therefore, this work considers a different load for islanding analysis. In particular, this load presents active and reactive power dependencies, which are comparable with the

Table 3.2: Total harmonic distortion (THD) index of the loads under investigation.

IEEE 1993 model coefficients

Load	THD
Fluorescent lamp	101.3
Halogen lamp	0
LED lamp	107.7
Neon lamp inductive reactor	11.08
Neon lamp electronic reactor	28.84
Sodium-vapor lamp	19.23
Metal halide lamps	15.27
Notebook	194.0
Monitor	193.4
PC desktop	81.92
Motor with auxiliary pole	29.29
Compressor	11.59
Electric pump	6.70
Washing machine	10.07

residential load type within the range of OUF and OUV limits. The load is presented in Fig. 6.5 and in chapter 6.This choice has been done also with the purpose to simplify the experimental validation.

a) Fluorescent lamp

b) Halogen lamp

c) LED lamp

d) Neon lamp (inductive reactor)

e) Neon lamp (electronic reactor)

f) Sodium-vapor lamp

g) Metal halide lamp

h) Notebook

i) Monitor

j) PC desktop

k) Fan motor (with auxiliary pole)

l) compressor

m) Electric pump

n) Washing machine

Figure 3.6: Loads adopted for the experimental model identification.

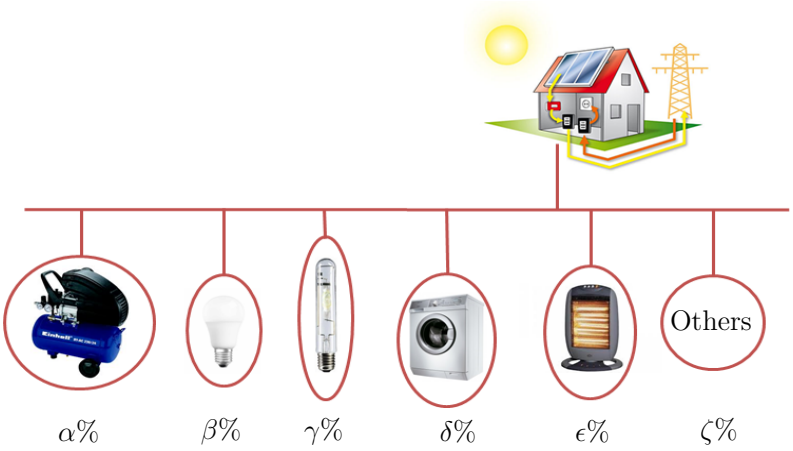

Figure 3.7: Residential system identified with a combination of load, based on the share of the total power.

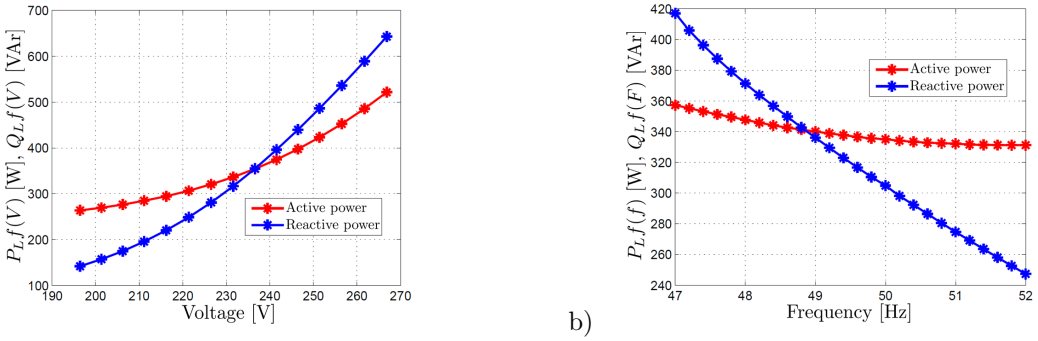

a) b)

Figure 3.8: Active and reactive power characteristic curves of the electro pump calculated in two cases: a) variations of the voltage amplitude level and b) variations of the voltage frequency value.

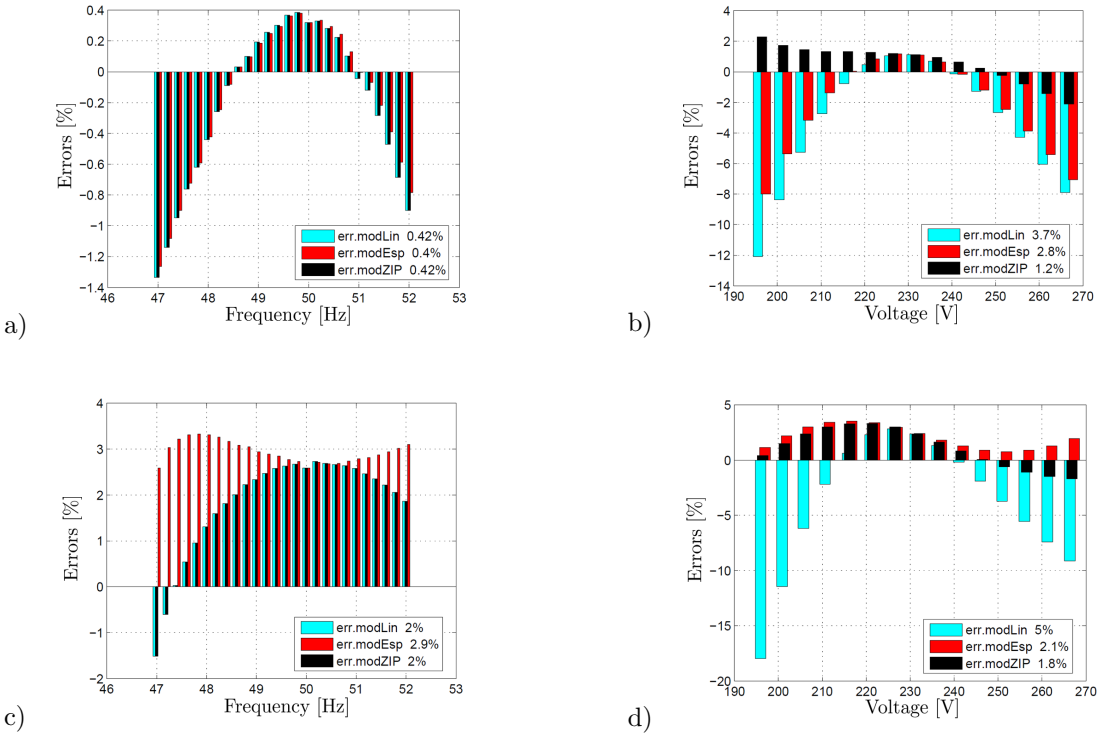

Figure 3.9: Active and reactive power errors introduced by the linear, the exponential and polynomial (or ZIP) model compared to the measurements. a) errors of active power in the range of frequency variations; b) errors of active power in the range of voltage variations; c) errors of reactive power in the range of frequency variations; d) errors of reactive power in the range of voltage variations.

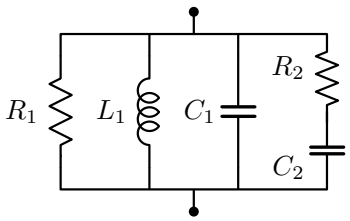

Figure 3.10: Generic local load with active and reactive power dependencies $P_L(f, u)$ and $Q_L(f, u)$.

Chapter 4

Power Converter Structure and Modeling

Electronic power converters are employed in DER systems with the main function of injecting the power generated by the energy source, such as PV panels, into the electric power system. They are needed for the connection and synchronization with the electric system. Control algorithms of the converter allow the grid synchronization, the control of the voltage and the current injected into the grid, the standards ancillary services and the internal protection functions required for the normal operation of the DER system. However, control concepts and characteristics of power electronic converters are significantly different from those of the conventional rotating machines. Therefore, the control strategies and dynamic behavior of the electrical grid having a large number of dispersed generators can be different from that of a conventional power system. Thus, the modeling of the DER power converter plays a key role in the analysis of the distribution networks with large penetration of inverter-based distributed generators.

In this thesis, the model of a DER PV system has been adopted in order to study the causes and the influencing factors of unintentional islanding in MV and LV distribution networks. The number of grid-connected PV systems has been significantly increased and this technology reached a large penetration in the grid, changing the traditional concept of passive distribution electric networks into active networks.

The model is implemented with the library Power System Blockset, a toolbox of Matlab and it is compliant to the Italian standard requirements for distribution electric networks. The model of the grid-connected PV inverter is reported in this chapter, including the description of the principal circuital and control blocks. This model enables the study of the dynamic behavior of the inverter during the disconnection from the main grid.

4.1 Power Converter Structure

Literature analysis shows different topologies for power converters [66–69]. All the converter topologies have to deal with the following constrains:

- conversion efficiency: the efficiency is usually required to be above 90%;
- electric grid connection: the converter has to be compliant with the technical requirements imposed by standard bodies, e.g. active and reactive power regulations;
- maximum power point tracker (MPPT): the converter has to reach the optimum working point in order to ensure the maximum power transfer to the grid.

Due to the high cost of solar energy, the PV inverter technology has been driven primarily by efficiency. New innovative topologies have been developed for PV inverters with the main purpose of increasing the efficiency and reducing the manufacturing cost. For example, a typical efficiency increase of 1–2 % can be obtained eliminating the galvanic isolation provided by high-frequency transformers in the DC–DC boost converter or by low-frequency transformer on the inverter output. As the lifetime of PV panels should be typically longer than 20 years, efforts to increase the lifetime of PV inverters are also under way.

Thus, a very large diversity of PV inverter topologies can be found on the market and in the literature over the recent years. However, it is possible to select two main categories based on: (*i*) the ratio between the numbers of PV modules and converters, and (*ii*) the number of converter stages. The first category is made up of different technologies: (a) centralized, (b) strings and (c) modules, while the second is based on: (a) single stage, (b) double stage and (c) multi-stage.

4.1.1 Centralized Technology

The first PV applications were based on centralized single stage technology, as shown in Fig. 4.1a. This scheme ensured high reliability, easy control strategies and good grid connected performance.

The introduction of higher switching frequency components helped the diffusion of this technology, reducing the current distortion injected in the electric system. Moreover, especially for single stage applications, the limited numbers of components have represented over the years a winning factor in the commercialization of this technology. However, it has to be mentioned that, in spite of the number of conversion stages, the input voltage level needs to be higher than the peak of the grid voltage. Therefore, this solution requires the series connection of multiple PV strings, with the drawback of reducing the efficiency

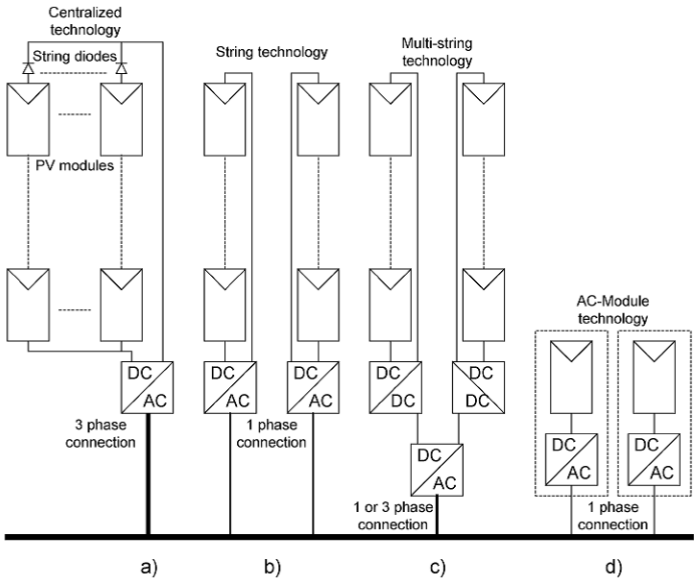

Figure 4.1: Typical PV converter systems: (a) centralized, (b) string, (c) multi-string and (d) modules technology.

in case of partial shading. The parallel connection of different strings requires the introduction of decoupling diodes, connected in series in each string, with corresponding power losses.

In single-phase applications, this technology requires a capacitor designed to compensate a full power swing at twice the line frequency, in order to reduce the corresponding voltage ripple at the input voltage of the conversion module. This electrolytic capacitor is the element that limits the reliability and the life time of the system. Finally, the conversion module becomes relatively inflexible, being optimized for a specific configuration of the PV modules. For all these reasons, in recent years the use of centralized solutions is decreased.

4.1.2 String Technology

The strings technology represents the state of the art in photovoltaic systems, although there are still various centralized solutions on the market. The conversion modules are of small-medium size and each module is connected to a string of PV modules in series, as shown in Fig. 4.1b.

The conversion modules are connected in parallel in order to supply the desired power. This technology provides high flexibility, being able to adapt to different power sizes. Moreover, the overall PV system efficiency is higher, given that each string can have its own MPPT. If the number of photovoltaic modules per string is sufficiently high (above 10), the conversion module may not require the voltage amplification. Otherwise, one DC/DC

boost converter stage, possibly with high frequency transformer, must be included in the module. It is important to note that the most recent implementations of string technology, called "multi-string" (Fig. 4.1c), are based actually on double stage conversion modules, using DC/DC converters connected in parallel. They supply a DC bus which feeds a single DC/AC converter, connected to the electric grid. Therefore, this solution combines the advantage of the better employment of the photovoltaic system, guaranteed by string converters and the presence of a single central inverter. For this reason, the multi-string is the basis of all the latest commercial products.

4.1.3 Modules Technology

The evolution of the multi-string solution is represented by modules technology (Fig.4.1d)), in which each PV module is equipped with converter connected to the electric grid. This solution provides maximum flexibility and the best possible use of the PV system (the modules are all in parallel and each has its own MPPT). Furthermore, it offers the possibility of an integrated converter in the photovoltaic module, with a consequent costs reduction.

Consider the realizations of the technology described above, it must be said that each of them is, in principle, compatible with topologies of converters with both single and multiple stages. As matter of fact, the literature presents several different solutions [69].

However, the main part related to this study is limited to the PV grid interface. To this end, regardless of the fact that the system is single-stage or double-stage or multi-string, the main part remains the grid-connected inverter. For this reason, the power electronics modeling is focused on the grid-connected inverter.

4.2 Two-Level PV Inverter

The power stage of DC/AC converters is characterized by several topologies. The most commonly used is the two level inverter shown in Fig. 4.2. In the literature, there are solutions to 3-level (neutral point clamped, T-type, etc.) and solutions using multiple levels (5, etc.). However, the two-level solution has been selected for the purposes of this study, since a fundamental role in the unintentional islanding is played by the inverter control. Any topology, which guarantees the capability of reactive power, provides very similar results. Hence, it is reasonable to use the most widespread and simple solution. Fig. 4.2 shows such two-level inverter together with the photovoltaic source, the DC side capacitor, the primary inductive filter, the EMI (Electromagnetic interference) filter and the connection to the electrical network.

This thesis is focused on the role of the inverter control during unintentional islanding

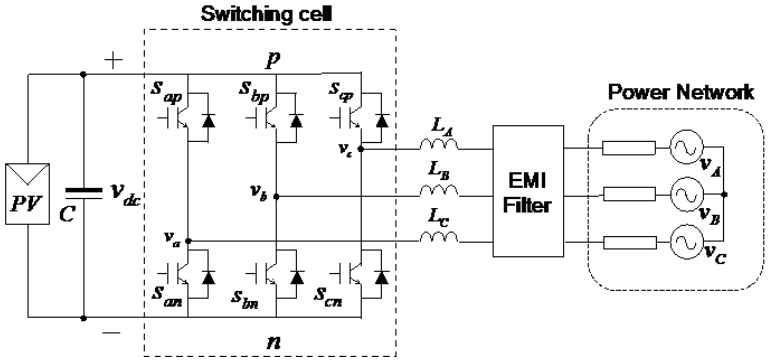

Figure 4.2: Block diagram of the three phase inverter.

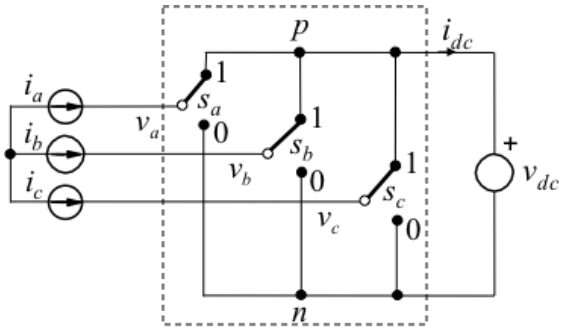

Figure 4.3: Ideal switching cell of a three phase inverter.

operations considering the possible interaction with the load, the protection system and the standard requirements. Therefore, it is possible to neglect issues like the switching losses and harmonics distortion. In fact, the case of ideal switches has been considered and the equivalent diagram of the switching cell is highlighted in Fig. 4.3. In following section, the derivation of the analytical steps is unfolded.

The mathematical model of the fundamental equations of the switching cell is performed using the switching function $s(t)$, that is 1 if the switch is closed and 0 if open. As highlighted in Fig. 4.3, $s_a(t)$, $s_b(t)$ and $s_c(t)$ are the switching functions for the phases a, b and c with $v_a(t)$, $v_b(t)$ and $v_c(t)$ voltages of the phase a, b and c referred to the point n.

It is possible to define the following line to line values:

$$\begin{aligned}
\overrightarrow{v}_{l-l} &= \begin{bmatrix} v_{ab} \\ v_{bc} \\ v_{ca} \end{bmatrix} = \begin{bmatrix} v_a - v_b \\ v_b - v_c \\ v_c - v_a \end{bmatrix}, \\
\overrightarrow{s}_{l-l} &= \begin{bmatrix} s_{ab} \\ s_{bc} \\ s_{ca} \end{bmatrix} = \begin{bmatrix} s_a - s_b \\ s_b - s_c \\ s_c - s_a \end{bmatrix}, \\
\overrightarrow{i}_{l-l} &= \begin{bmatrix} i_{ab} \\ i_{bc} \\ i_{ca} \end{bmatrix} = \frac{1}{3} \begin{bmatrix} i_a - i_b \\ i_b - i_c \\ i_c - i_a \end{bmatrix}.
\end{aligned} \tag{4.1}$$

Therefore, the equations that connect the DC side to the AC side are:

$$\begin{cases} \overrightarrow{v}_{l-l} = \overrightarrow{s}_{l-l} \cdot V_{DC} \\ i_{DC} = \overrightarrow{s}^{T}_{l-l} \cdot \overrightarrow{i}_{l-l} \end{cases}. \tag{4.2}$$

The differential equations of the schematics in Fig. 4.4 are:

$$v_{ab} = L\frac{d}{dt} \begin{bmatrix} i_a - i_b \\ i_b - i_c \\ i_c - i_a \end{bmatrix} + \begin{bmatrix} v_a - v_b \\ v_b - v_c \\ v_c - v_a \end{bmatrix} = 3L\frac{d}{dt} \begin{bmatrix} i_{ab} \\ i_{bc} \\ i_{ca} \end{bmatrix} + \begin{bmatrix} v_{ab} \\ v_{bc} \\ v_{ca} \end{bmatrix}, \tag{4.3}$$

$$i_{DC} = C\frac{dV_{DC}}{dt} + i_{PV}. \tag{4.4}$$

Resulting:

$$\begin{aligned}
\frac{dV_{DC}}{dt} &= \frac{1}{C}(i_{DC} - i_{PV}), \\
\frac{\overrightarrow{i}_{l-l}}{dt} &= \frac{1}{3L}\overrightarrow{v}_{L-L} - \frac{1}{3L}\overrightarrow{v}_{l-l},
\end{aligned} \tag{4.5}$$

where: $\overrightarrow{v}_{L-L} = \begin{bmatrix} v_{AB} & v_{BC} & v_{CA} \end{bmatrix}^T$. Using the (4.2), the switching model is described

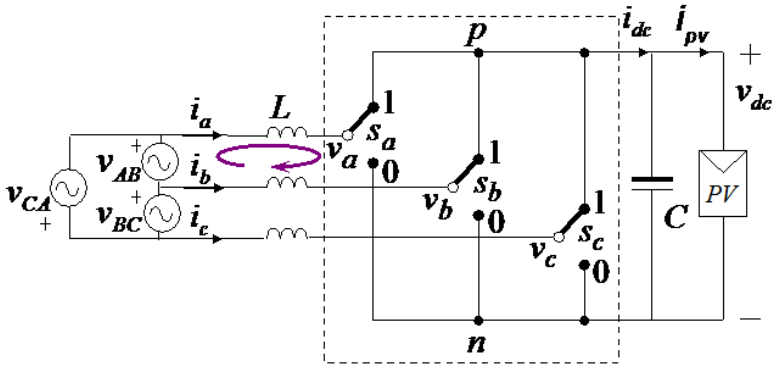

Figure 4.4: Three phase PV inverter switching model.

by:

$$\begin{aligned} \frac{dV_{DC}}{dt} &= \frac{1}{C}(\overrightarrow{s}^{T}_{l-l} \cdot \overrightarrow{i}_{l-l} - i_{PV}), \\ \frac{\overrightarrow{i}_{l-l}}{dt} &= \frac{1}{3L}\overrightarrow{v}_{L-L} - \frac{1}{3L}\overrightarrow{s}_{l-l} \cdot V_{DC}. \end{aligned} \tag{4.6}$$

The switching model is able to reproduce the switching operations and can be very useful for studying high frequency phenomenons, such as harmonic distortions, electromagnetic compatibility (EMC) problems, interference with power line communication (PLC) used by the distribution system operator (DSO), etc. However, the switching model also introduces some drawbacks, resulting in long simulation times and high computational resources. Therefore, a simplified model, which is capable of reproducing the static and dynamic behavior of the average voltage and current values inside the switching period, is needed.

4.3 Average Time Model

The average time model can reproduce the behavior of the PV system in a low-frequency range with easier deployment and higher computing speed (at least a factor of 10). Thus, for the purpose of this thesis, the behavior of the PV inverter in the high-frequency range is not required. This section continues from the previous mathematical derivation, introducing the time averaging of the voltage, current and switching function values within the switching period. Consider the following average operator:

$$\overline{x}(t) = \frac{1}{T}\int_{t-\tau}^{t} x(\tau)d\tau, \tag{4.7}$$

where the $\overline{x}(t)$ is the average of x within the switching period. The average value of the switching function $s(t)$ is the duty-cycle $d = t_{ON}/T_{sw}$, with t_{ON} the closing time of the switch and T_{sw} the switching period. Therefore, it is possible to obtain:

$$d = \overline{s}(t) = \frac{1}{T}\int_{t-\tau}^{t} s(\tau)d\tau. \tag{4.8}$$

This averaging function is linear. Thus, the Kirchhoff law can be applied. With the hypothesis of small or linear ripple, it is possible to include the non linear elements, i.e.:

$$\begin{aligned}
&\overline{\overrightarrow{s}_{l-l} \cdot V_{DC}} \approx \overline{\overrightarrow{s}_{l-l}} \cdot \overline{V}_{DC} = \overrightarrow{d}_{l-l} \cdot \overline{V}_{DC}, \\
&\overline{\overrightarrow{s}^{T}_{l-l} \cdot \overrightarrow{i}_{l-l}} \approx \overline{\overrightarrow{s}^{T}_{l-l}} \cdot \overline{\overrightarrow{i}}_{l-l} = \overrightarrow{d}^{T}_{l-l} \cdot \overline{\overrightarrow{i}}_{l-l}.
\end{aligned} \tag{4.9}$$

Using the average operator (4.7) in the switching model (4.6), we obtain:

$$\begin{aligned}
\tfrac{1}{T}\textstyle\int_{t-\tau}^{t} \frac{dV_{DC}(\tau)}{dt}\,\mathrm{d}\tau &= \frac{1}{T}\int_{t-\tau}^{t}\left(\frac{1}{C}\overrightarrow{s}^{T}_{l-l}(\tau)\cdot\overrightarrow{i}_{l-l}(\tau) - \frac{1}{C}i_{PV}\right)d\tau \\
&, \\
\frac{1}{T}\int_{t-\tau}^{t}\frac{\overrightarrow{i}_{l-l}(\tau)}{dt}d\tau &= \frac{1}{T}\int_{t-\tau}^{t}\left(\frac{1}{3L}\overrightarrow{v}_{L-L}(\tau) - \frac{1}{3L}\overrightarrow{s}_{l-l}(\tau)\cdot V_{DC}(\tau)\right)d\tau,
\end{aligned} \tag{4.10}$$

and applying the (4.9), the system becomes:

$$\begin{aligned}
\frac{d\,\overline{\overrightarrow{i}}_{l-l}}{dt} &= \frac{1}{3L}\left(\overline{\overrightarrow{v}}_{L-L} - \overrightarrow{d}_{l-l}\overline{V}_{DC}\right), \\
\frac{d\overline{V}_{DC}}{dt} &= \frac{1}{C}\left(\overrightarrow{d}^{T}_{l-l}\cdot\overline{\overrightarrow{i}}_{l-l} - i_{PV}\right),
\end{aligned} \tag{4.11}$$

where: $\overrightarrow{v}_{L-L} = \begin{bmatrix} v_{AB} & v_{BC} & v_{CA} \end{bmatrix}^{T}$.

The time averaging model is presented in Fig. 4.5. This model implementation requires the use of generators controlled on voltage and current level based on the (4.11). There are no appreciable differences between the switching and averaging models for the phenomena occurring at frequency below half of the switching frequency. Furthermore, the harmonic distortion of the injected current is negligible, due to the absence of the dead time.

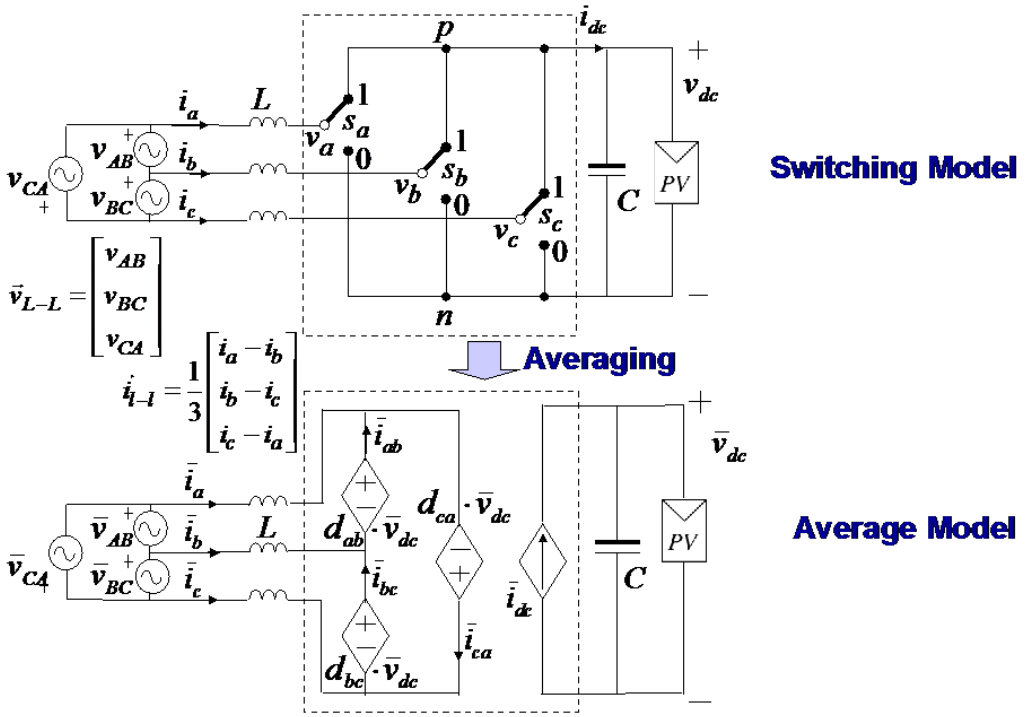

Figure 4.5: Three phase PV inverter - averaging time model.

4.4 Simulink/Matlab Inverter Model

The Simulink/Matlab model implementation is reported in Fig. 4.8 and Fig. 4.9. Fig. 4.8 shows the average time inverter model, where the typical six switches inverter structure is replaced by ideal voltage sources controlled by the block diagram in the upper portion. This block diagram implements the average time model of the inverter output voltage with the DC component V_{DC} implemented as a constant DC voltage source. This is a voltage source inverter (VSI) with an inner current closed-loop in order to provide the active and reactive power. Fig. 4.8 shows the output inductive filter and the EMI filter. The reference current values I_{ref} are generated by the external power closed-loop represented in Fig. 4.9, where three-phase voltage source inverter model of Fig. 4.8 is included in the orange subsystem called $Three-phase\ Inverter$. The control architecture of the inverter is proposed in Fig. 4.9. In this configuration, two different phase locked loop (PLL) blocks have been implemented. The PLL called PLL_{meas} is used for the external measurement of frequency and amplitude of the voltage during unintentional islanding operation, while the $PLL_{inverter}$ block tuned with a lower bandwidth (5 Hz) realizes the inverter grid synchronization used to generate the desired active and reactive power. Furthermore, the $PLL_{inverter}$ block generates the reference values of f and V for the regulation droop

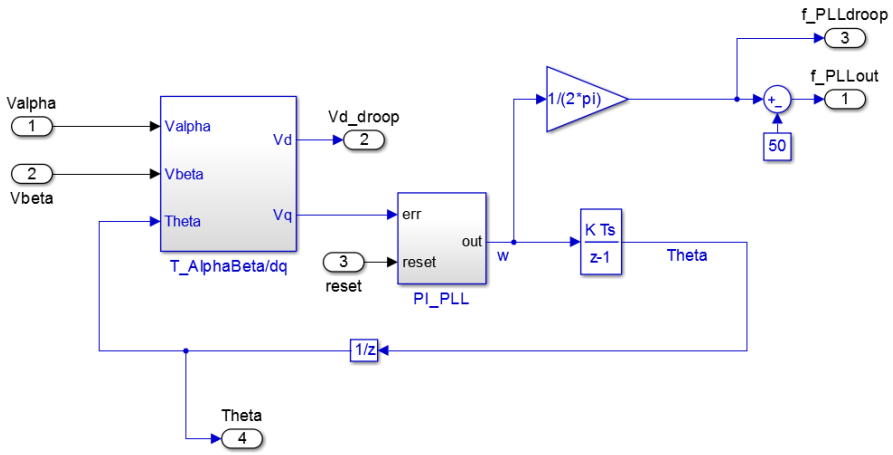

Figure 4.6: Three phase PV inverter - PLL for grid synchronization.

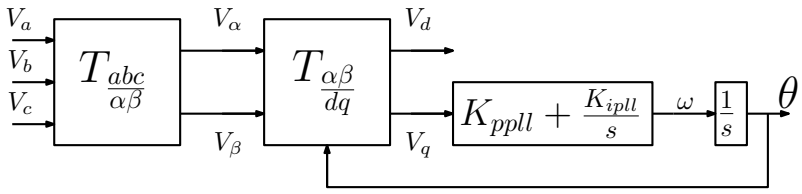

Figure 4.7: Typical three-phase SFR-PLL scheme.

functions P/f and Q/V. The PLL model is reported in Fig. 4.6, and it is adopted for both the PLL_{meas} and $PLL_{inverter}$ block, changing only the PI regulator parameters.

In this model, a synchronous reference frame (SRF) PLL has been implemented. SRF-PLL are widely applied in three-phase DER. Previous papers [70–74] have focused on the PLL performance, such as nonlinear PLL techniques [70, 71], during distorted and unbalanced grid conditions, to improve the trade off between tracking bandwidth and filtering. Fig. 4.7 shows the widely used three-phase SRF PLL system [75, 76].

It uses a abc/dq transformation block as the phase-detector (PD) to convert the measured utility positive-sequence phase-voltages into the q channel signal.

Though many sophisticated PLLs are proposed with different PDs, the results drawn from the SRF PLL are still applicable to others solutions, since they share the same phase locking principle [75, 77].

In Fig. 4.9 the active and reactive external closed-loops are presented. The blocks $droop_{P(f)}$ and $droop_{Q(V)}$ elaborate the reference value of the active and reactive power starting from the nominal external value and the PLL frequency and voltage measurements at the point of common coupling terminals. Thus, in grid connected operations the voltage frequency and amplitude are imposed by the main grid, while in islanding operations the inverter maintains the voltage supplying the local load. Furthermore, the blocks $droop_{P(f)}$

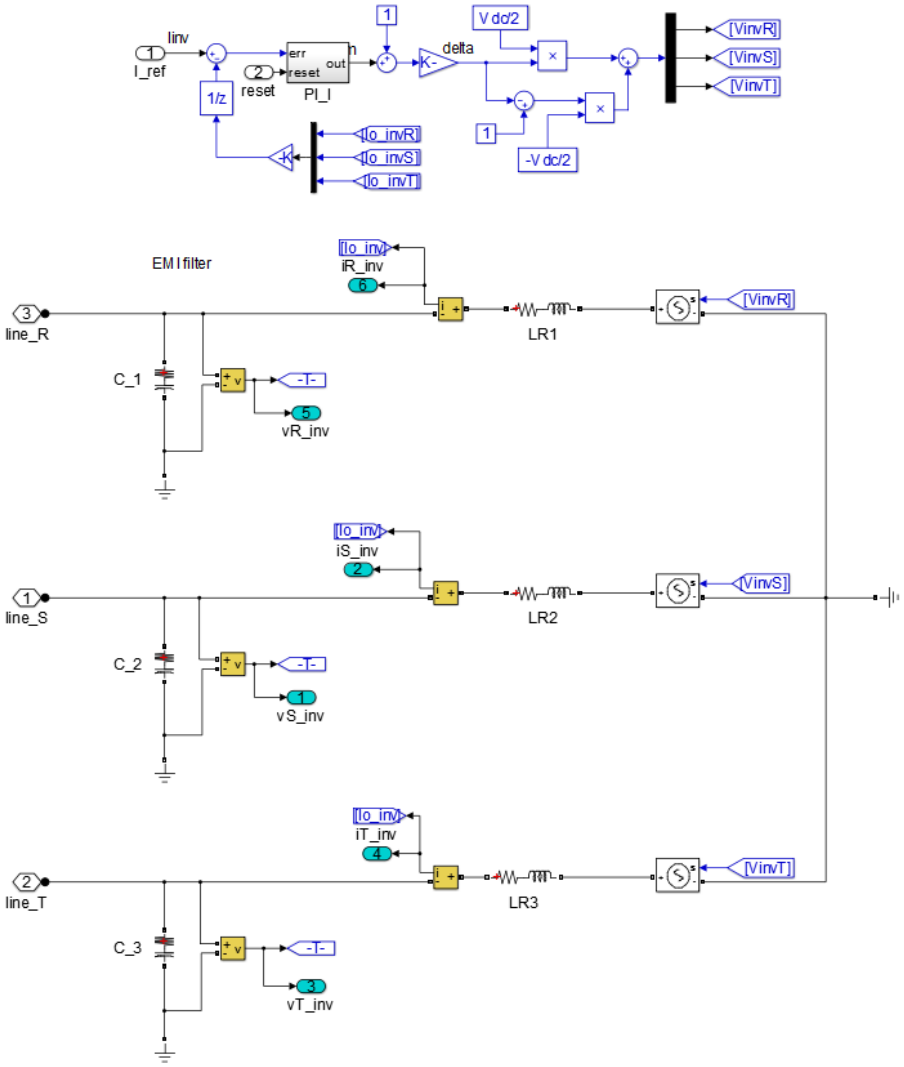

Figure 4.8: Three phase PV inverter - averaging time model voltage sources.

and $droop_{Q(V)}$ have been designed in order to perform the following functions:

- constant power references;
- activate the active and reactive power droop P/f and Q/V, with the possibility to select one or both of them;

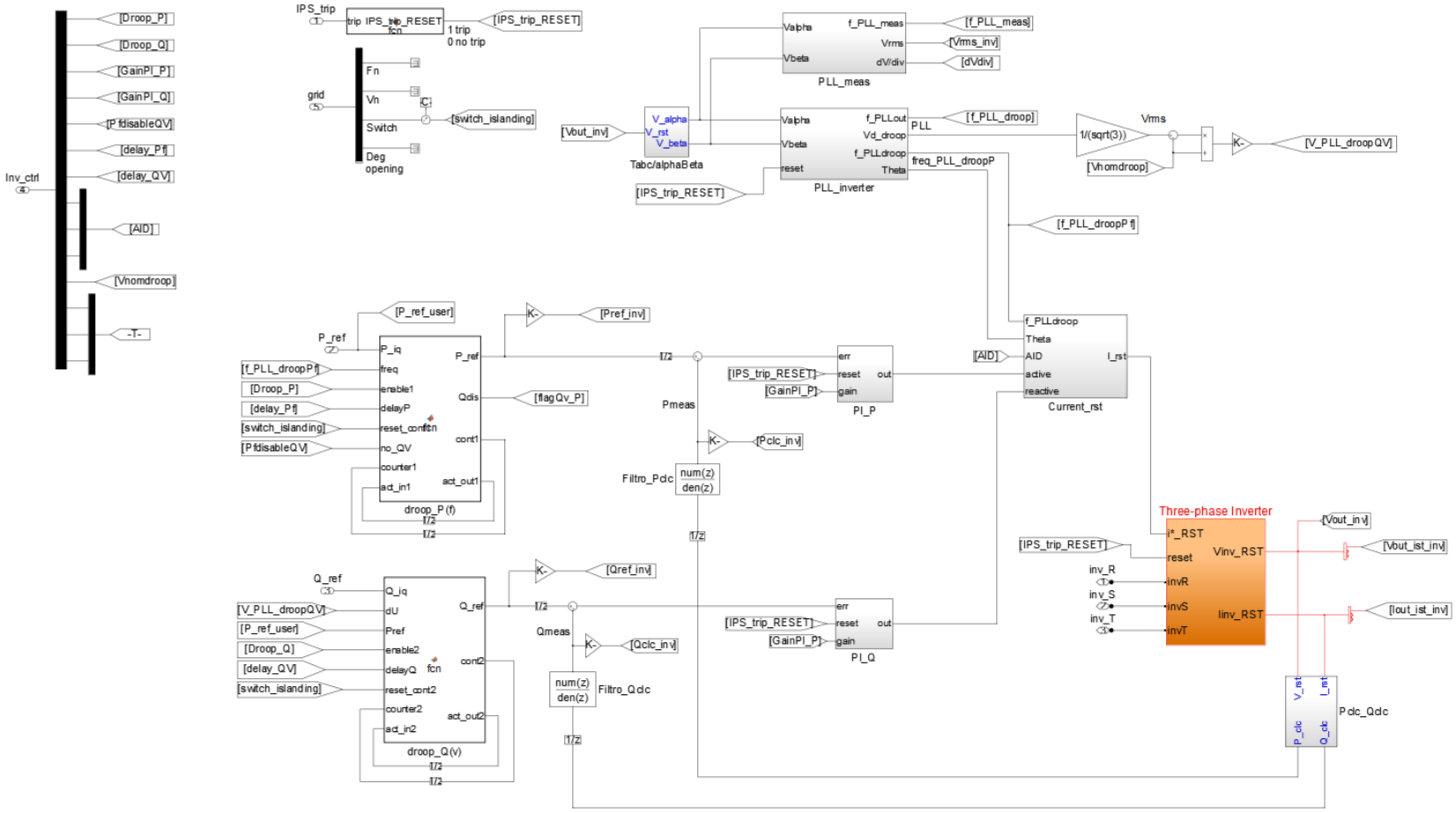

Figure 4.9: Three phase PV inverter - averaging time model implemented in simulink/powersystem blockset.

The inverter control model has been implemented with the possibility to change the active and reactive power regulation loop bandwidth. Fig. 4.9 shows the active and reactive power regulator, which lead to the current reference values for the inner current loop in Fig. 4.8. The regulator comprises PI blocks with the possibility to change the bandwidth of the power closed-loops. Hence, the role of the power speed response has been analyzed during unintentional islanding operations.

Finally, the block diagram $Current_{rst}$ elaborates the current reference values using the PLL system to synchronize to the measured voltage and to generate the required active and reactive power. The $Current_{rst}$ block is designed with the possibility to activate the active anti-islanding (AI) method called SFS (Sandia frequency shift), as shown in Fig. 4.10.

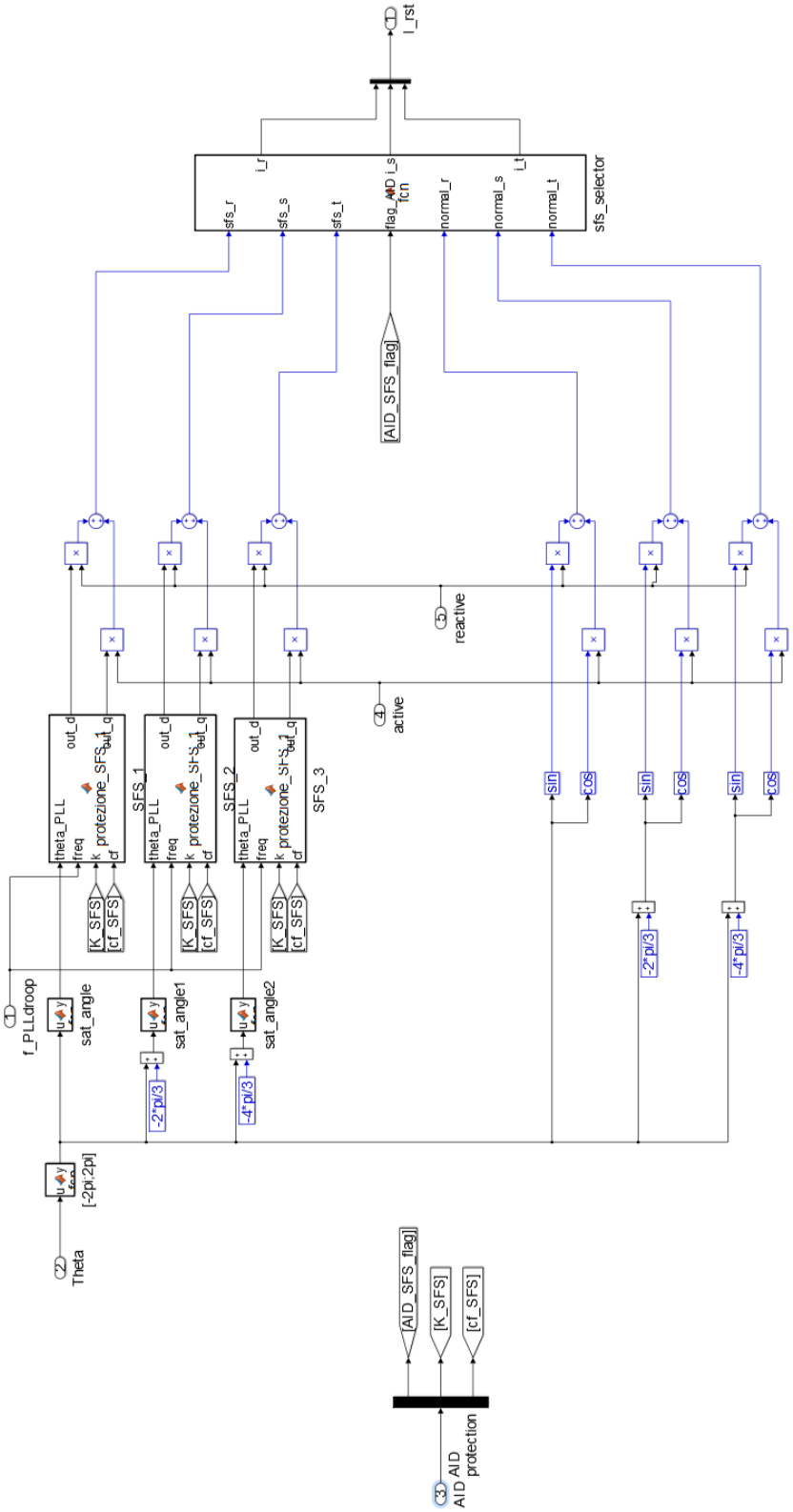

Figure 4.10: Three phase PV inverter - averaging time model voltage sources

This active anti islanding protection injects a slightly distorted current. The implementation of this methods is described in chapter 9.

Chapter 5

Hardware in the loop and Experimental setups validation

This chapter describes the two setups adopted for the validation of the unintentional islanding analysis. The study-case scenario, selected for islanding operation investigations, is depicted in Fig. 5.1, where a three-phase PV inverter, at the point of common coupling (PCC), is connected in parallel to a local load and to the main grid, which can be disconnected by the switching of the utility breaker. The first setup is experimental and it is implemented in a lab-scale prototype, where the control algorithms of the PV inverter are implemented in a 15 kVA UPS, whereas, the hardware in the loop (HIL) configuration is used as second setup. The HIL setup, which is much more flexible than the experimental hardware one, allows the test of islanding operations in complex scenarios as the multiple inverter case. In this work, the HIL simulations permitted to interface the simulated study-case, shown in Fig. 5.1, with a physical interface protection system (IPS) of the type required by the Italian standard [57].

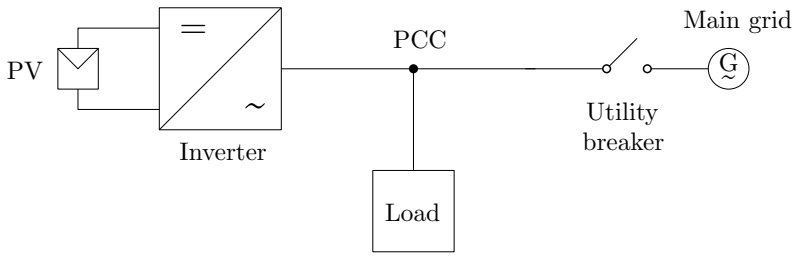

Figure 5.1: Study-case scenario. Single-phase equivalent representation of a three-phase PV inverter connected in parallel to a local load and the main grid at the point of common coupling (PCC).

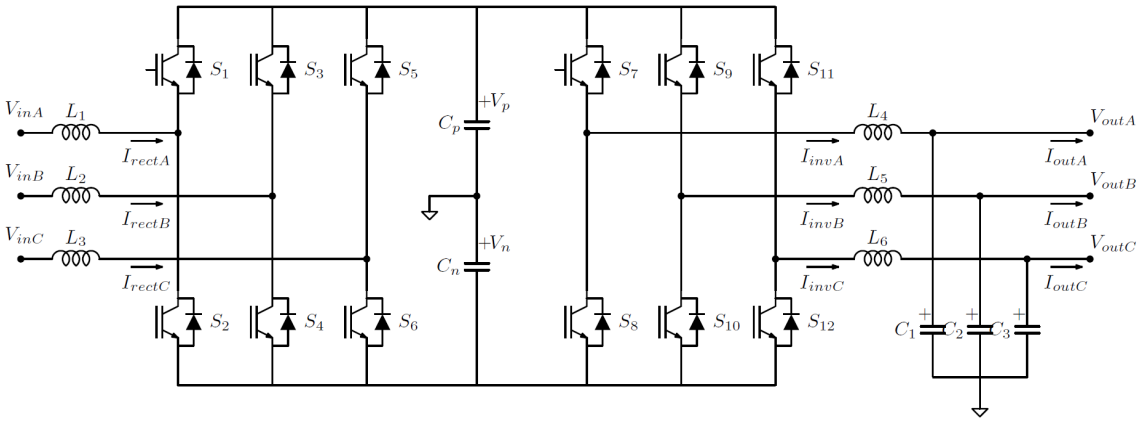

Figure 5.2: UPS used for the experimental setup of unintentional islanding operations.

5.1 Experimental Setup

As shown in Fig 5.2, a three phase experimental setup has been implemented. This system is a double conversion UPS, i.e the grid voltage ($V_{inA,B,C}$) is first rectified to DC bus (650 V) and an inverter supplies the desired amplitude and frequency of the voltage waveform. All the control is performed by a micro-controlled interfaced digital signal processor (DSP), which can be programmed in order to obtain the desired operation at the switching frequency of 12.5 kHz.

For the experimental setup an external rectifier has been implemented to supply directly the DC bus with the rectified utility voltage. Than, the UPS rectifier has been programed as *PV inverter* with the DC source representing the DC voltage of the emulated solar panels, while the UPS inverter AC voltage source acts as *Emulated Grid*. Thus with the UPS it is possible to have both the distributed energy resource (DER) unit and the main grid for unintentional islanding operations. The load has been connected in parallel with the *PV inverter* an the *Emulated Grid*, and a switch has been inserted to disconnect the *Emulated Grid* from the islanded portion and Load.

The single-phase equivalent diagram of the three-phase experimental setup is reported in Fig. 5.3. The *Emulated Grid* plays the role of distribution grid and is controlled as voltage generator with a voltage loop bandwidth of 500 Hz. The *PV Inverter*, as DER unit, is controlled with a current loop bandwidth of about 2.7 kHz on the inductor current of L_1. A Synchronous Rotating Frame (SRF) PLL has been used to synchronize the current controller of the inverter to the grid voltage and to get the frequency and amplitude measures for the P/f and Q/V droop functions. The PLL bandwidth of *PV Inverter* is about 5 Hz. The PV inverter is equipped with closed loop controllers to ensure that the active and reactive power references are properly tracked, and these closed-loops are designed in order to change the bandwidths and select the desired active and reactive power

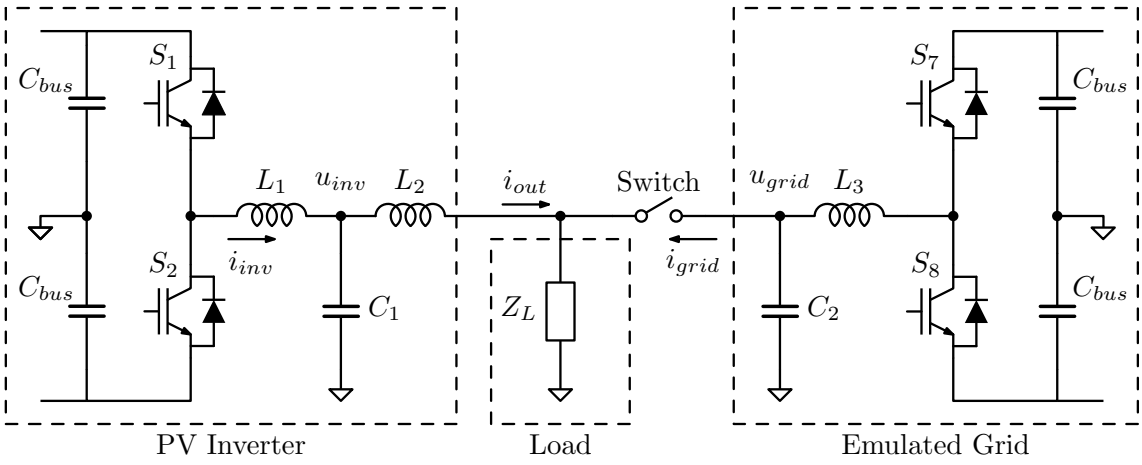

Figure 5.3: Single-phase equivalent diagram of the experimental setup.

settling. The detailed *PV Inverter* model implementation is the same of the simulation model and it is described in chapter 4.

The nominal phase voltage is $230\,\mathrm{V_{rms}}$ and the nominal power is $15\,\mathrm{kVA}$, although the test, reported below, has been performed using $V_b = 151\,\mathrm{V_{rms}}$ and $I_b = 12\,\mathrm{A_{rms}}$ as the base quantity to evaluate the per-unit values. Since the current control of *PV Inverter* is performed on L_1 current, C_1 can be considered as part of the Z_L that consists of a set of passive components: it is a parallel connection of a resistor $R_{L1} = 18\Omega$, an inductor $L_{L1} = 87.5mH$, a capacitor $C_{L1} = 14.4\mu F$ and a resistive-capacitive series ($R_{L2} = 82.5\Omega$ and $C_{L2} = 60\mu F$). Due to its low value the $L_2 = 1600\mu H$ has been neglected in the analytical analysis of islanding events.

In Fig. 5.4 the lab-scale prototype for unintentional islanding is represented . This experimental setup comprises the rectifier, the supply, the DC bus of the two three-phase inverters of the UPS and the elements that compose the load in parallel with the two inverter. A manual switch has been positioned to disconnect the *Emulated Grid* inverter from the islanded system.

5.2 Hardware in the Loop Simulations

The hardware-in-the-loop (HIL) process has been in use for no more than 15 to 20 years. Its roots are found in the Aviation industry. The reason the use of an HIL process is becoming more prevalent in all industries is driven by two major factors: time to market and complexity. HIL simulation is a technique that is used in the development and test of complex systems. The definition for HIL simulator is a setup that emulates a system by connecting in real-time physical subsystems with a simulated mathematical representation of the remaining subsystems. Hardware-in-the-loop is a form of real-time simulation,

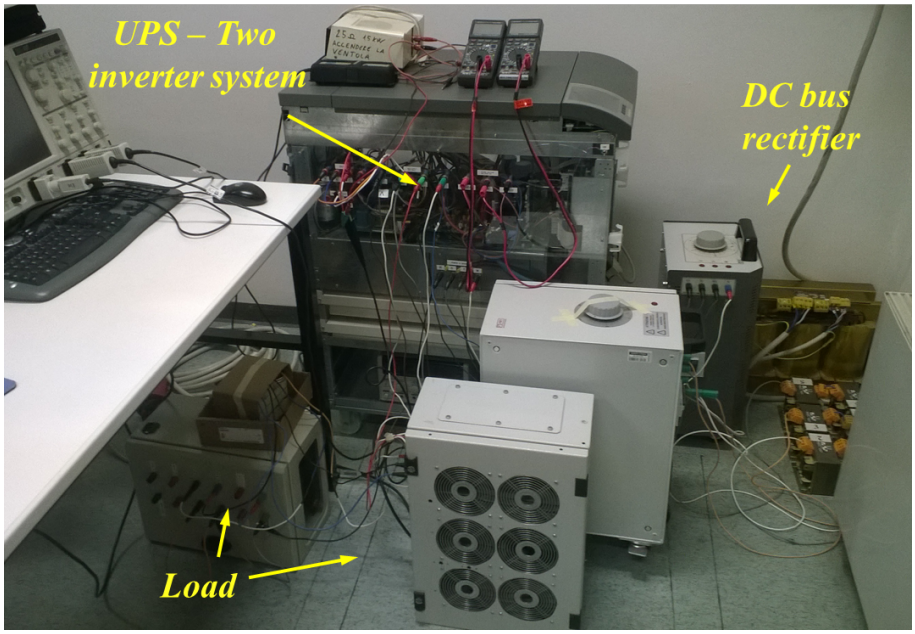

Figure 5.4: Experimental laboratory setup

but differs by the addition of physical components in the closed-loop, using bidirectional interactions between the physical and simulated subsystems. HIL simulation represents an efficient approach to the development, testing and validation of prototypes under investigation. The HIL introduction in the engineering processes enables to limit the cost of testing or developing equipments or prototypes, to have more flexibility in reproducing a variety of testing conditions and to guarantee the safety depending on the applications. Furthermore, HIL provides the efficient control and safe environment where test or application engineer can focus on the functionality of the controller.

In recent years, HIL simulation for power systems has been used for verifying the stability, operation, and fault tolerance of large-scale electrical grids. Current-generation real-time processing platforms have the capability to model large-scale power systems in real-time. This includes complex systems with associated generators, loads, power factor correction devices, and network interconnections and many other devices, which are present in the power electric system. These platforms enable the evaluation and testing of large scale power systems in realistic emulated environments. Moreover, HIL for power systems has been used for studying next-generation SCADA systems and power management units, and static synchronous compensator devices.

5.2.1 Hardware in the Loop Setup Implementation

HIL is used to investigate the integration of distributed energy resources in the distribution electric network. Most of low-power DER units use power electronic converters, which increase the complexity of the network management and operation for the distribution system operator (DSO) [17]. Many literature studies addressed the topic of DERs integration in the existing power system, focusing on different aspects (e.g. control strategies, converter technology, protection systems, etc.). However, none of them have investigated the effect the physical IPS operations and the DER control operations during unintentional islanded conditions. For such purpose, a specific HIL test bed is proposed in this work, where the DER is modeled with a real-time simulator that drives, through a signal amplifier, the physical IPS.

In detail, the HIL setup is composed by the real time simulator OP4500 by OPAL-RT and the signal amplifier in order to interface signals from simulations with the external commercial IPS, which by monitoring the simulated voltage at the PCC can disconnect the DER, if required. Fig. 5.5 presents the HIL setup, where the study-case of PV inverter (with the embedded control algorithms), the local load and the main grid are simulated in real-time by the OP4500.

Such platform enables a more comprehensive understanding of the physical operation and interaction of the IPS with the DER control action during unintentional islanding operations, especially in terms of P/f and Q/V droop functions. The proposed HIL setup is suitable to address the effects of different inverter control actions or of different network configurations. As in any HIL test-bench, it is very easy to modify parameters or to simulate more complex test cases without the need to change the experimental hardware configuration.

The model has been developed in the real-time simulator using Matlab/Simulink environment, including DER inverter-interfaced, local passive load and the main grid with embedded voltage control. The main grid is disconnected by controlling the switch/recloser in order to start the islanding events. The model of a typical PV unit DER is implemented with active and reactive power loops control, droop regulating function and embedded PLL synchronization system.

The configuration of the inverter model is described in chapter 4. In detail, the model has been implemented as the average model of a three-phase inverter, with its inner current closed-loop and the external power closed-loop in order to generate the required active and reactive power using constant $P_{G,ref}$ and $Q_{G,ref}$ reference values or calculated by the regulating droop functions P/f and Q/V. Furthermore, the control uses the synchronous frame reference (SFR) phase locked-loop (PLL) to ensure the synchronization and con-

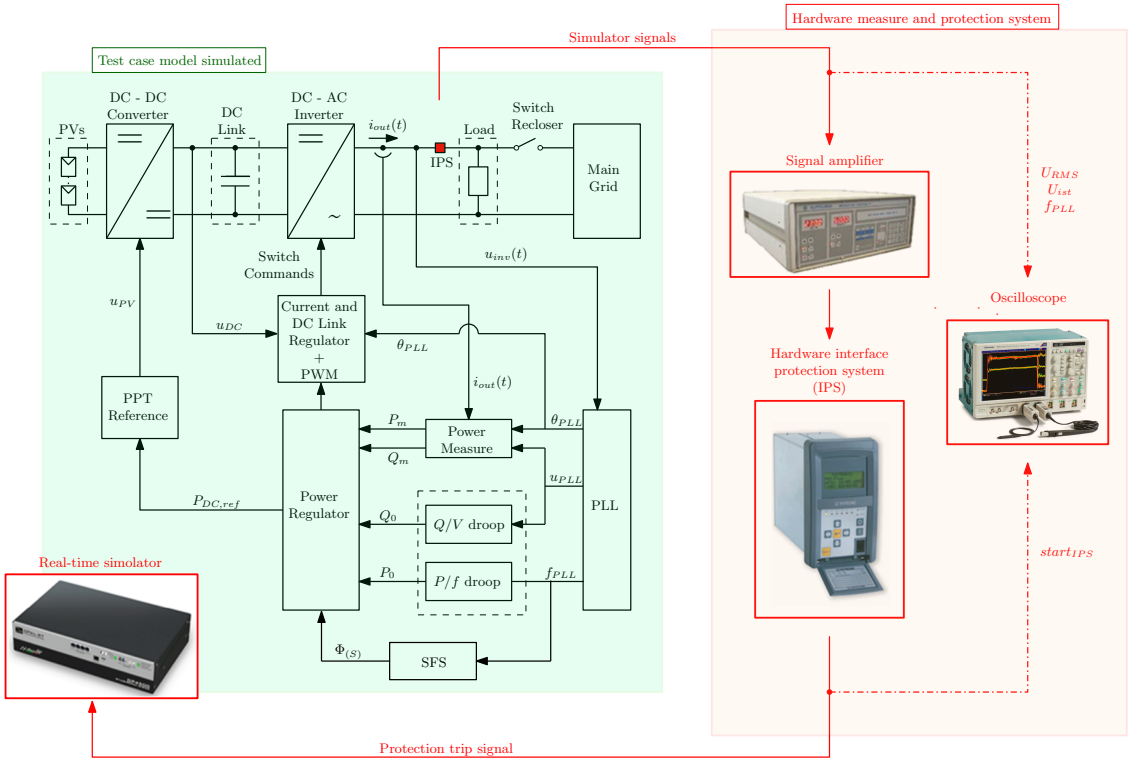

Figure 5.5: Single phase equivalent of the HIL setup implemented to analyze the real IPS during unintentional islanding operations.

nection with the grid voltage.

This specific inverter configuration is implemented for discrete-time simulations with fixed time step $T_{sim} = 20\mu s$, imposed by the real-time simulator as the minimum step size in order to prevent errors during simulations. Therefore, the control loops of the inverter could not have the same dynamic of the simulated electric components such as inductances, capacitors and resistances. Thus, a factor of ten has been introduced in the control dynamic, i.e. $T_{control} = 10 \cdot T_{sim}$. While the experimental setup switching frequency is 12.5 kHz (80 μs), the inverter model control is simulated at 5 kHz (200 μs). This means that the dynamic behavior of the two systems may differ at high frequency, but they present the same response at low frequency (under 1 kHz). Typical unintentional islanding events present dynamic behavior near the nominal grid frequency ($\pm$10 Hz), where simulation model and experimental setup have the same dynamics.

Hence, it is worth mentioning that the inverter models have been validated comparing to lab-scale setup, using the same configuration and control schemes implemented in the experimental inverter digital signal processor (DSP) described in [26, 27, 29]. This validation has been established comparing the islanding transients after the disconnection of the main grid, as shown in Fig.5.6. The tests are performed with a power unbalance of

$\Delta P = 0.9$ and $\Delta Q = -0.2$, with different settling time for the power regulating droop functions:

- *Case I*: constant $P_{G,ref}$ and $Q_{G,ref}$;
- *Case II*: $\tau_P = 5s$, $\tau_Q = 7.5s$;
- *Case III*: $\tau_P = 2s$, $\tau_Q = 3.5s$;
- *Case IV*: $\tau_P = 0.6s$, $\tau_Q = 1.4s$.

Fig. 5.6 shows how the dynamic of the inverter model of HIL simulations is the same of the experimental setup. It may also be noticed in Fig. 5.6g and 5.6h that the HIL model has the same transient behavior of the hardware setup, due mainly to the selected settling time which creates oscillations in the droop controls.

Once the model has been properly and accurately tuned, the analysis of different situations and conditions of the system is more flexible with respect to real full power test beds. Results of the presented study show many dynamic phenomena of the system, ranging from the increase of uncontrolled islanding probability, to different behaviors of inter-operating system components (protection, inverters controls, etc.), such as the speed response of the inverter power regulation. Therefore, it would be of paramount importance to predict the behavior of IPS, P/f and Q/V functions and even the presence of active anti-islanding protection implemented in the DER inverter and, in general terms, to enable the DSO to predict how the large diffusion of DERs in the distribution grids would affect the unintentional islanding and other transient phenomena.

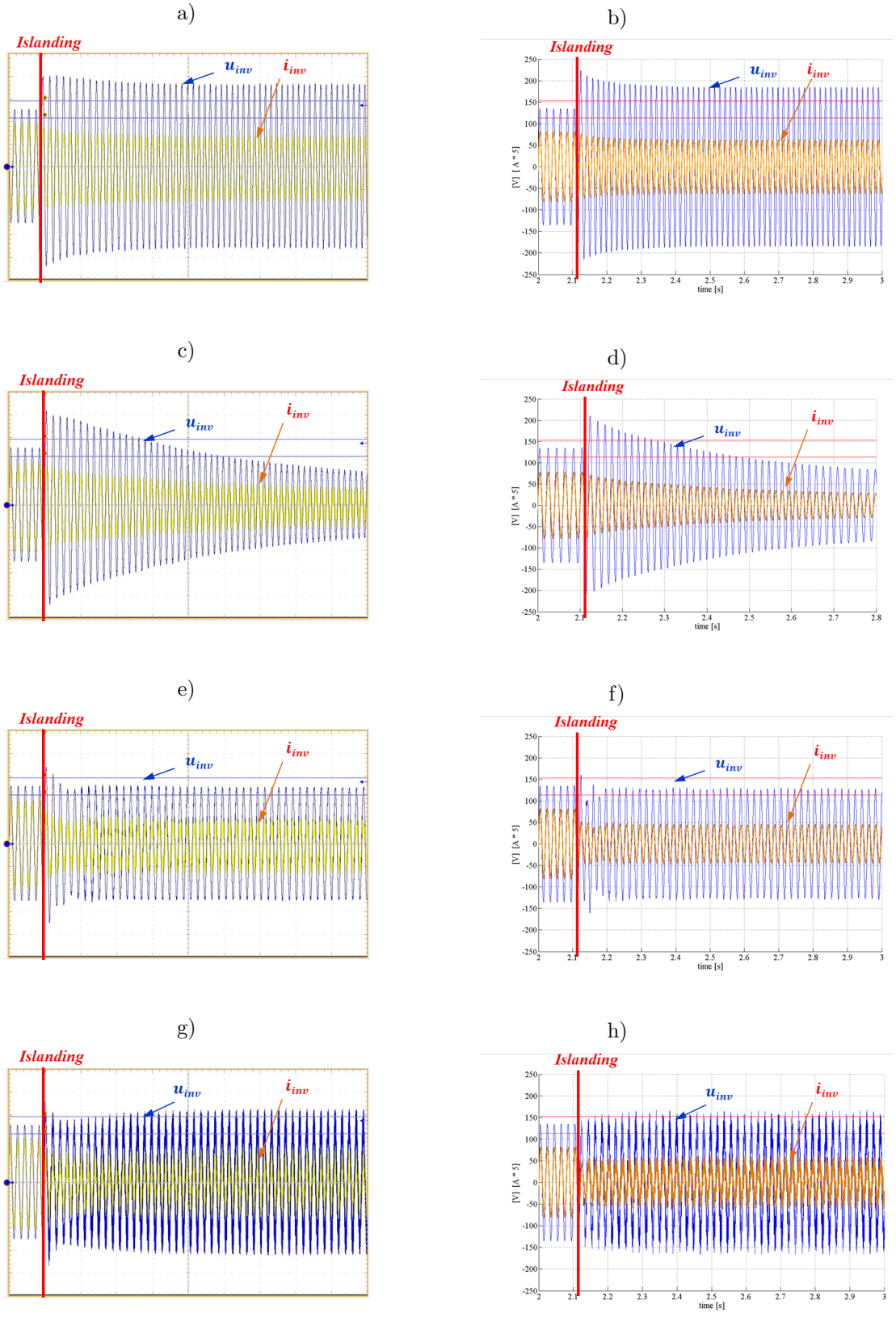

Figure 5.6: Results of $\Delta P = 0.9$ and $\Delta Q = -0.2$ unintentional islanding: a) experimental (constant $P_{G,ref}$ and $Q_{G,ref}$), b) HIL (constant $P_{G,ref}$ and $Q_{G,ref}$), c) experimental ($\tau_P = 5s$, $\tau_Q = 7.5s$), d) HIL ($\tau_P = 5s$, $\tau_Q = 7.5s$), c) experimental ($\tau_P = 2s$, $\tau_Q = 3.5s$), d) HIL ($\tau_P = 2s$, $\tau_Q = 3.5s$), g) experimental ($\tau_P = 0.6s$, $\tau_Q = 1.4s$), h) HIL ($\tau_P = 0.6s$, $\tau_Q = 1.4s$)

Chapter 6

Unintentional Islanding Non Detection Zone

6.1 Introduction

The diffusion of renewable energy resources (RESs), such as photovoltaic and wind energy sources, is continuously increasing and changing the structure and operations of the medium and low voltage (MV and LV) distribution networks. Residential environments have experienced one of the most relevant growth of distributed-generation power systems [13–15, 78]. Most of low-power DERs units consist of power electronic converters with limited number of sensors and communication capabilities [16], increasing the complexity of the network management and operations for the distribution system operator (DSO) [17]. The proliferation of such systems has led to an increasing concern about the problem of unintentional islanding on distribution networks. The islanding condition is defined as a portion of the utility system containing both loads and DER units that remains energized while it is isolated from the main grid. The analysis of unintentional islanding has been addressed in several literature studies, such as [24, 26, 27, 44, 79], and interesting studies on the determination of non detection zone (NDZ) can be found in [80–83].

This complex scenario has also influenced the latest grid codes and country-level requirements for DER units [19, 20]. At this time, no universal standard for anti-islanding (AI) requirement has been adopted. Over the years several different AI algorithms have been proposed and they can be classified in passive and active methods [42]. Passive methods verify grid parameters at DER point of common coupling (PCC), such as over/under voltage (OUV) and over/under frequency (OUF) [43], detection of the voltage/current harmonics [21, 44] and phase variations [16]. Anti-islanding techniques for inverter have been proposed so far for DER applications and surveys are given for instance by [21, 36, 37, 84]. However, when there is a large number of DERs, the behavior of such provisions, being

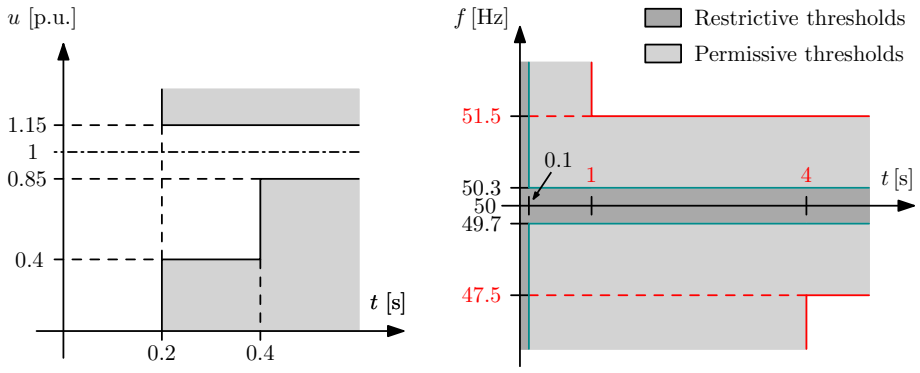

Figure 6.1: Voltage and frequency thresholds imposed by the standard for inverter based DER.

different from each manufacturer and not specified by standards, is unpredictable and in some cases these techniques can lack to detect the operation mode and so the disconnection of the inverter may not happen [24,29]. Grid-connected DER systems are required by standards and technical rules to adopt OUV and OUF protections which disconnect the DER system from the utility when the magnitude or frequency at the point of common coupling (PCC) is out of the prescribed limits [57,58]. This protection system is used to protect the electric equipments but also has the role of passive islanding detection method. Therefore, this analysis is focused on passive AI methods OUV and OUF, since active AI methods present a set of fundamental drawbacks to be used for a general analysis: they are not regulated by standards, they are different from each manufacturer, the different perturbations, each inverter is generating, tend to be compensated each other in a large distribution network and, last but not least, they are not mandatory in all countries. The OUV and OUF are implemented in the interface protection system (IPS) presented in Fig. 6.1 [57].

New European standards state the reference technical rules for the connection of active users to the grid and for their behavior during temporary voltage and frequency variations [19,20,59]. Moreover, these standards together with some country-level ones are imposing the participation of DERs to the voltage and frequency regulation to improve the system stability, through the $P/f$and Q/V droop characteristics (Fig. 6.2) [57]. One of the most relevant modification are the extension of the frequency range that is allowed during normal operation of DERs from the traditional thresholds 49.7 Hz and 50.3 Hz to the less stringent values 47.5 Hz and 51.5 Hz, and the extension of the voltage levels to 15% of the rated voltage (Fig. 6.1).

This work focuses on the risk of permanent islanding operation [26,27,31], that is the risk of an unintentional islanding whose steady-state frequency and voltage remain within the allowed thresholds, for instance those reported in Fig. 6.1.

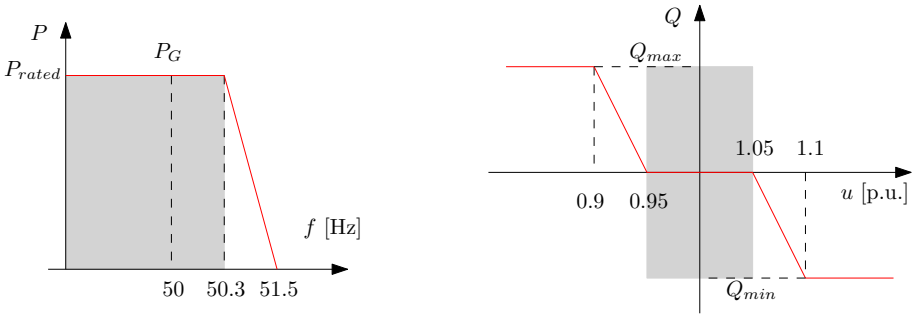

(a) Active power regulation P/f (b) Reactive power regulation Q/V

Figure 6.2: Active and reactive power regulations stated by standards. These droop regulating actions modify the active power in (a) and reactive power in (b) of the inverter output set-point due to local frequency and voltage amplitude measurements.

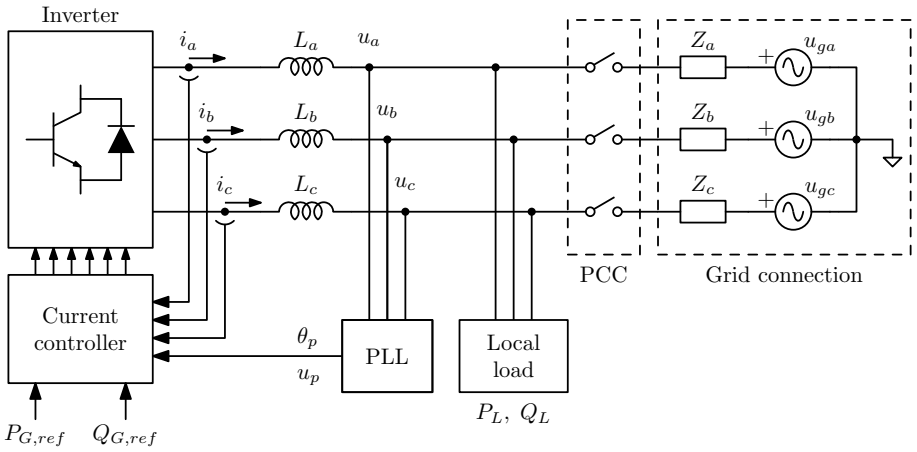

Figure 6.3: Considered scenario of a DER inverter connected in parallel with a local load in the low voltage distribution network.

6.2 System Description and Area of Uncontrolled Islanding

The goal is to analyze the DER unintentional islanding risks in the case of the supporting functions P/f and Q/V are activated. In particular, it is addressed the mapping of the IPS NDZ considering the individual contribution of the P/f and Q/V droop regulations, first enabling only one of them, either P/f or Q/V, and then both. In order to simplify the analysis, the test-case shown in Fig. 6.3 has been adopted, where a low voltage PV three-phase inverter and a local load are considered.

Regarding the active and reactive generated power references P_G, ref and Q_G, ref of the DER, four Cases are considered:

- *Case I* of a DER with constant active and reactive power references;
- *Case II* of a DER with only Q/V droop characteristic as in Fig. 6.2;
- *Case III* of a DER with only P/f droop characteristic as in Fig. 6.2;

- *Case IV* of a DER with both Q/V and P/f droop characteristics as in Fig. 6.2,

where Cases II and III are usually not considered in the literature.

After the transition from grid-connected to islanded operation, the active and reactive powers P_G and Q_G generated by the inverter have to balance the ones absorbed by the load P_L and Q_L, i.e.

$$\begin{cases} P_L(f,u) = P_G(f) \\ Q_L(f,u) = Q_G(u). \end{cases} \tag{6.1}$$

Here in general, P_L and Q_L are functions of the frequency f and the voltage amplitude u, while P_G is a function of the frequency f and Q_G is a function of the voltage amplitude u, considering the droop characteristics 6.2. Notice that this choice is general and it can be done also for the case of an inverter with constant power references. After the disconnection, the power balancing between generation and local load leads to a new steady-state solution (f^*, u^+) for the system. If f^* and u^* do not trigger the DER protections, for instance those in Fig. 6.1, then an unintentional islanding is possible [25]. Here, the permissive allowed ranges are considered

$$\begin{array}{rcccl} u & \in & [u_{min}, u_{max}] & = & [0.85, 1.15] \quad \text{p.u.} \\ f & \in & [f_{min}, f_{max}] & = & [47.5, 51.5] \quad \text{Hz} \end{array} \tag{6.2}$$

Taking into account the variability of the power source and the load components in terms of grid-connected active and reactive powers, a set of solutions is found that defines the non detection zone (NDZ), i.e. an area representing the power mismatch $\Delta P = P_G(f_0) - P_L(f_0, u_0)$ versus $\Delta Q = Q_G(u_0) - Q_L(f_0, u_0)$ at the PCC, where the islanding condition is possible, where f_0 and u_0 are respectively the nominal frequency and nominal voltage amplitude. If, for a certain ($\Delta P^*, \Delta Q^*$), the corresponding steady-state solution (f^*, u^*) is within the voltage and frequency thresholds and if such operating point is stable, then a permanent islanding operation can be maintained, in other words ($\Delta P^*, \Delta Q^*$) points belongs to the NDZ. The frequency and voltage thresholds of (6.2) identify a rectangular area on the plane of allowed deviation of voltage amplitude $\Delta u = u - u_0$ versus deviation of frequency $|Deltaf = f - f_0$. The borders of this region is given by

$$\begin{aligned} \Delta u_{min} &= u_{min} - u_0, \\ \Delta u_{max} &= u_{max} - u_0, \\ \Delta f_{min} &= f_{min} - f_0, \\ \Delta f_{max} &= f_{max} - f_0, \end{aligned} \tag{6.3}$$

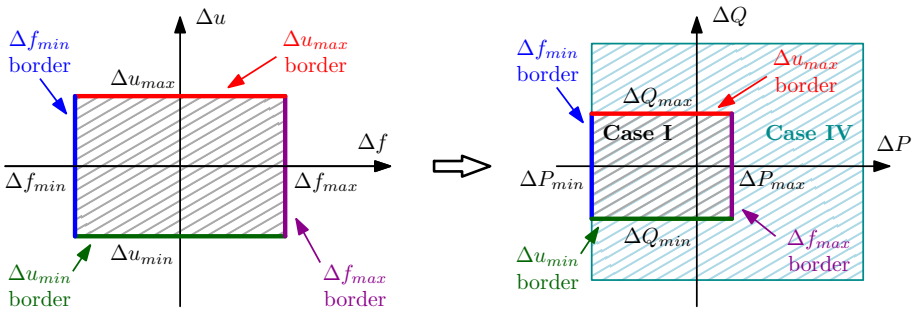

Figure 6.4: Mapping of the Δf_{max}, Δf_{min}, Δu_{max} and Δu_{min} borders from $\Delta f - \Delta u$ plane to $\Delta P - \Delta Q$ plane.

and they are mapped on the $\Delta f - \Delta u$ plane to the $\Delta P - \Delta Q$ plane. In this reference frame, other four borders are identified and thus the NDZ of unintentional islanding, as shown schematically in Fig. 6.4.

It is possible to draw the NDZ regions (for each different Case), considering the load power dependencies $P_L(f, u)$ and $Q_L(f, u)$, with the following procedure:

1. the load power point P_L^* and Q_L^* is evaluated for a precise point (f^*, u^*) on the $\Delta f - \Delta u$ border;

2. then, because in islanded operation P_L^* and Q_L^* must be equal to the inverter active and reactive powers, P_G^* and Q_G^*, for (f^*, u^*), knowing the particular case and the droop characteristics of the inverter, the active and reactive powers $P_G(f_0)$ and $Q_G(u_0)$ in grid-connected mode can be calculated;

3. the $(\Delta P, \Delta Q)$ point on the NDZ border (Fig. 6.4) are derived from the grid-connected powers of the inverter and from those of the load, $P_L(f_0, u_0)$ and $Q_L(f_0, u_0)$, which are known;

4. the previous points are then repeated for all the border in the $\Delta f - \Delta u$ plane of Fig. 6.4.

In this analysis, the grid-connected operating point is (f_0, u_0) regardless the power absorbed or generated by the main grid, meaning that the small voltage drop due to the output impedance of the grid is neglected.

This analysis is general and it can be applied for a generic local load, whose active and reactive power dependencies are known, $P_L(f, u)$ and $Q_L(f, u)$. For instance, it can be used with standard modeling choices of loads, as residential, agricultural and industrial described in [47]. In this work, it has been considered a local load that consists of a set of passive components, as shown in Fig. 6.5 : it is a parallel connection of a resistor R_1, an inductor L_1, a capacitor C_1 and a resistive-capacitive series (R_2 and C_2), whose values

Table 6.1: Load parameters: base power is the active load power at (f_0, u_0).

R_1	=	17	=	0.873 p.u.
R_2	=	82.5	=	0.180 p.u.
L_1	=	87.5 mH	=	0.551 p.u.
C_1	=	14.4 μF	=	0.067 p.u.
C_2	=	60 μF	=	0.280 p.u.

are in Tab. 6.1 and whose power dependencies $P_L(f, u)$ and $Q_L(f, u)$ are shown in Fig. 6.6. This choice has been done for the sake of experimental validation and simplicity.

For such load, the NDZ areas, evaluated using the method described before, are reported in Fig. 6.7, where Fig. 6.7a refers to the Case I, while Fig. 6.7.b shows that including the Q/V droop control (Case II) causes a slight widening of the unintentional islanding region. On the other hand, introducing only the P/f droop control (Case III) produces a larger area widening (Fig. 6.7c).

Finally, in Fig. 6.7d for Case IV, the islanding risk is maximum since the region is by far the largest. Notice that introducing the P/f droop originates a potential unbounded area. However, in a real application, this area will be limited by the rated power of the inverter. To quantify the area enlargement, the areas of the regions of Fig. 6.7 limited to

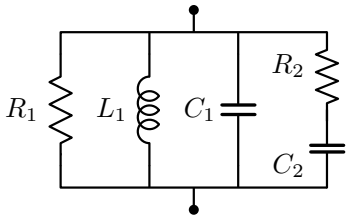

Figure 6.5: Generic local load with active and reactive power dependencies: $P_L(f, u)$ and $Q_L(f, u)$.

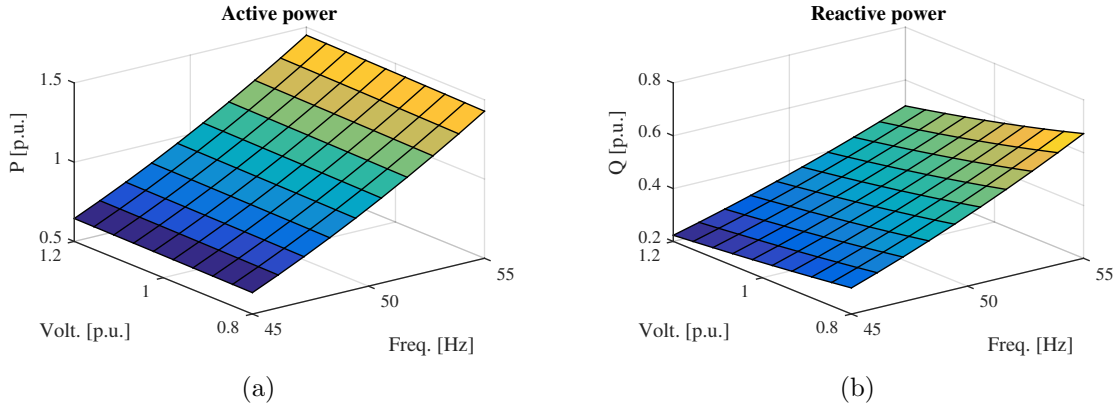

(a) (b)

Figure 6.6: Active P_L and reactive Q_L powers of the load as functions of frequency f and voltage u: powers are normalized to the active power of the load at nominal frequency f_0 and nominal voltage u_0.

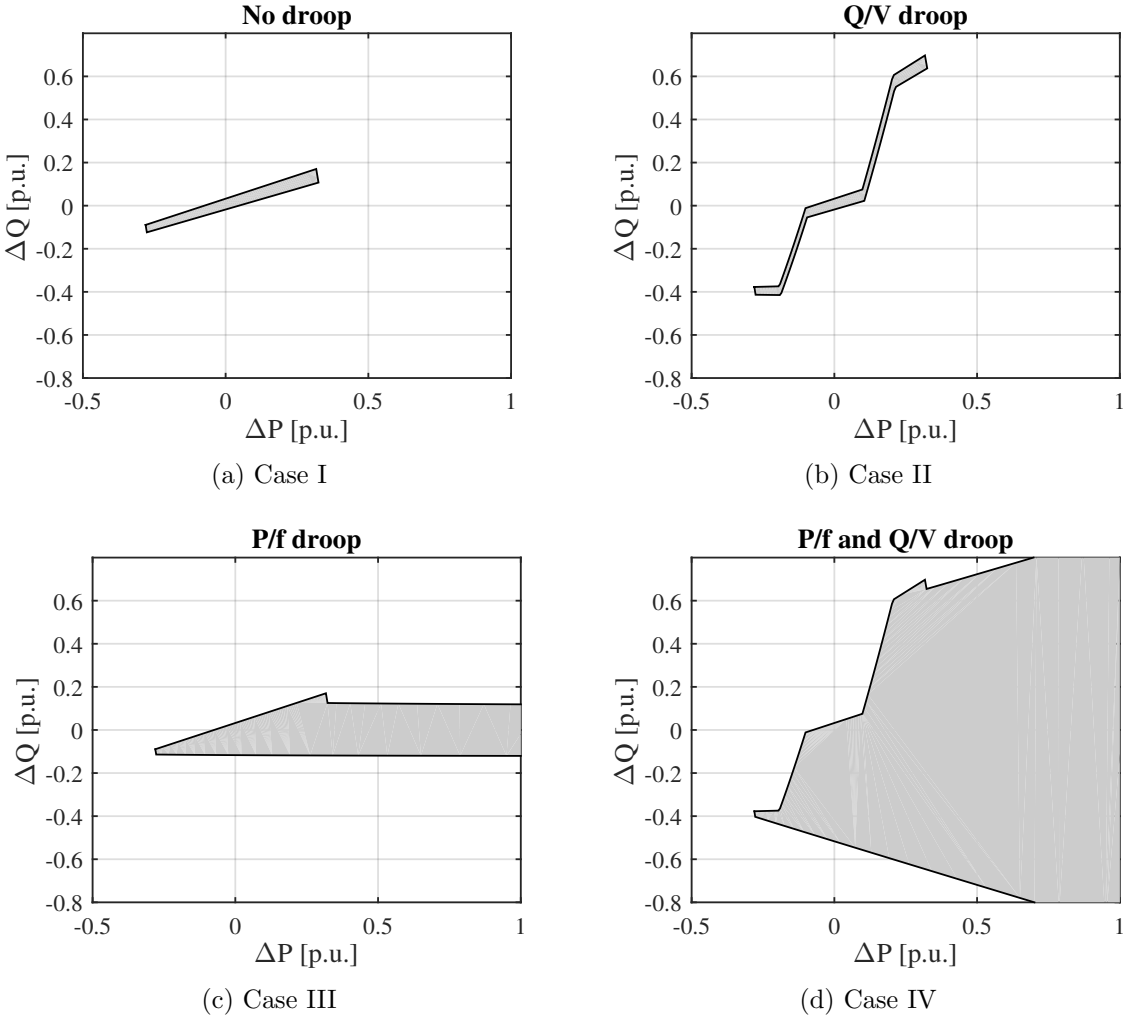

(a) Case I

(b) Case II

(c) Case III

(d) Case IV

Figure 6.7: $\Delta P - \Delta Q$ area of possible permanent unintentional islanding when the inverter operates with droop characteristics: a) no droop, b) only Q/V droop, c) only P/f droop and d) both Q/V and P/f droop.

Table 6.2: Areas of NDZ: values are normalized to the area of Case I.

Case I	1
Case II	1.16
Case III	8.41
Case IV.16	45.9

those axis ranges, that is inside the plane $\Delta P \in [0.5, 1]$ p.u. and $\Delta Q \in [-0.8, 0.8]$ p.u., have been evaluated and reported in Tab. 6.2.

This analysis shows that in the last three cases (II-III-IV), the risk of islanding increases compared to Case I, where the unintentional islanding operation can be formed due to the regulation characteristics of the load, i.e. the dependencies of the active and reactive load powers to the frequency and the amplitude of the voltage. In the other cases the risk is increased due to the droop characteristics of the inverter-interfaced generator.

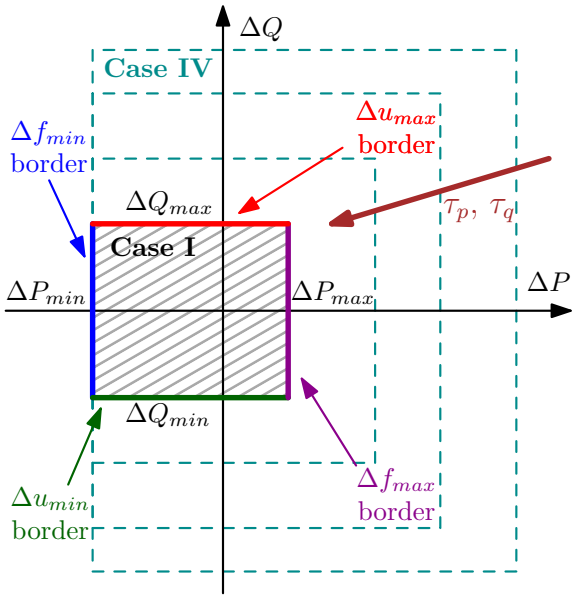

Figure 6.8: Qualitative example of NDZ extension in the plane $\Delta P - \Delta Q$ due to the P/f and Q/V droop characteristics, depending on the embedded inverter power control scheme [27].

The regions of this NDZ analysis refer only to the steady-state solutions of a permanent islanding operation. Further investigation, as reported in Chapter 8, 9 and 10 will describe how the NDZ extension is not only influenced by the load characteristic or the presence of the P/f and Q/V droop regulating functions, but also by speed response of the power regulation implemented in the inverter.

6.2.1 Power Regulation Speed Response in the Single Inverter Case

The investigation on the role of the speed response of the droop functions P/f and Q/V during unintentional islanding is a recent topic, introduced by the latest grid code and standards. Recently, inverter interface DER units are required to perform fast droop regulation functions in order to increase the stability of the electric power system, as recalled in chapter 2.6.

In Fig. 6.8, it is shown a qualitative example on how the speed of the power control plays a fundamental role in the NDZ sizing and in the unintentional islanding issue in general.

In particular, the response time of the closed-loop for active power regulation T_P and reactive power regulation T_Q may increase the size of the NDZ.

As a matter of fact, by increasing the time response of the power regulating functions, the NDZ will be reduced to the Case I, where the active and reactive power generation is constant. Hence, the required fast droop characteristics may play a useful stabilizing

role by quickly responding to the temporary grid perturbations, whereas in this work it is highlighted how they may play a negative role in terms of unintentional islanding events.

The analysis of power regulation speed response influence on the sizing of the NDZ obtained in Fig. 6.7d has been validated via experimental tests.

6.3 Experimental Results

A lab-scale prototype has been implemented in order to perform experimental validations as described in chapter 5. A switch allows the islanding operation by isolating the PV inverter and the passive load Z_L from the main grid. The same load structure described in Section 6.2 is adopted in the experimental setup, where the nominal phase voltage is 182 V_{rms} and the nominal line frequency is $f_0 = 50$ Hz.

A synchronous rotating frame (SRF) PLL has been used to synchronize the current controller of the inverter to the grid voltage and to get the frequency and amplitude measures for the P/f and Q/V droop control. If one of the droop characteristics is disabled, the corresponding power reference will be constant regardless the frequency or the voltage amplitude. The outputs of the PLL together with the output current measure of the inverter are used to evaluate the output active and reactive powers of the inverter: these are feedback variables for the power regulator.

In Fig. 6.10, the test 20 of Fig. 6.9 is considered. It exhibits a frequency value out of the thresholds for the Case II (64.8 Hz in Fig. 6.10a), a voltage close to the minimum voltage threshold $182 \cdot 0.85 = 154.7 V_{rms}$ for Case III (158.7 V_{rms} in Fig. 6.10b) and frequency and voltage values within the thresholds for Case IV (50.59 Hz and 173.5 V_{rms} in Fig. 6.10c).

Experimental results prove the widening of the NDZ in the plane $\Delta P - \Delta Q$ and are reported in Fig. 6.9: in particular Fig. 6.9.a refers to Case II, Fig. 6.9.b to Case III and 6.9.c to Case IV. All the results indicate that the risk of unintentional islanding increases introducing inverter droop control with respect to the case of a constant power inverter and that such risk is higher introducing both P/f and Q/V droop control: there is a extremely good agreement between analytic and experimental results. Moreover, the effect of the P/f droop is stronger in terms of area change than the Q/V droop one. In such results, a stable steady-state is reached, but this does not always happen: for example, Case IV for Test 31 in Fig. 6.11 shows a system behavior that is not perfectly stable and so oscillations on the voltage amplitude appear. However, such instability does not trigger the DER protections and so a permanent islanding operation is still achieved. Another cause that can trigger the DER protections is related to the initial transient just after

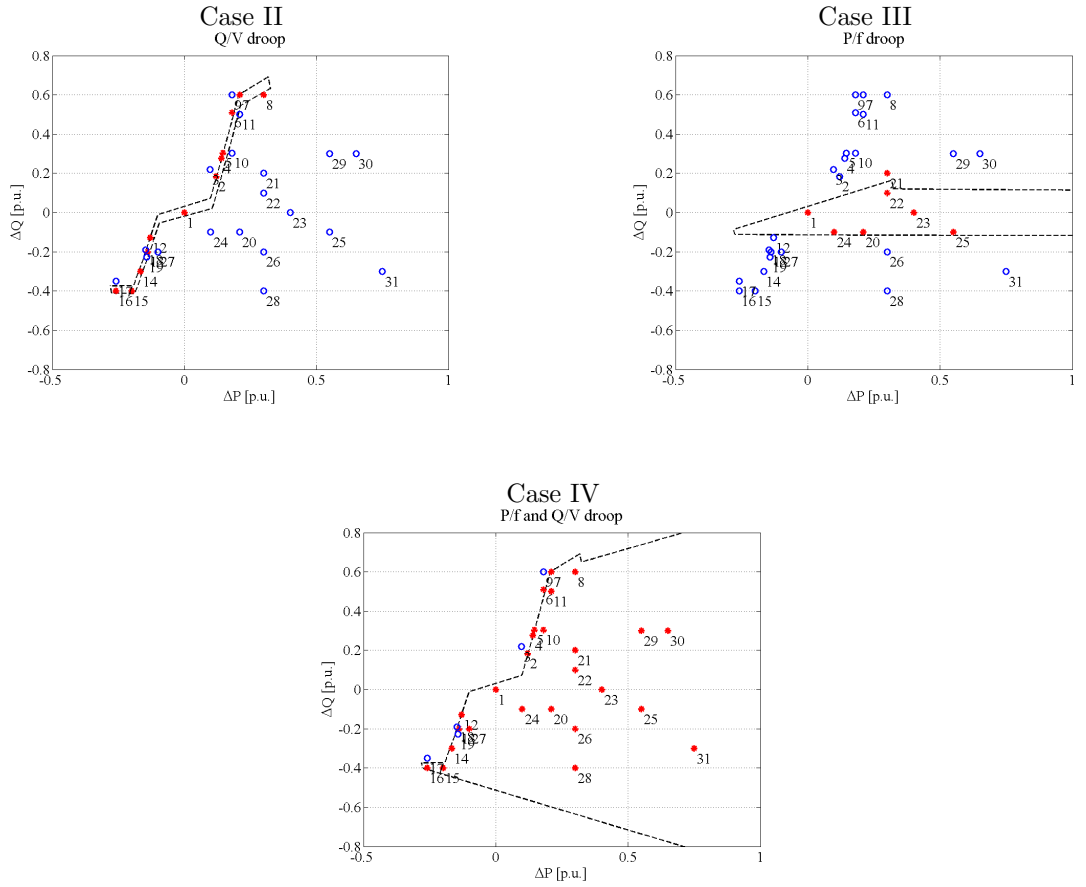

Figure 6.9: Experimental results of$\Delta P - \Delta Q$ area of permanent unintentional islanding: a) Case II, b) Case III and c) Case IV; blue circles refer to an islanding operation out of the protection thresholds, red asterisks refer to an islanding operation within the protection threshold.

the disconnection. During this transient, the frequency and the voltage of the islanded grid can exhibit some oscillations that can bring those quantities out of the protection thresholds. Two examples of such oscillating transients are in Fig. 6.12, however they do not trigger the protections.

The resulting points of unintentional islanding on the plane $\Delta P - \Delta Q$ represent the steady-state islanding conditions. As shown the Fig. 6.9.c the Case IV present the activation of both P/f and Q/V. This condition allows the enlargements of the NDZ, increasing the number of stable steady-state islanding operations. It has been reported that the transient to reach this condition may cause the intervention of the interface protection system and this is mainly due to the speed response of the power regulation.

The experimental results reported in Fig. 6.13 show that with different regulation speed response, it is possible to obtain different results in terms of NDZ. Using a small

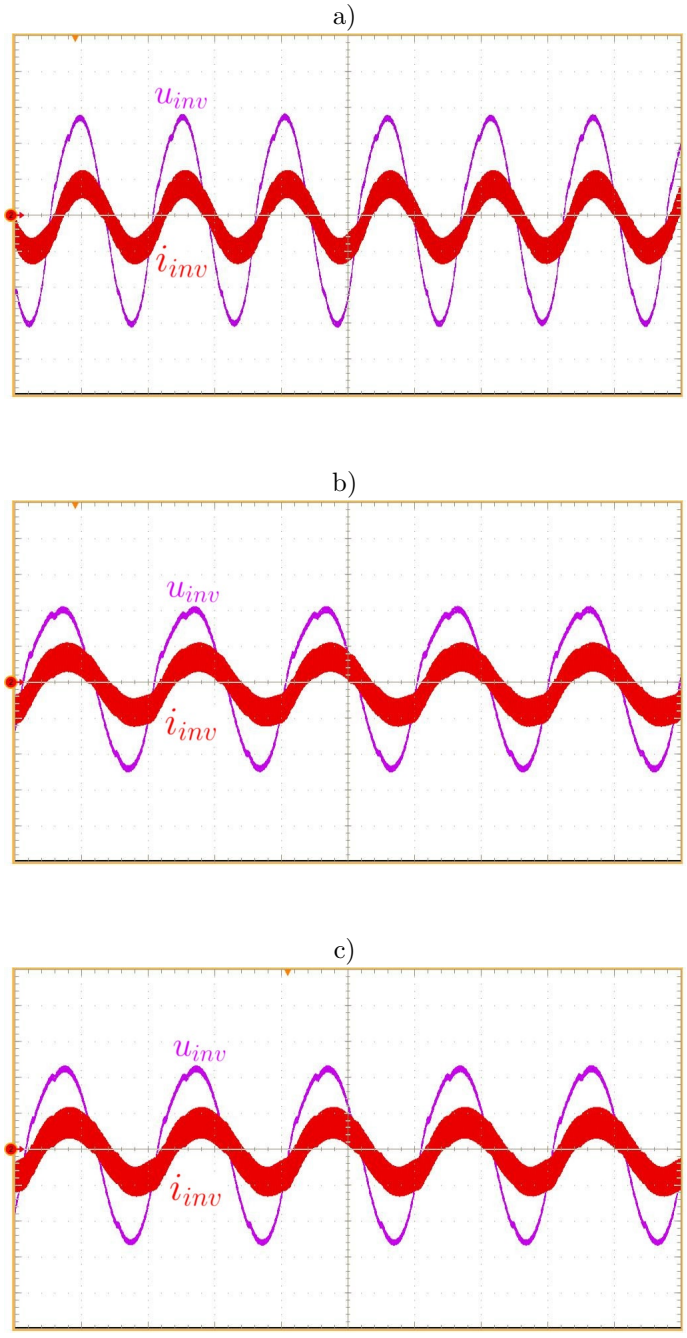

Figure 6.10: Experimental results of inverter output voltage u_{inv} (100 V/div) and current i_{inv} (30 A/div) for Test 20 of Fig. 6.9: a) Case II where the frequency is 64.8 Hz and the voltage 203.6 V_{rms}, b) Case III where the frequency is 50.62 Hz and the voltage 158.7 V_{rms} and c) Case IV where the frequency is 50.59 Hz and the voltage 173.5 V_{rms}; time with 10 ms/div scale.

bandwidth for the power regulation closed-loop the system reacts very slowly to voltage frequency and amplitude variations. Therefore, the equilibrium point is reached with a slow transient, which may be characterized by frequency and voltage values out of the

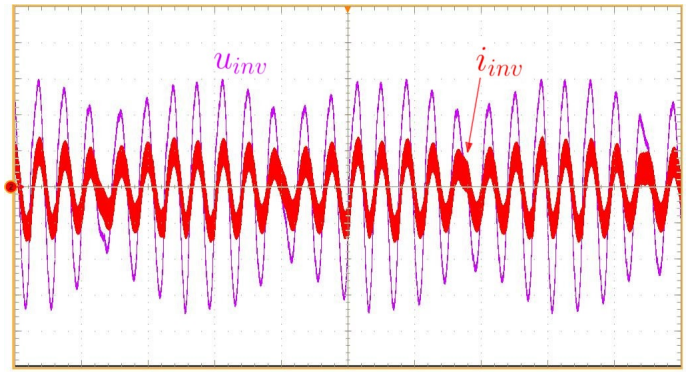

Figure 6.11: Experimental results of inverter output voltage u_{inv} (100 V/div) and current i_{inv} (30 A/div) for Case IV for Test 31 of Fig. 6.9; time with 50 ms/div scale

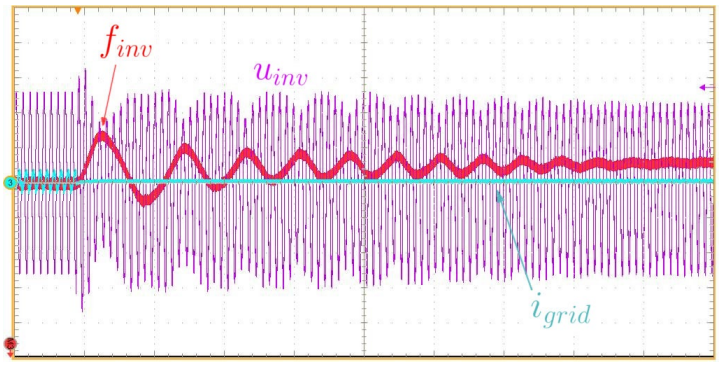

(a)

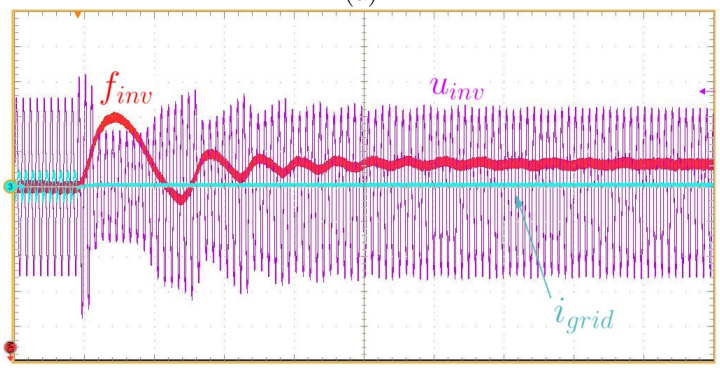

(b)

Figure 6.12: Experimental results of islanding transients a) for Case IV of Test 26 and b) for Case IV of Test 28 of Fig. 6.9: inverter output voltage u_{inv} (100 V/div), its measured frequency f_{inv} (1 Hz=div) and current i_{inv} (30 A/div); time with 200 ms/div scale.

protection thresholds causing the disconnection of the DER and the islanding detection. Fig. 6.13 Case C presents an increased size of the NDZ compared to Fig. 6.13 Case B. This is due to the change of the power control bandwidth: from $\omega_p = \omega_q = 2\pi 4.2\,\text{Hz}$ (Case B) to $\omega_p = \omega_q = 2\pi 5\,\text{Hz}$ (Case C).

Fig. 6.14 compares the islanding transition of the test 5 in Fig. 6.13. It is possible to

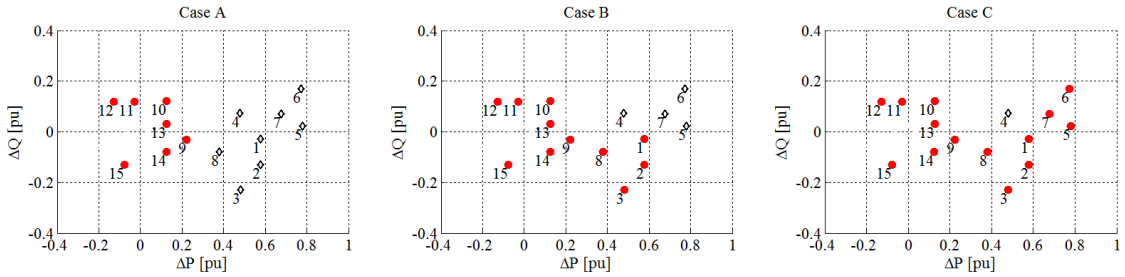

Figure 6.13: Experimental test results are reported in the plane $\Delta P - \Delta Q$ with different response times of the droop characteristics: Case A constant power references, Case B droop regulation with $\omega_p = \omega_q = 2\pi 4.2\,\text{Hz}$ and Case C droop regulation with $\omega_p = \omega_q = 2\pi 5\,\text{Hz}$; red dot tests allow islanding operations, while black diamonds do not

note that using even a small difference on the bandwidth of the power regulation control loop (4.2 Hz and 5 Hz) the transient behavior of the islanding operation is drastically different. Hence, in Fig. 6.14b the islanding conditions leads to an over voltage transient, which will cause the disconnection of the DER system. In this specific configuration, the experimental tests were not equipped with the interface protection system, because of the interest on the transient behavior with different power regulation bandwidths. However as reported in Fig. 6.14b the system voltage exceed the limit of the over voltage relay, while in Fig. 6.14a the faster regulation guarantees a shorter transient, without exceeding the protection thresholds. In Fig. 6.14, it is also reported the automatic re-closure time (600 ms) when the islanded grid should be reconnected to the main grid in presence of an automatic re-closing procedure. In this test case, due to the use of fast droop regulation the DER could not be disconnect before the automatic re-closure with the serious danger of out-of-phase reconnection with the main grid. This topic is presented in chapter 8.

6.4 Conclusions

The proposed investigation shows that the risk of permanent unintentional islanding increases introducing P/f or Q/V droop regulation to the control of DERs and that the $\Delta P - \Delta Q$ area widens more including both the P/f and Q/V droop regulations, rather than only one of them. Thus, the non-simultaneous operation of P/f and Q/V seems to be an effective approach to reduce the NDZ, for example disabling the Q/V function when activated the P/f under over-frequency operation.

In future generation of distribution grid with large penetration of renewable energy sources, the understanding of the stabilizing effects of droop control in islanded operation is of paramount importance in order to provide insights on design criteria for the DER connections and on settings of P/f and Q/V droop functions on future standards. Moreover, the speed of the power regulation plays an important role in the unintentional

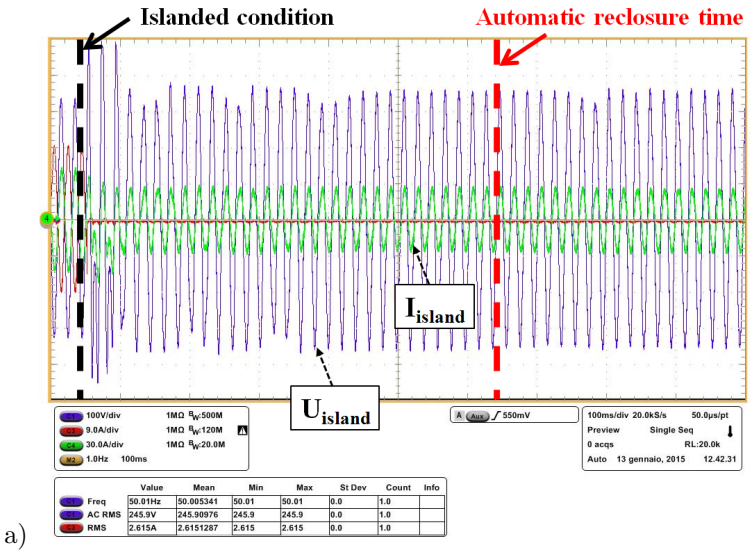

a)

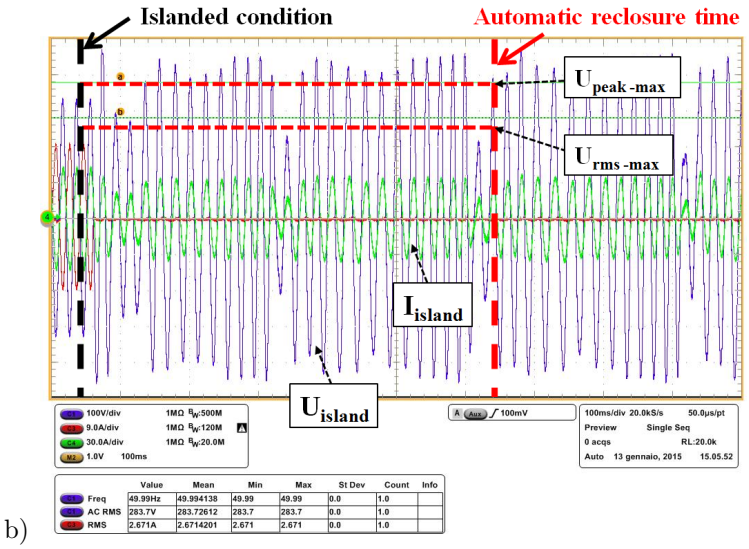

b)

Figure 6.14: Test 5 of Fig. 6.13 for $\Delta P = 0.67$ p.u. and $\Delta Q = 0.07$ p.u.: example of islanded operation: a) droop control with $\omega_p = \omega_q = 2\pi 5$ Hz and b) with $\omega_p = \omega_q = 2\pi 4.2$ Hz (U_{island} - 100 V/div, U_L - 100 V/div, I_{island} - 30 A/div, time - 100 ms/div).

islanding forming and NDZ and show as the criteria of requiring fast DER system has a major drawback in terms of unintentional islanding an so in terms of security of people and electric devices.

All the aspects reported in this analysis may allow the selection of new requirements for the upcoming standard and technical specifications, in order to reduce the risks associated with unintentional islanding events. These results give also the opportunity to the DSO to endorse corrective actions limiting the possible islanding events in order to guarantee the quality of the distribution electric system, as adopting non-simultaneous P/f and Q/V droop regulations and requiring a slow power regulation in order to minimize the NDZ.

Chapter 7

Non Detection Zone with Single Phase PLL Synchronization System

The significant increasing number of generating units connected to the low voltage (LV) level is interesting the residential level, such as single-phase PV sources. The dynamic behavior of distributed generators depends on the embedded control system of the inverter more than the structural characteristic of the source, as it is for the synchronous generators. The control systems are designed by the manufactures using different techniques, and when all different inverters are connected to the same grid, instability or interaction issues may occur during steady-state and transient conditions [85, 86].

The LV distribution networks are characterized by the presence of three-phase and even more small sized single-phase inverters (under $3kW$) connected to different phases and with different control techniques, as presented in literature [87, 88]. The differences among each embedded control systems lead to different responses and behaviors during network alterations of operative conditions [89].

Specific focus has been dedicated to unintentional islanding operations in presence of different synchronization control scheme. In particular, the single-phase and three-phase synchronous reference frame phase locked loop (SRF-PLL) behaviors have been compared in order to study their influence in the unintentional islanding non-detection zone (NDZ) of the protection system.

7.1 System Description

The investigation on the SRF-PLL single-phase contributions on the unintentional islanding forming is carried out in a LV 4-wire electric distribution network, where single-phase

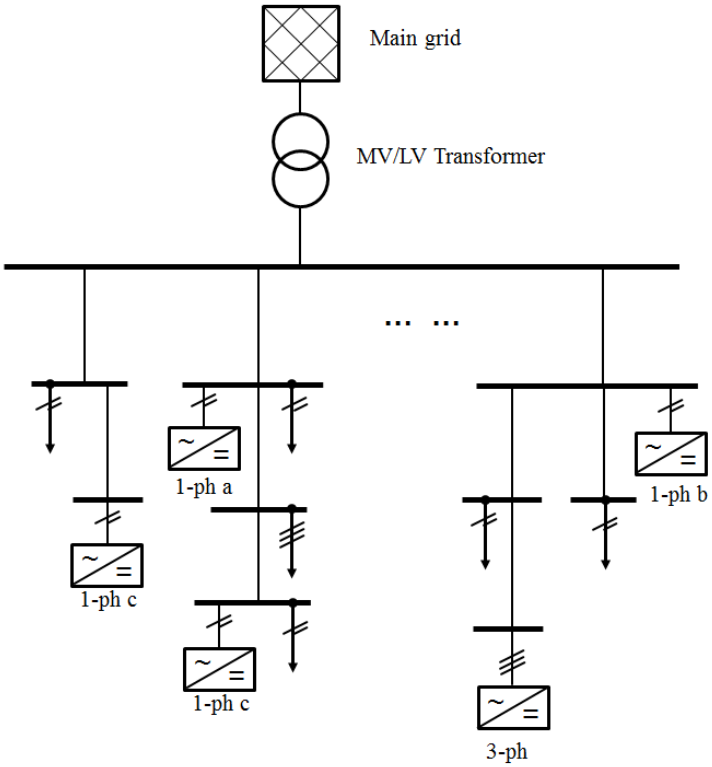

Figure 7.1: Distributed generator and load units three-phase and single-phase, connected to the distribution LV network.

and three-phase DER inverters are connected, as presented in Fig. 7.1. Lately, standards have imposed permissive thresholds for interface protection systems that could lead to a failure on the detection of unintentional islanding events, due to the sensitivity loss on the deviation of voltage amplitude and frequency from the nominal (grid connected) values. This protection system is equipped with a fault ride through (FRT) logic in order to avoid unintentional DERs disconnections during voltage and frequency temporary deviations from the nominal values. Only the mandatory protection system required by the Italian standard are here considered. Therefore, the inverter is equipped with an interface protection system (IPS) with over/under voltage (OUV) and over/under frequency (OUF) passive protections. Other anti-islanding protections have been neglected so the only possibility to detect an islanding forming operation is by the tripping of the IPS OUV and OUF.

The OUV and OUF protections system required by Italian standard for LV inverter based DER units are reported in Tab. 7.1, as described in Chapter 2.6.

A simplified scenario, has been considered: a three-phase LV inverter is connected to the main grid at the PCC with in parallel a local load. The grid-interface inverter is provided by internal current feedback and PLL to ensure the desired generation of active and

Table 7.1: Interface Protection System thresholds.

	Value	Tripping time
OV	1.15 p.u.	0.2 s
UV_1	0.85 p.u.	0.4 s
UV_2	0.4 p.u.	0.2 s
OF	51.5 Hz	1 s
UF	47.5 Hz	4 s

reactive power references during steady-state and grid connected operations, as presented in 7.4. Furthermore, the embedded control of inverter is designed to work on constant active and reactive power reference. Hence, in this section the regulating functions P/f and Q/V are not considered, because they are required for DER units above the rated power of 6 kW. Usually the single-phase current source inverters, on which the investigation is made, are characterized by lower rated power (around 3 kW). Even if the level of power of each generator is small, this study earns importance by the huge diffusion of this small DER units (especially PV systems) in the LV distribution network at the residential level.

Many grid-synchronization techniques have been proposed in literature [75, 90, 91]. Regarding the PLL, the following two cases are considered:

1. three-phase SRF-PLL;

2. single-phase SRF-PLL.

The single-phase SRF-PLL case is the main focus of this analysis. Different techniques for single-phase inverter have been studied in [92, 93]. The PLLs structure used are presented in Fig. 7.5 and Fig. 7.6. In the single-phase PLL the quadrature component is generated introducing a second order filter (Eq. 7.1). There are several other possible solutions to realize the quadrature component for a single-phase systems and (7.1) is adopted for the sake of explanation.

$$\begin{cases} F_s(s) = \dfrac{1}{\frac{s^2}{w_s^2} + s \cdot \frac{2\xi}{w_s} + 1} \\ w_s = 2\pi f \;\; rad/sec \\ \xi = 0.5, \end{cases} \tag{7.1}$$

where f is the grid voltage frequency.

In order to study the contribution of each type of PLL, it is possible to consider the islanded portion of the grid composed by the inverter and a local load, in order to make a

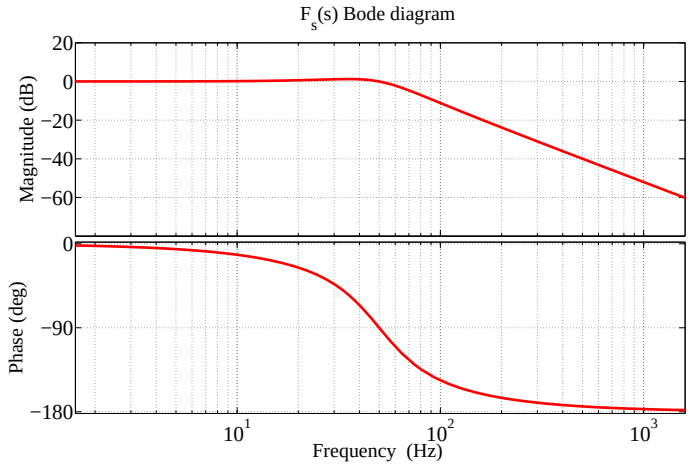

Figure 7.2: Bode diagram of the single-phase PLL filter.

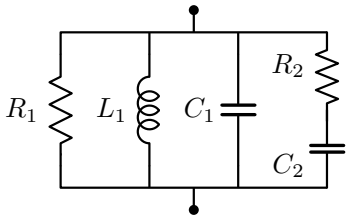

Figure 7.3: Generic local load with active and reactive power dependencies: $P_L(f,u)$ and $Q_L(f,u)$.

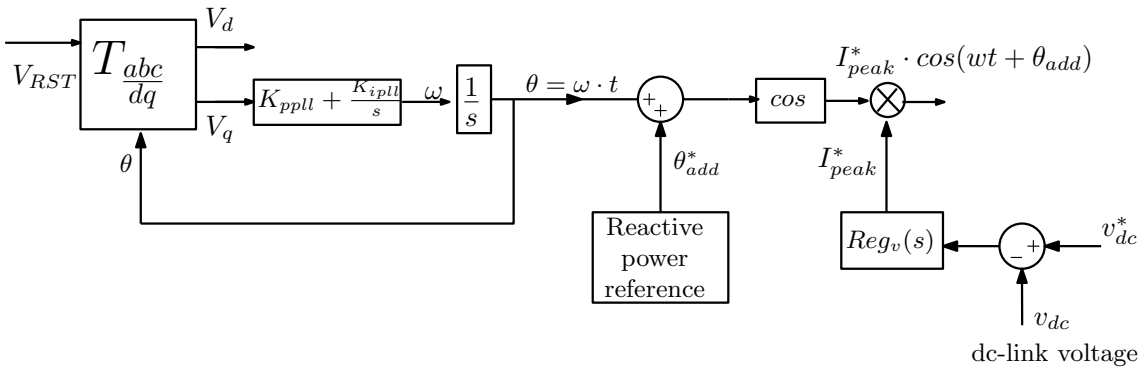

Figure 7.4: Scheme of the embedded current control of the inverter.

simplified approach with the aim to analyze a more complex system composed by different inverters and loads. The local load has been considered as RLC parallel impedance shown in Fig. 7.3, where the active P_L and reactive Q_L powers depend both on the frequency and the amplitude of the voltage waveform, as presented in Chapter 6.

After the transition from grid-connected to islanded operation there must be a balance between the generated power of the inverter and the absorbed power of the load. That is:

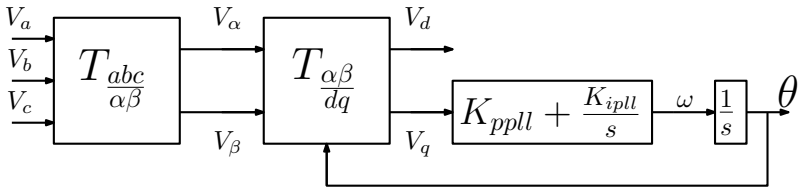

Figure 7.5: Typical three-phase SRF-PLL scheme.

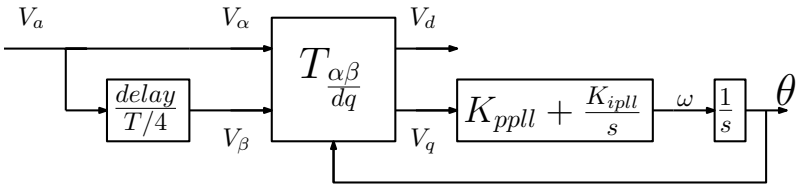

Figure 7.6: single-phase PLL scheme with fixed delay for the quadrature component, where T is the period of the voltage waveform.

$$\begin{cases} P_L(f,u) = P_G \\ Q_L(f,u) = Q_G, \end{cases} \tag{7.2}$$

where P_G and Q_G are the inverter generated active and reactive powers. Solving the system in Eq. (7.2), it is possible to evaluate the frequency and amplitude (f^* and u^*) of the steady-state point of uncontrolled islanded grid. Then, such solution can or can not meet the standards. We define:

$$\begin{array}{rcll} \Delta P & = & (P_G - P_L)/P_L & u_{min} < u^* < u_{max}, \\ \Delta Q & = & (Q_G - Q_L)/P_L & f_{min} < f^* < f_{max}, \end{array} \tag{7.3}$$

with $u_{max} = 1.15$ p.u., $u_{min} = 0.85$ p.u., $f_{max} = 51.5$ Hz and $f_{min} = 47.5$ Hz for permissive protection thresholds [57] and considering the P_L the nominal power value of the system.

As explained in Chapter 6, a set of solutions is found that define the non detection zone (NDZ), i.e. an area representing the power mismatch (ΔP versus ΔQ) at the PCC where the islanding condition is possible [27]. The PLL scheme have a role on the sizing of the NDZ with current source PV inverter as reported in Fig. 7.4.

7.2 Three-phase and single-phase SRF-PLL

One of the most common technique for grid synchronization in grid connected inverter applications is the SRF-PLL. In grid connected operations it is essential to be synchronized to the network voltage at the PCC in order to supply the active and reactive power

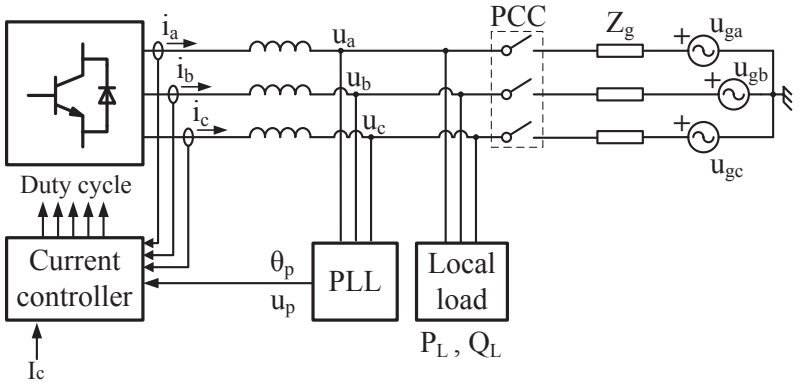

Figure 7.7: Three-phase inverter system connected to the main grid at the PCC, with a local load.

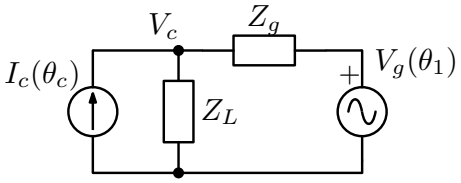

Figure 7.8: Single-phase equivalent scheme with the inverter as a current source.

references required. The typical SRF-PLL three-phase model implemented in our analysis is shown in Fig. 7.5. Where the first system transformation $T_{abc/\alpha\beta}$ allows to generate a two-phase quadrature rotating system $V_{\alpha\beta}$ from the three-phase rotating system V_{abc}. Then a second transformation $T_{\alpha\beta/dq}$ introduces two static quadrature components V_{dq} as reported in eq.7.4, considering symmetrical and balance conditions of the V_{abc} system. Other applications have been analyzed under unbalanced and frequency polluted conditions as in [94–96] and faulty conditions [97].

$$\begin{cases} V_a = V_m \cdot e^{j(\omega t)} \\ V_b = V_m \cdot e^{j(\omega t - \frac{2\pi}{3})} \\ V_c = V_m \cdot e^{j(\omega t + \frac{2\pi}{3})} \end{cases} \quad \begin{cases} V_\alpha = V_m \cdot e^{j(\omega t)} \\ V_\beta = V_m \cdot e^{j(\omega t - \frac{\pi}{2})} \end{cases} \quad \begin{cases} V_d = V_m \cdot e^{j\theta} \\ V_q = V_m \cdot e^{j(\theta - \frac{\pi}{2})} \end{cases} \tag{7.4}$$

$\theta = \int \omega(t) dt$.

Using a regulator, for example a PI controller $(K_p + K_i/s)$, it is possible to synchronize the voltage dq components in order to obtain $V_d = V_m$ and $V_q = 0$. Under hypothesis of symmetrical and balance conditions of the V_{abc} system, the three-phase model in Fig. 7.7 can be represented as a single-phase equivalent as shown in Fig. 7.8. Thus it is easier to study the contribution of the particular single-phase PLL presented in this work, compared with the common three-phase PLL scheme.

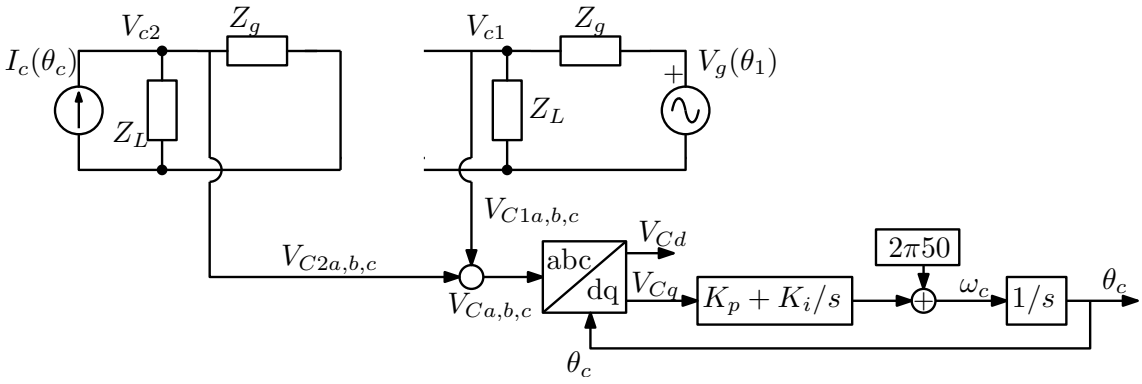

Figure 7.9: Scheme of the superposition of the effects on the inverter in Fig. 7.8.

The voltage contributions of the current and voltage generator in Fig. 7.8 are separated by the superposition of the effects as shown in Fig. 7.9.

$$\begin{cases} V_{C1,abc} = \dfrac{Z_L}{Z_g + Z_L} \cdot V_g = \mid \dfrac{Z_L}{Z_g + Z_L} \mid \cdot V_g \cdot e^{j(\theta_g + \varphi_1)} \\ V_{C2,abc} = \dfrac{Z_g Z_L}{Z_g + Z_L} \cdot I_C = \mid \dfrac{Z_g Z_L}{Z_g + Z_L} \mid \cdot I_C \cdot e^{j(\theta_C + \varphi_2)}, \end{cases} \tag{7.5}$$

where the φ_2 is the phase of the local load. Considering the two contributions, we can describe the PLL behavior as follow:

$$V_{abc} = V_{C1,abc} + V_{C2,abc}, \tag{7.6}$$

$$V_a = G \cdot cos(\theta_1 + \varphi_1) + C \cdot cos(\theta_2 + \varphi_2), \tag{7.7}$$

where:

$$\begin{cases} G = V_g \cdot \mid \dfrac{Z_L}{Z_L + Z_g} \mid \\ C = I_c \cdot \mid \dfrac{Z_L \cdot Z_g}{Z_L + Z_g} \mid, \end{cases} \tag{7.8}$$

$$\begin{bmatrix} V_d \\ V_q \end{bmatrix} = \frac{2}{3} \begin{bmatrix} cos(\theta_2) & cos(\theta_2 - \frac{2\pi}{3}) & cos(\theta_2 + \frac{2\pi}{3}) \\ -sin(\theta_2) & -sin(\theta_2 - \frac{2\pi}{3}) & -sin(\theta_2 + \frac{2\pi}{3}) \end{bmatrix} \begin{bmatrix} v_a \\ v_b \\ v_c \end{bmatrix}. \tag{7.9}$$

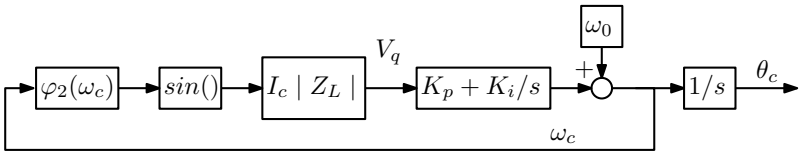

Figure 7.10: Scheme of the three-phase SRF-PLL in unintentional islanding operation.

In order to be synchronized with the grid voltage at the PCC, the V_q component (7.10) is the regulator input. The system under consideration for unintentional islanding operation is presented in Fig. 7.10 with $Z_g = \infty$ after the disconnection from the main grid. Thus,

$$V_q = G \cdot sin(\theta_1 + \varphi_1 - \theta_2) + C \cdot sin(\varphi_2), \tag{7.10}$$

$$V_q = C \cdot sin(\varphi_2), \tag{7.11}$$

$$\begin{cases} \mid Z_L \mid = \frac{R_L}{\sqrt{1-Q_F^2(\frac{\omega_2}{\omega_r}-\frac{\omega_r}{\omega_c})^2}} \\ \varphi_L(\omega_2) = arctan\left[Q_F(\frac{\omega_r^2-\omega_2^2}{\omega_r\omega_2})\right] \\ \omega_r = \frac{1}{\sqrt{(L_L C_L)}} \\ Q_F = R_L\sqrt{\frac{C_L}{L_L}}. \end{cases} \tag{7.12}$$

This configuration presents a positive feedback that depends on the $\varphi_L(\omega_2)$. The three-phase PLL system is unstable if $\omega_2 \neq \omega_r$, which means that there is no equilibrium point between load and inverter. Such balance condition is found in case of a generation of active and reactive power matching the load consumption.

The three-phase is than compared with the single-phase SRF-PLL, where the quadrature component V_β is obtained with the second order filter in Eq. 7.1. This single-phase PLL guarantees a correct synchronizing with the PCC voltage only with a stable frequency at 50 Hz. In presence of a frequency deviation from the nominal value, the filter introduces a $\varphi_F \neq -\pi/2$ as presented in the Bode diagram in Fig. 7.2. However, this specific PLL implementation is suitable for grid-connected applications, because in presence of the main bulk system, the frequency is fixed at the nominal value and the possible frequency temporary variations are usually near to 50 Hz value (± 0.5 Hz); therefore do not introduce an error in the V_β that compromises the grid synchronization.

Consider the same consideration of superposition of the effects made for the three-phase PLL. The single-phase PLL system is defined:

$$\begin{cases} V_\alpha = G \cdot e^{j(\theta_1+\varphi_1)} + C \cdot e^{j(\theta_2+\varphi_{add}+\varphi_2)} \\ V_\beta = W_F \cdot G \cdot e^{j(\theta_1+\varphi_1+\varphi_F)} + W_F \cdot C \cdot e^{j(\theta_2+\varphi_{add}+\varphi_2+\varphi_F)} \end{cases}, \tag{7.13}$$

$$\begin{bmatrix} V_d \\ v_q \end{bmatrix} = \begin{bmatrix} cos(\theta_2) & sin(\theta_2) \\ -sin(\theta_2) & cos(\theta_2) \end{bmatrix} \begin{bmatrix} V_\alpha \\ V_\beta \end{bmatrix}, \tag{7.14}$$

$$\begin{aligned} V_q = &- G \cdot cos(\theta_1 + \varphi_1) \cdot sin(\theta_2) + \\ &- C \cdot cos(\theta_2 + \varphi_{add} + \varphi_2) \cdot sin(\theta_2) + \\ &+ W_F \cdot cos(\theta_1 + \varphi_1 + \varphi_F) \cdot cos(\theta_2) + \\ &+ W_F \cdot C \cdot cos(\theta_2 + \varphi_{add} + \varphi_2 + \varphi_F) \cdot cos(\theta_2). \end{aligned} \tag{7.15}$$

Considering islanding operation ($Z_g = \infty$):

$$\begin{aligned} V_q = &- C \cdot cos(\theta_2 + \varphi_{add} + \varphi_2) \cdot sin(\theta_2) + \\ &+ W_F \cdot C \cdot cos(\theta_2 + \varphi_{add} + \varphi_2 + \varphi_F) \cdot cos(\theta_2), \end{aligned} \tag{7.16}$$

$$\begin{aligned} V_q = &- \frac{C}{2}[sin(2\theta_2 + \varphi_{add} + \varphi_2) - sin(\varphi_{add} + \varphi_2) + \\ &- W_F \cdot sin(\frac{\pi}{2} + 2\theta_2 + \varphi_{add} + \varphi_2 + \varphi_F) \\ &- W_F sin(\frac{\pi}{2} + \varphi_{add} + \varphi_2 + \varphi_F)]. \end{aligned} \tag{7.17}$$

The single-phase PLL model in islanding operation is presented in Fig. 7.11.

Substituting $W_F = 1$ and $\varphi_F = -\pi/2$ the system is reduced to the three-phase PLL scheme in in Fig. 7.10. It is demonstrated in the simulations (Section 7.3) that during islanding operation the single-phase configuration, when the frequency deviates from the nominal value the positive feedback is reduce by the presence of the filter, starting from the same ϑ_{add} condition in comparison with the three-phase PLL case.

7.3 Simulations

The validation of the study is proposed using a time domain Simulink/Matlab model of a current controlled voltage source inverter in parallel with a local load (RLC parallel).

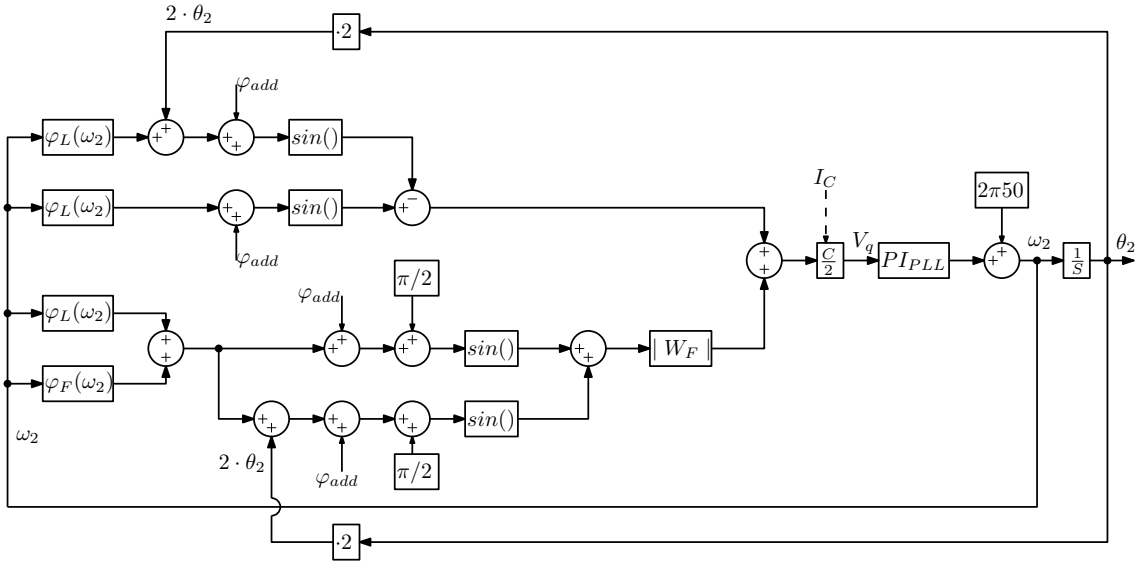

Figure 7.11: Scheme of the single-phase SRF-PLL in unintentional islanding operation.

The inverter embedded control has been designed following the scheme in Fig. 7.4, in which the inverter power injection (P_G - Q_G) is regulated by PLL synchronization and current control loop. In order to compare the effects, different unintentional islanding events have been simulated using the two PLL selected configurations in different power balance condition with the load. The maximum power mismatch ($\Delta P = (P_G - P_L)/P_N$ and $\Delta Q = (Q_G - Q_L)/P_N$ with P_N as the load nominal power) has been considered in order to allow unintentional islanding operations in which voltage amplitude and frequency are within the protection thresholds stated by the standard.

In particular, the initial power mismatch $\Delta P - \Delta Q$ corresponds to specific reference values of I_c and ϑ_{add} in the inverter current control, which leads to the islanding voltage amplitude V^* and frequency f^*. Therefore, the limits of the NDZ have been determinate considering this constrains $V_{min} \leq V^* \leq V_{max}$ and $f_{min} \leq f^* \leq f_{max}$. The simulation results allowed to determinate an enlargement of the NDZ for the single-phase PLL respect to the three-phase PLL, as presented in the analysis due to the compensation of the positive feedback in presence of $\varphi_F(\omega_2)$ described in Fig. 7.11. This means that with this single-phase PLL configuration, the protection limits are respected by wider power unbalance conditions on the plane ΔP - ΔQ. In Fig. 7.12 are presented the NDZ of the single and three-phase PLL contributions, where the ΔP - ΔQ before the islanding event is presented in terms of I_c - ϑ_{add} in order to validate the study referring to the analytical model presented in Fig. 7.11. Thus, with this specific single-phase PLL, the ϑ_{add} range which allows unintentional islanding conditions is enlarged by the contribution of the filter in Eq. 7.1 respect to the case of three-phase PLL system.

This result leads to a wider NDZ in the plane $\Delta P - \Delta Q$ for the inverter adopting this

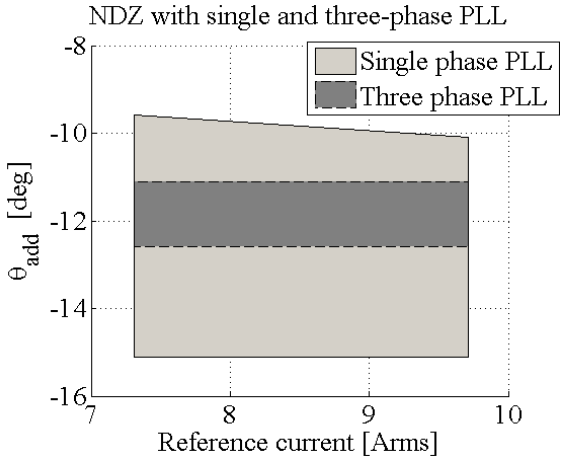

Figure 7.12: Analytic area resulting of simulink simulations; I_c - ϑ_{add} combination that allows islanding operations.

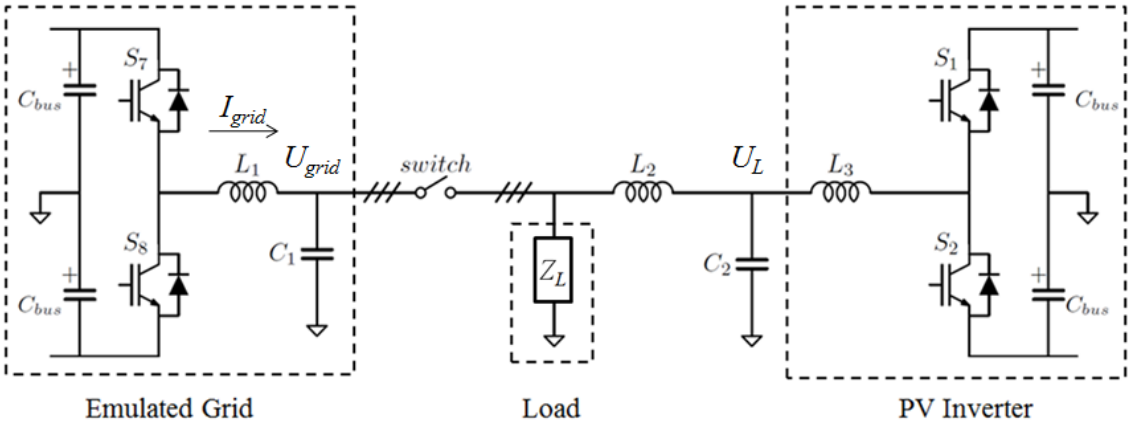

Figure 7.13: Experimental test-bed equivalent single-phase configuration. The Inverter controlled as a PV DER (PV Inverter) and the passive load (Z_L) are separated by the emulated grid using a manual switch.

specific single-phase SRF-PLL, as demonstrated by the experimental result of a lab-scale prototype in Section 7.4.

7.4 Experimental setup

The test-bed used to perform experimental validations is reported in Fig. 7.13. The PV inverter is equipped with a current control loop and the PLL bandwidth is about 10 Hz. The nominal phase voltage is 230 V_{rms} and the nominal power is 15 kVA, however the following tests have been performed at reduced voltage and current levels. In the tests, we have used $V_b = 150\ V_{rms}$ and $I_b = 8.5\ A_{rms}$ as the base quantities to evaluate the per-unit values.

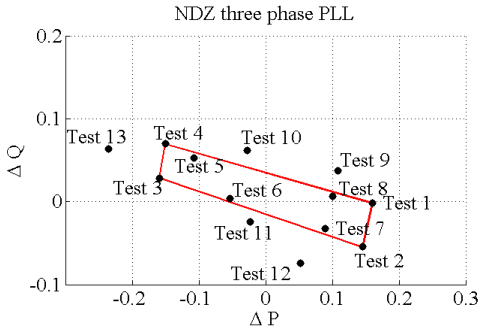

Figure 7.14: Analytic area resulting of simulink simulations; I_c - ϑ_{add} combination that allows islanding operations.

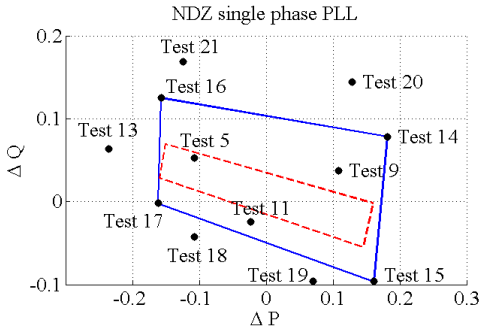

Figure 7.15: Analytic area resulting of simulink simulations; I_c - ϑ_{add} combination that allows islanding operations.

The experimental results confirm a different behavior of the inverter depending on the PLL implementation: a single-phase with a filter-delay PLL and a three-phase PLL. In Fig. 7.14 and 7.15, the NDZ comparison in the plane $\Delta P - \Delta Q$ is presented.

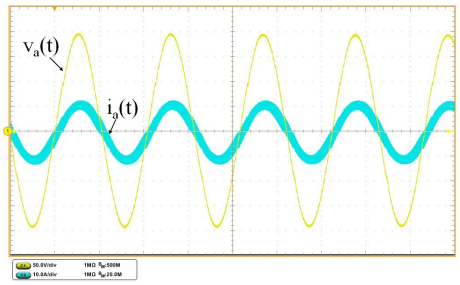

Figure 7.16: Test 5 using three-phase PLL, output voltage $v_a(t)$ (50V/div), inverter output current $i_a(t)$ (10A/div), 10ms/div, islanding operation frequency 48.1 Hz and voltage 135 Vrms (0.90 p.u.).

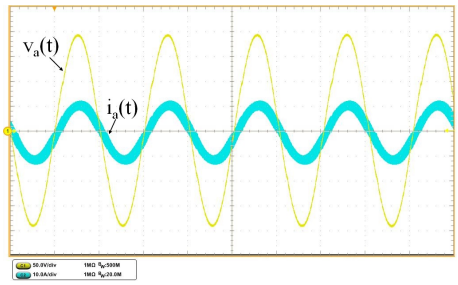

Figure 7.17: Test 5 single-phase PLL, output voltage $v_a(t)$ (50V/div), inverter output current $i_a(t)$ (10A/div), 10ms/div, islanding operation frequency 49.4 Hz and voltage 135.5 Vrms (0.90 p.u.).

In Tab. 7.2 and 7.3 are presented the experimental results. The case with single-phase PLL presents a wider NDZ in the plane ΔP - ΔQ, as shown in Fig. 7.15. In Fig. 7.16 and 7.18 the waveform of the islanding operations presents a higher values of frequency, while in Fig. 7.17,7.19 the tests have been repeated starting from the same ΔP - ΔQ, but the frequencies are closer to the nominal frequency. This effect is due to the presence of the filter for the quadrature component that reduce the deviation of the frequency from the nominal value.

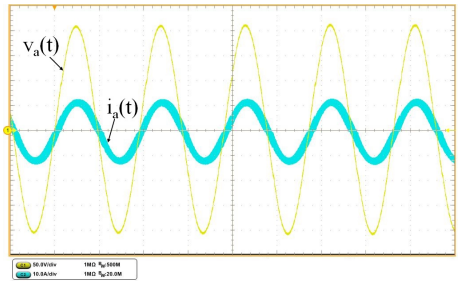

Figure 7.18: Test 11 three-phase PLL, output voltage $v_a(t)$ (50V/div), inverter output current $i_a(t)$ (10A/div), 10ms/div, islanding operation frequency 52.3 Hz and voltage 145 Vrms (0.97 p.u.).

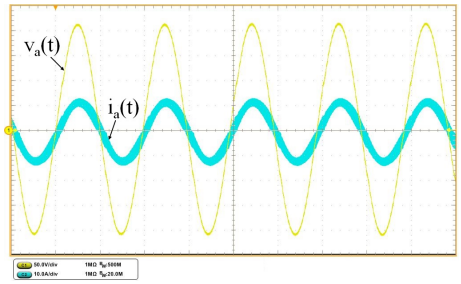

Figure 7.19: Test 11 single-phase PLL, output voltage $v_a(t)$ (50V/div), inverter output current $i_a(t)$ (10A/div), 10ms/div, islanding operation frequency 51.0 Hz and voltage 146.1 Vrms (0.97 p.u.).

Table 7.2: Test with three-phase PLL.

Test	ΔP	ΔQ	f [Hz] *island*	V_{rms} [p.u.] *island*
1	0.160	-0.002	47.7	1.13
2	0.145	-0.055	51.4	1.15
3	-0.159	0.029	51.4	0.85
4	-0.151	0.070	47.5	0.86
5	-0.108	0.052	48.1	0.90
6	-0.054	0.004	51	0.94
7	0.089	-0.032	50.6	1.07
8	0.100	0.007	47.9	1.10
9	0.108	0.037	45.8	1.09
10	-0.027	0.062	46.1	0.97
11	-0.023	-0.024	52.3	0.97
12	0.052	-0.075	54.4	1.04
13	-0.236	0.064	49.2	0.79

7.5 Conclusions

This chapter has proposed an analysis of the interface protection system NDZ for unintentional islanding operations, considering the mismatch $\Delta P - \Delta Q$ between load and generation. We have shown the single-phase PLL important role in the sustain of islanding conditions compared with a typical three-phase PLL. In particular, the investigation was focused on the single-phase SRF-PLL with orthogonal component obtained by a fixed filter (nominal condition 50 Hz). The size of the $\Delta P - \Delta Q$ NDZ is not negligible and it should be analyzed for the future generation of LV distribution grids with large penetration of renewable energy sources.

Table 7.3: Test with single-phase PLL.

Test	ΔP	ΔQ	f [Hz] *island*	V_{rms} [p.u.] *island*
5	-0.108	0.052	49.4	0.90
9	0.108	0.037	48.6	1.10
11	-0.023	-0.024	51	0.97
13	-0.236	0.064	50	0.79
14	0.181	0.078	47.5	1.14
15	0.161	-0.096	51.4	1.13
16	-0.157	0.125	47.5	0.85
17	-0.162	-0.002	51.5	0.85
18	-0.107	-0.042	52.3	0.91
19	0.070	-0.096	52.1	1.07
20	0.128	0.145	46.1	1.09
21	-0.124	0.169	46.3	0.87

Chapter 8

Temporary Unintentional Islanding

The number of distributed energy resources (DER) units connected to medium and low voltage (MV and LV) distribution grids through inverters has increased and new introduced European standards regulate the connections of active users to the grid, in particular during temporary variations of voltage and frequency [19, 20, 59]. These standards, with some country-level ones, state the support of DERs to voltage and frequency regulations via P/f and Q/V droop characteristics. Furthermore, these grid codes have recently extended the frequency range of normal operation of DERs.

Inverters introduce fast dynamics into the grid and they could continue to feed parts of the grid also when the mains disconnect. In this case, undesired islanded portions of the grid can still be energized [22, 98].The temporary islanding operation, below 600 ms, caused by the automatic re-closing procedure is also considered herein, because it may increase the risk of possible out-of-synchronism reconnection [27, 29]. This automatic procedure is adopted in some distribution networks of European countries and has the purpose of fast localization and separation of the faulted line segment of a MV distribution network [57,99]. In order to avoid out-of-synchronism reconnection during the main switch re-closing, unintentional islanded conditions must be detected by the DERs, which have immediately to disconnect from the grid [23, 39].

In this chapter, it is shown that the risk of temporary unintentional islanding can potentially increase with the introduction of P/f and Q/V droop characteristics. Such risk may also change according to the speed of such regulators, i.e. the faster the droop regulators, the greater the islanding probability.

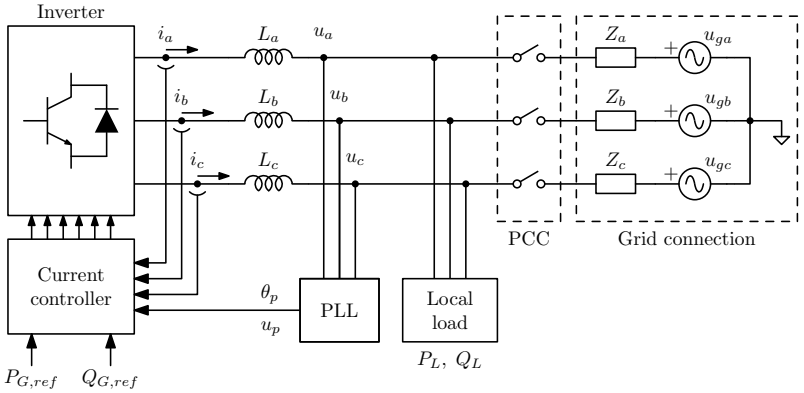

Figure 8.1: Considered scenario.

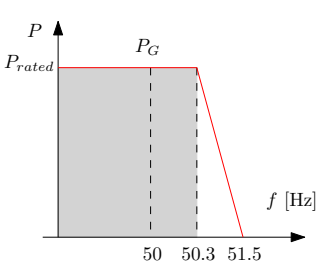

(a) Active power regulation P/f

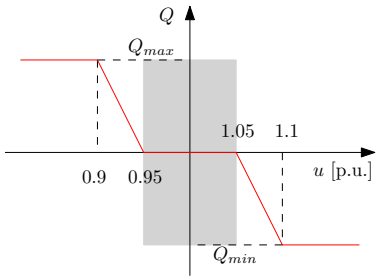

(b) Reactive power regulation Q/V

Figure 8.2: P/f and Q/V droop characteristics for inverter [57]; Q_{max} and Q_{min} are respectively $0.483 \cdot P_{G,ref}$ and $-0.483 \cdot P_{G,ref}$.

8.1 System Description of Temporary Islanding

The considered scenario includes a LV inverter connected to the main grid and having a local loads as Fig. 8.1 shows. This is a three-phase system, but similar results can also be obtained for the single-phase case [27, 34]. The inverter has internal current/voltage feedbacks and phase-locked loop (PLL) to ensure the desired generation of active and reactive powers while grid-connected.

Two Cases are considered for the power generation:

- *Case I* for an inverter with constant active and reactive power references $P_{G,ref}$ and $Q_{G,ref}$;
- *Case II* for an inverter with P/f and Q/V droop characteristics as in Fig. 8.2.

After the breaker opening at the point of common coupling (PCC) in Fig. 8.1, the active P_G and reactive Q_G powers of the inverter balance those of the load, P_L and Q_L:

$$\begin{cases} P_L(f,u) = P_G(f) \\ Q_L(f,u) = Q_G(u) \end{cases} \tag{8.1}$$

where the load has been modeled with its active P_L and reactive Q_L powers as functions of the frequency f and the voltage amplitude u, as in [47]. The permissive limits of [57] are considered: steady-state operation is allowed within $0.85 \div 1.15$ p.u. for the voltage and within $47.5 \div 51.5$ Hz for the frequency.

After the disconnection and the initial transient, a new operating point can be reached. This steady-state point is the solution of the system (8.1) in terms of frequency and voltage, that is ($f^\star$, $u^\star$). If $f^\star$ and $u^\star$ remain within the previously defined voltage and frequency ranges, then a permanent unintentional islanding is possible. In grid-connected operations, active and reactive powers flow toward the grid because of imbalances between load and generation: these powers are $\Delta P = P_G - P_L$ and $\Delta Q = Q_G - Q_L$. Considering these imbalances, a set of solutions is found that defines the NDZ on the plane ΔP versus ΔQ where the islanding condition is possible.

The temporary islanding problem has been introduced in [27] as the problem of understanding if the disconnection transient in terms of frequency f and voltage u of the islanded system fulfills the standard thresholds, for a defined time interval after the break opening. It is analyzed if during a 600 ms transient, due to the automatic re-closing procedure, the islanding operation can be maintained according to the protections of [57]. However, for the temporary islanding the voltage and frequency have to be within the allowed ranges in an established time, and so the speeds of the P/f and Q/V droop regulations play an important role on the $\Delta P - \Delta Q$ region shaping. Describing these speeds with two response times of the droop control loops, respectively τ_p and τ_q, it has been verified that larger time constants lead to smaller NDZ. This phenomenon is qualitatively shown in chapter 6 at section 6.2.1 and it should be adopted also for the temporary unintentional islanding operations. Note that, when studying the temporary islanding during the automatic re-closing time, only the voltage protections may trip within the intervention time of 600 ms [57].

8.2 Dynamic Analysis for NDZ

In this section, the islanded system of Fig. 8.1 is modeled to analytically derive the NDZ. The inverter is managed with multiple control loops as in Fig. 8.3. It has an inner current controller that ensures the tracking of two current references which are evaluated by outer power loops that track power references from the P/f and Q/V droop regulators. Moreover, the SRF-PLL (synchronous reference frame phase-locked loop) is included in order to synchronize the current regulator to the output voltage. This PLL evaluates also the frequency and voltage amplitude for the droop regulation scheme. Here, the active power loop of the inverter is an abstraction to simplify the analysis and to describe the

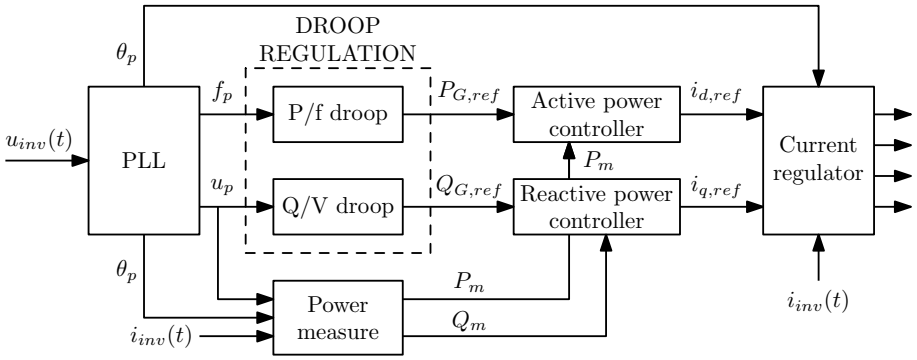

Figure 8.3: Control architecture of the inverter with active and reactive power loops and P/f and Q/V droop functions.

behavior of a real PV inverter.

8.2.1 Modeling of the Inverter with Constant Power

Now a dynamic model for Case I is proposed to predict the temporary NDZ. This model exploits the time scale separation of the dynamics of the system in Fig. 8.1, meaning that there are fast dynamics due to the current and power regulators and the load that are negligible to describe the 600 ms transient for the automatic re-closure procedure and others that are slower, as those due to the PLL. With this observation, we can provide a static description of the faster dynamics, i.e. the current and power regulation loops, while all the dynamic contributions of this model are related to the PLL [29]. These approximations will be validated with simulations.

In a SRF-PLL that is synchronized to the q component of the voltage [86], the d component can be used as measure of voltage amplitude u_p:

$$\begin{cases} u_d = u\cos\xi \triangleq u_p \\ u_q = u\sin\xi \end{cases} \tag{8.2}$$

where u is the actual voltage amplitude at the inverter output and ξ is the phase shift between the actual voltage space vector and the PLL reference frame.

If the current and power loop dynamics are neglected as said before, the feedback powers are always equal to their reference powers (the tracking error is always zero):

$$\begin{aligned} S_{G,ref} = P_{G,ref} + jQ_{G,ref} &= \frac{3}{2}u_p\left[\frac{ue^{j\xi}}{Z_L(f)}\right]^* = \\ &= \frac{3}{2}\frac{u^2\cos\xi e^{-j\xi}}{Z_L(f)^*} \end{aligned} \tag{8.3}$$

where * is the complex conjugation operation and its argument is the space vector of

the inverter current in the PLL reference frame. The small-signal model is obtained by linearized in the grid-connected operating point just before the grid transition. The overall model can be described with the Laplace transfer functions $H_{\delta f}(s)$ and $H_{\delta u}(s)$:

$$\begin{aligned} H_{\delta f}(s) &= \frac{\mathfrak{L}\left[\hat{f}\right]}{\mathfrak{L}\left[\hat{\delta}\right]} \\ H_{\delta u}(s) &= \frac{\mathfrak{L}\left[\hat{u}\right]}{\mathfrak{L}\left[\hat{\delta}\right]} \end{aligned} \tag{8.4}$$

where the input $\hat{\delta}$ of this model is a phase perturbation that triggers the PLL transient caused by the sudden cancellation of the grid current. The expressions in (8.4) can be used to evaluate the PLL frequency and voltage amplitude for a certain time $\bar{t}$ after the grid disconnection or to predict the whole transient after the disconnection, exploiting the Laplace anti-transform. This model description and a possible extension in order to account the droop regulations can be found in [29].

8.2.2 Analytic results for constant power inverter

A validation of the model of section 8.2.1 based on Matlab/Simulink simulations is now proposed. The simulation model is a detailed description of the architecture of Fig. 8.1 and 8.3. Nominal voltage amplitude is $u_0 = 150\,\mathrm{V_{RMS}}$ (phase to neutral) and nominal frequency is $f_0 = 50\,\mathrm{Hz}$. This choice has been done to have the same parameters both in simulation and for the experiments of Section 8.4.

The closed-loop bandwidths are: 5 Hz for the SRF-PLL, 7 Hz for the active power control loop and 5 Hz for the reactive power control loop. The load, i.e. Z_L, is a set of passive components, including in parallel connected a resistor R_1, an inductor L_1, a capacitor C_1 and a series of a resistor R_2 and a capacitor C_2, where their values are in Tab. 8.1.

Table 8.1: Load parameters: base impedance is at the nominal value of voltage amplitude and frequency u_0 and f_0.

R_1	=	$18\,\Omega$	=	0.798 p.u.
R_2	=	$82.5\,\Omega$	=	0.174 p.u.
L_1	=	87.5 mH	=	0.534 p.u.
C_1	=	$14.4\,\mu$F	=	0.065 p.u.
C_2	=	$60\,\mu$F	=	0.271 p.u.

A simulation of the disconnection transient is proposed in Fig. 8.4 in terms of frequency f measured by the PLL and voltage amplitude u, with $\Delta P = 0.2$ p.u. and $\Delta Q = 0.4$ p.u.

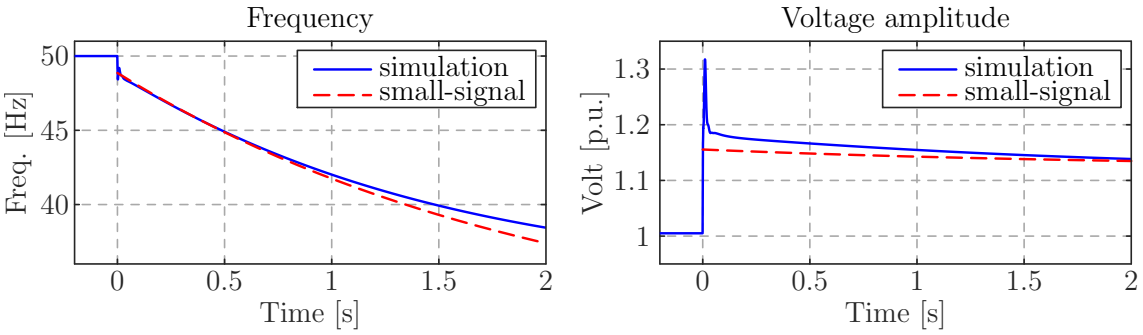

Figure 8.4: Time-domain comparison between the small-signal model and a detailed simulation: the frequency measured by the PLL and the actual voltage amplitude for a grid disconnection with $\Delta P = 0.2\,\text{p.u.}$ and $\Delta Q = 0.4\,\text{p.u.}$ for Case I [29].

(base power is the apparent load power). In Fig. 8.4, it is shown the good matching between the mathematical model, i.e. (8.4), and the simulation results: only a fast initial transient is not described in the small-signal model because of the approximations described in Section 8.2.1.

Evaluating the Laplace anti-transform of $H_{\delta u}(s) \cdot \hat{\delta}$, the voltage, for instance, at $\bar{t} = 600\,\text{ms}$ can be set equal to the higher or lower protection thresholds and the resulting system can be solved backward in order to evaluate $\hat{\delta}$ and then back again to ΔP and ΔQ (NDZ border). Therefore, it is possible to identify the analytical NDZ ($\Delta P - \Delta Q$ plane) which includes the temporary unintentional islanding region [29]. An example of these results is in Fig. 8.5 for the constant power inverter, where the red solid lines delimit the NDZ. These results are obtained considering the voltage within $0.4 \div 1.15\,\text{p.u.}$ at $\bar{t} = 200\,\text{ms}$ and within $0.85 \div 1.15\,\text{p.u.}$ at $\bar{t} = 400\,\text{ms}$ and $\bar{t} = 600\,\text{ms}$. This is an approximation because the small-signal model can be applied only a finite number of $\bar{t}$, while the inverter protections continuously check the voltage in the $0 \div 600\,\text{ms}$ interval; for analytic, simulation and experimental results [29].

The NDZ obtained with the small-signal model is compared to one obtained with simulation in Fig. 8.5. Blue dots are unintentional islanded operations verified by simulations, checking if the voltage remains within the protection ranges for all the interval $0 \div 600\,\text{ms}$. In these simulations, also frequency limits have been included to maintain the islanded operation: such limits are $45 \div 55\,\text{Hz}$, instead of the protection thresholds (47.5 Hz and 51.5 Hz) which time intervention is higher (respectively 4 s and 1 s) than the temporary islanding time considered (600 ms). The comparison shows a good agreement between the analytic approach and the simulation-based results in terms of NDZ. The missing region within the analytic borders is due to the frequency limits (not tested analytically), while the voltage thresholds are well approximated [29].

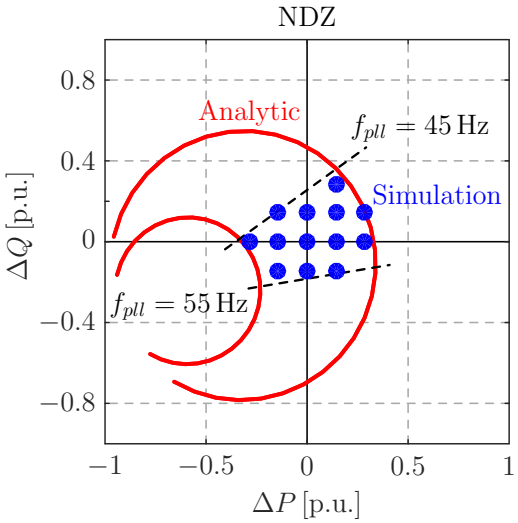

Figure 8.5: Analytic and simulation NDZs below 600 ms for Case I (powers normalized to the nominal load power) [29]

8.3 Temporary Islanding Simulation Results

Simulations are presented to describe how the temporary unintentional islanding risk increases introducing the P/f and Q/V droop functions and with respect to their speeds. The system in Fig. 8.1 is simulated with the same control architecture described in the section 8.2 (also same parameters). The NDZs are evaluated with the same method of section 8.2.2.

The NDZs for an inverter with P/f and Q/V droop functions with different rise times of the active τ_p and reactive τ_q power loops are in Fig. 8.6. As presented in chapter 6, the results of Fig. 8.6 clearly show that the risk of unintentional islanding operation increases introducing droop functions. Moreover, the considerations in chapter 6.2.1 are also visible here, since the $\Delta P - \Delta Q$ area widens more with faster P/f and Q/V droop controllers (i.e. for smaller τ_p and τ_q). With other words, the temporary unintentional islanding risk increases with faster systems. However, in some cases fast droop regulation may destabilize the autonomous system, leading to a reduction of the temporary NDZ [29].

Examples of time-domain simulations are reported in Fig. 8.7 for the disconnection transient in terms of the grid voltage and PLL frequency. They are for the same $\Delta P = 0.29$ p.u. and $\Delta Q = -0.14$ p.u. and for different τ_p and τ_q rise times.

8.4 Temporary Islanding Experimental Results

The lab-scale three-phase prototype has been used for the experimental validation [27,34]. The configuration is described in chapter 5, where a switch allows the islanding operation

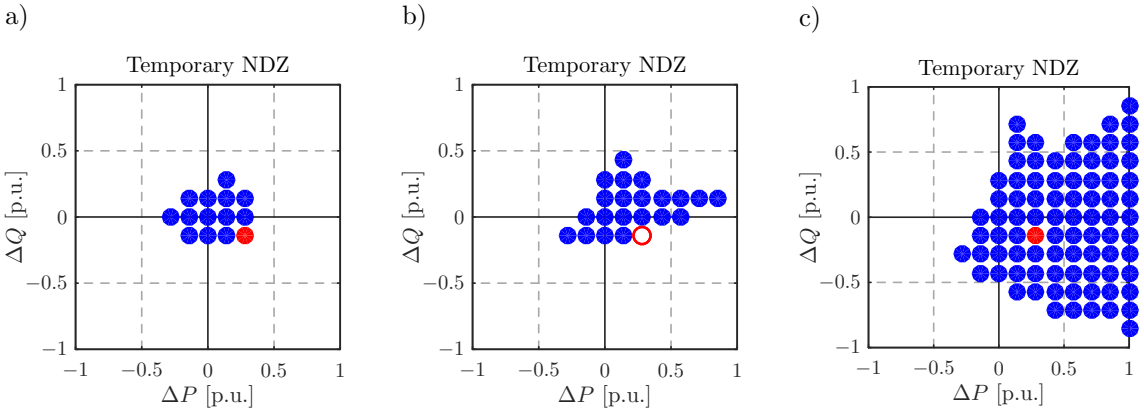

Figure 8.6: Simulation results for $\Delta P - \Delta Q$ area of unintentional islanding (for a 600 ms time) when the inverter operates with droop characteristics according to [57] for different power response times (Case IV): a) with $\tau_p = 5\,\text{s}$ and $\tau_q = 5.8\,\text{s}$; b) with $\tau_p = 1\,\text{s}$ and $\tau_q = 1.5\,\text{s}$ and c) with $\tau_p = 0.24\,\text{s}$ and $\tau_q = 0.35\,\text{s}$ (ΔP and ΔQ are normalized to the nominal load power) [29].

by isolating the PV inverter and the passive load Z_L from the main grid. The nominal phase voltage is $150\,\text{V}_{\text{rms}}$ and the nominal line frequency is $f_0 = 50\,\text{Hz}$ and the same load described in Section 8.2 for the simulation analysis is used here.

The control scheme for a typical PV application with active and reactive power closed-loop controllers and SRF-PLL (in this implementation the PLL closed-loop bandwidth is equal to 4 Hz) is reported in Fig. 8.8.

Experimental results show an enlargement of the NDZ in the plane $\Delta P - \Delta Q$ in Fig. 8.9, in which tests indicated with a blue dot represent unintentional islanding operation within 600 ms. Furthermore, each test is performed with different τ_p and τ_q response times of the P/f and Q/V droop characteristics. Some disconnection transients from the experimental setup are reported in Fig. 8.10 for $\Delta P = 0.9\,\text{p.u.}$ and $\Delta Q = -0.2\,\text{p.u.}$ for the same conditions of Fig. 8.9.

These results confirm that the risk of unintentional islanding increases using droop control for supporting functions with respect to the case of a constant power inverter. Moreover, the enlargement of the NDZ depends on the time response of the inverter regulation functions, i.e. the fast droop controllers (small τ_p and τ_q) lead to wider NDZs. However, *potential* increase of the temporary unintentional islanding risk due to fast droop regulations have been shown. It has to be reported that, in some cases, especially with large unbalance conditions, this is not always true. In some cases the temporary islanding risk may decrease with faster droop controllers because they may destabilize the islanded system [29]. This can be due to several aspects that can be different for different PV installations in the distribution grid, for example due different control implementation, bandwidths of the inner inverter regulators, local load structures, etc.

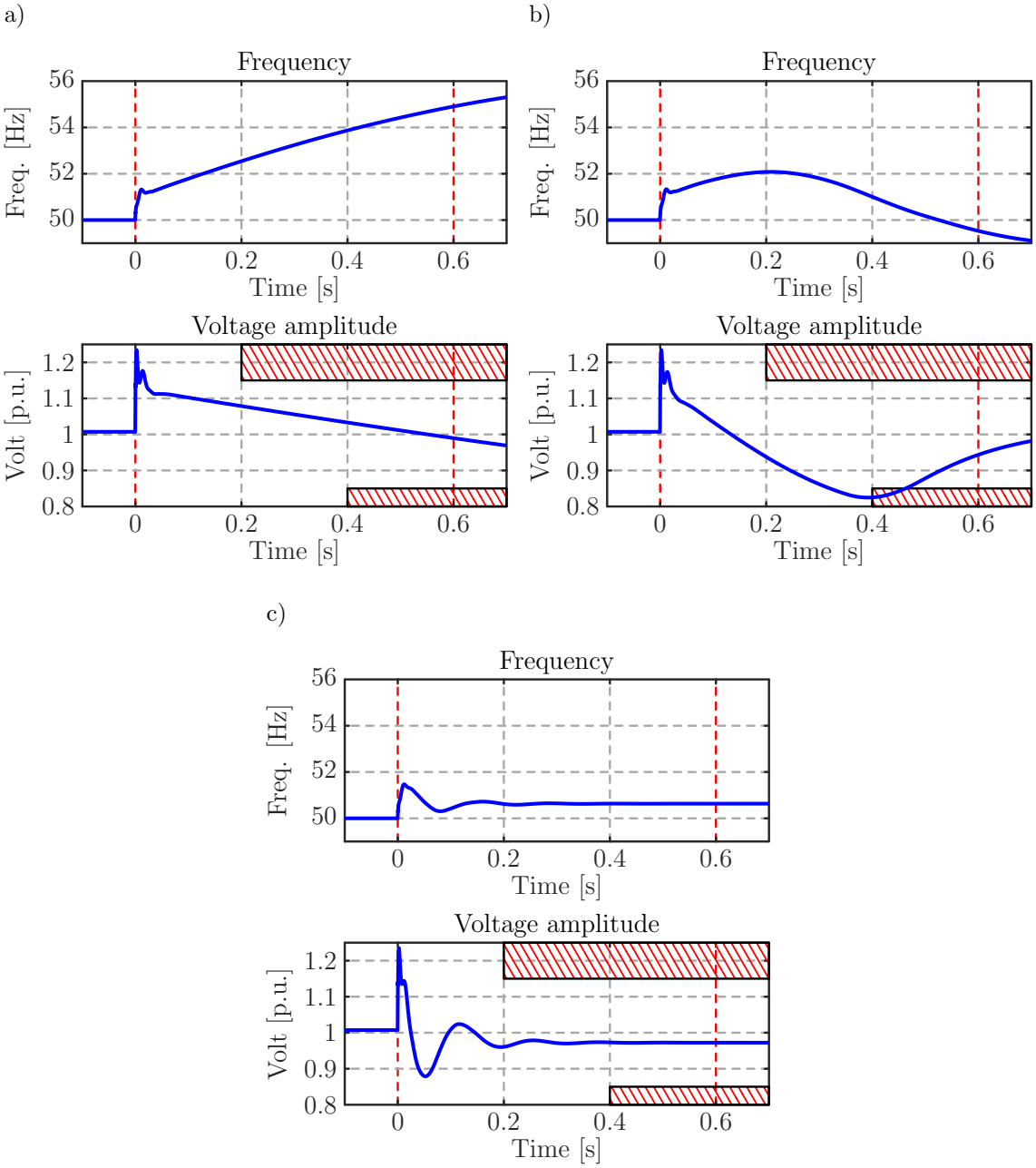

Figure 8.7: Test of Fig. 8.6 for $\Delta P = 0.29\,\text{p.u.}$ and $\Delta Q = -0.14\,\text{p.u.}$: examples of temporary islanded operation (simulation results) a) with $\tau_p = 5\,\text{s}$ and $\tau_q = 5.8\,\text{s}$; b) with $\tau_p = 1\,\text{s}$ and $\tau_q = 1.5\,\text{s}$ and c) with $\tau_p = 0.24\,\text{s}$ and $\tau_q = 0.35\,\text{s}$ (ΔP and ΔQ are normalized to the nominal load power) [29].

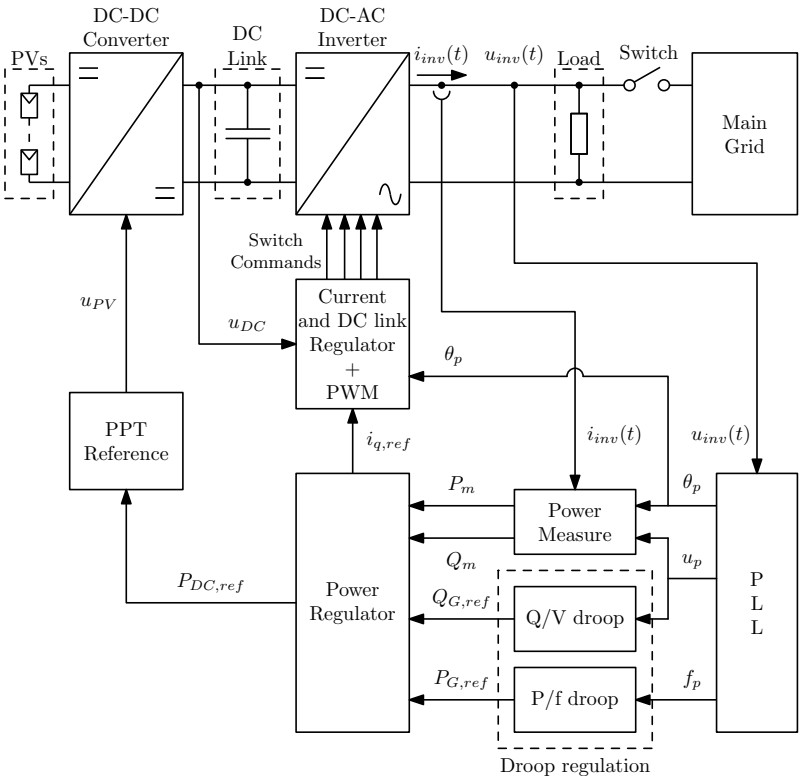

Figure 8.8: Inverter control structure with active and reactive power loops and P/f and Q/V droop regulation [26].

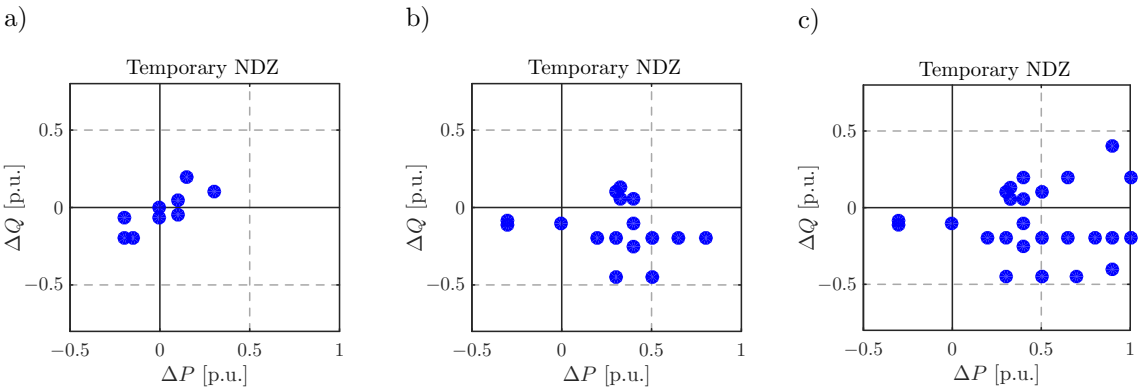

Figure 8.9: Experimental test results in the plane $\Delta P - \Delta Q$ with different response times of the droop characteristics: a) constant power references, b) $\tau_p = 5\,\mathrm{s}$ and $\tau_q = 7.5\,\mathrm{s}$ and c) $\tau_p = 2\,\mathrm{s}$ and $\tau_q = 3.5\,\mathrm{s}$; blue dot tests allow temporary islanding operations [29].

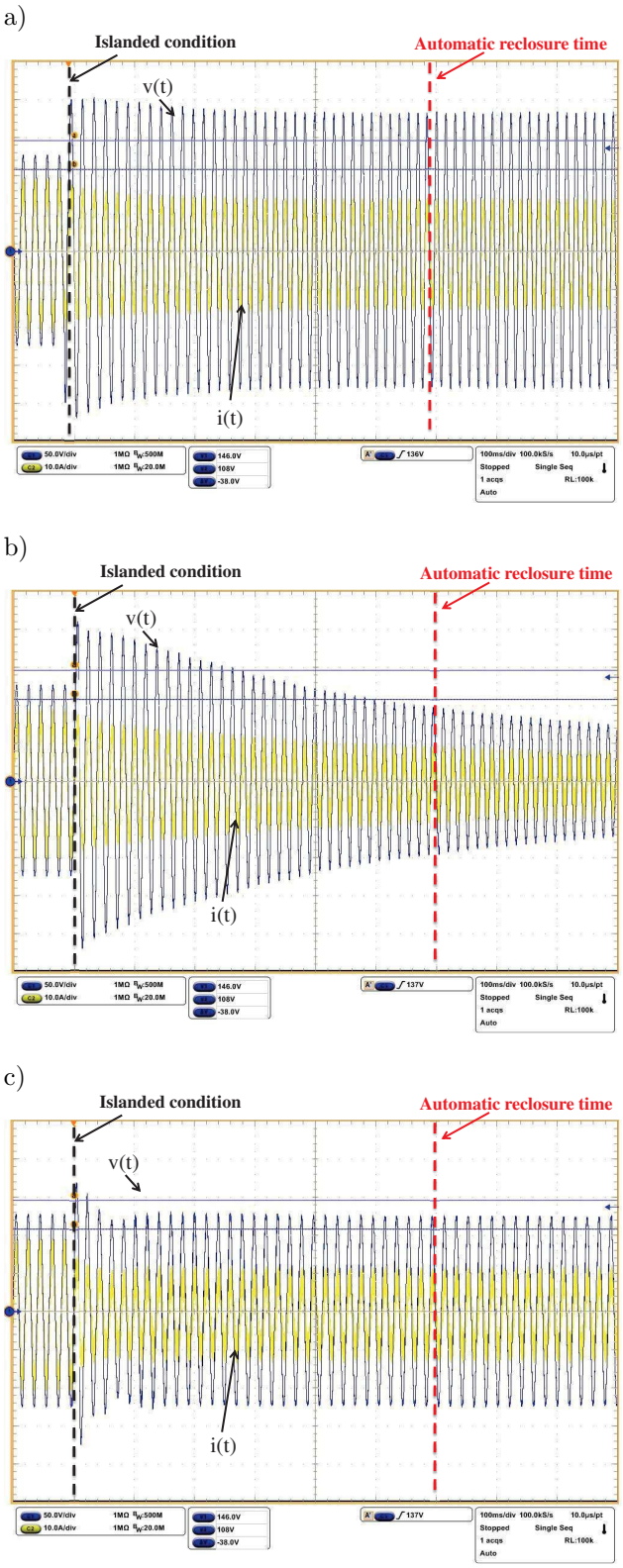

Figure 8.10: Test with $\Delta P = 0.9\,\text{p.u.}$ and $\Delta Q = -0.2\,\text{p.u.}$ of Fig. 8.9: examples of temporary islanded operation (experimental results) a) for constant power inverter, b) for droop control with $\tau_p = 5\,\text{s}$ and $\tau_q = 7.5\,\text{s}$ and c) for $\tau_p = 2\,\text{s}$ and $\tau_q = 3.5\,\text{s}$; $v(t) \rightarrow 50\,\text{V/div}$, $i(t) \rightarrow 10$ A/div, time $\rightarrow 100\,\text{ms/div}$ [29].

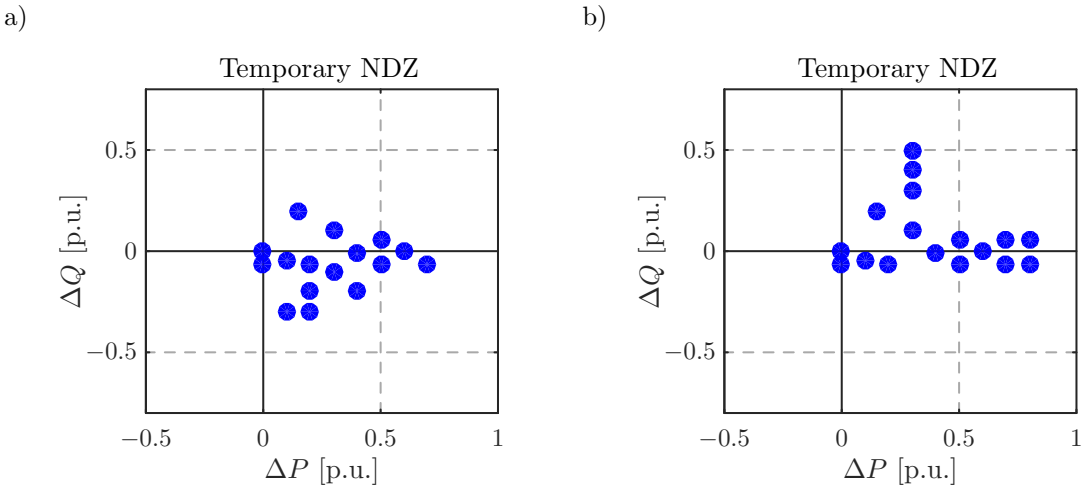

Figure 8.11: Experimental test results for the proposed control technique in order to reduce the NDZ in the plane $\Delta P - \Delta Q$ with different response times: a) $\tau_p = 5\,\mathrm{s}$ and $\tau_q = 7.5\,\mathrm{s}$ and b) $\tau_p = 2\,\mathrm{s}$ and $\tau_q = 3.5\,\mathrm{s}$; blue dot tests allow temporary islanding operations.

8.5 Conclusions

The proposed analysis gives an evaluation of the $\Delta P - \Delta Q$ region where temporary unintentional islanding can occur, the case of 600 ms automatic re-closure procedures is investigated. The analysis shows that the risk of temporary unintentional islanding increases introducing P/f or Q/V droop regulation to the control of DERs. Moreover, the speed of the P/f and Q/V droop functions has a strong impact on the $\Delta P - \Delta Q$ area: the faster the time responses, *potentially* the larger the risk of temporary islanding.

These results are shown by small-signal modeling, simulation and experimental validations. The understanding of the effects of droop characteristics and their time responses stated by the standards for PV connection is strongly advisable for the future generation of LV distribution grids with large penetration of renewable energy sources, providing insights on design criteria for the DER connections and on their settings.

Chapter 9

Active Anti-islanding Detection Method

This analysis refers to the complex scenario, where several photo-voltaic (PV) sources are connected to the medium and low voltage (MV and LV) distribution networks. Islanding detection methods are essential in the design of the inverter control strategies, with the role of recognizing the islanding conditions and disconnecting the islanded renewable energy resources (DERs). Islanding protection methods are classified into passive and active, where the passive ones detect the islanding operations setting thresholds on specific measured parameters as frequency and voltage amplitude, while the active methods are based on a particular inverter control designed to force a certain system parameter to drift once the islanding event occurs [42] [100]. Usually, manufacturers protect DERs from the unintentional islanding with active methods, which are not regulated by standards as they may be different for each manufacturer to another and they are not mandatory in all countries.

In this thesis an active frequency shift anti-islanding (AI) method has been considered, such as one of the most widely used in the DER inverter interfaced systems, in order to interrupt unintentional islanding operations. In particular, the Sandia frequency shift (SFS) active protection algorithm has been implemented in the embedded inverter control system. This active anti-islanding detection protection is characterized by a positive feedback that forces the frequency drifting in islanding conditions. It has been establishes a hardware in the loop (HIL) method to assess the interactions between active anti-islanding methods and grid codes requirements, as supporting functions in steady state conditions and even during fast transient, in order to understand and predict the behavior of interface protection system (IPS) and DER during islanding operations.

In order to simplify the analysis and study the interactions between the active anti-islanding method and the control actions of the PV inverters, the test-case shown in Fig.

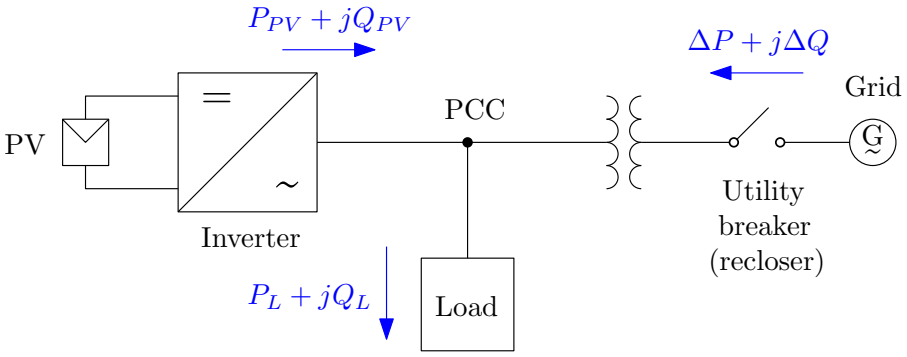

Figure 9.1: Test-case adopted to study unintentional islanding operations on a LV system composed by one PV unit, one local load and the main grid that provides the power mismatch ($\Delta P + j\Delta Q$) between the PV generation ($P_{PV} + jQ_{PV}$) and the load demand ($P_L + jQ_L$).

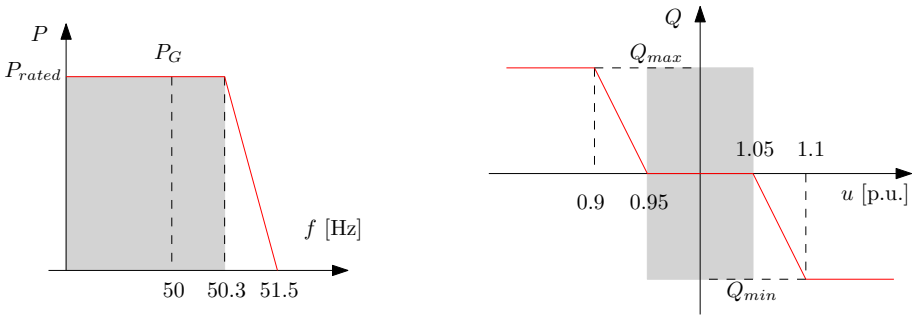

(a) Active power regulation P/f

(b) Reactive power regulation Q/V

Figure 9.2: Active and reactive power regulations stated by standards. These droop regulating actions modify the active power in (a) and reactive power in (b) of the inverter output set-point due to local frequency and voltage amplitude measurements.

9.1 has been adopted, where a PV three-phase inverter and a local load are considered.

In particular, the performance of the SFS method has been tested taking into account the load frequency dependence, as in chapter 6. It should be noted that this is not taken into consideration in the design of active methods such as the SFS method, which is tested on a parallel-connected RLC load, according to IEEE Std 1547-1 [39]. This resonant loading condition is assumed to be the worst case in terms of unintentional islanding detection. However, the loads connected at the distribution level present different characteristics in active and reactive power dependency on voltage frequency and amplitude, with dynamic behavior depending on the type, being residential, commercial or industrial [47] [48].

9.1 Sandia Frequency Shift Implementation

Chapter 6 addressed effects of power regulating actions (P/f, Q/V) during unintentional islanding, demonstrating a non-detection zone (NDZ) increase with respect to the case of

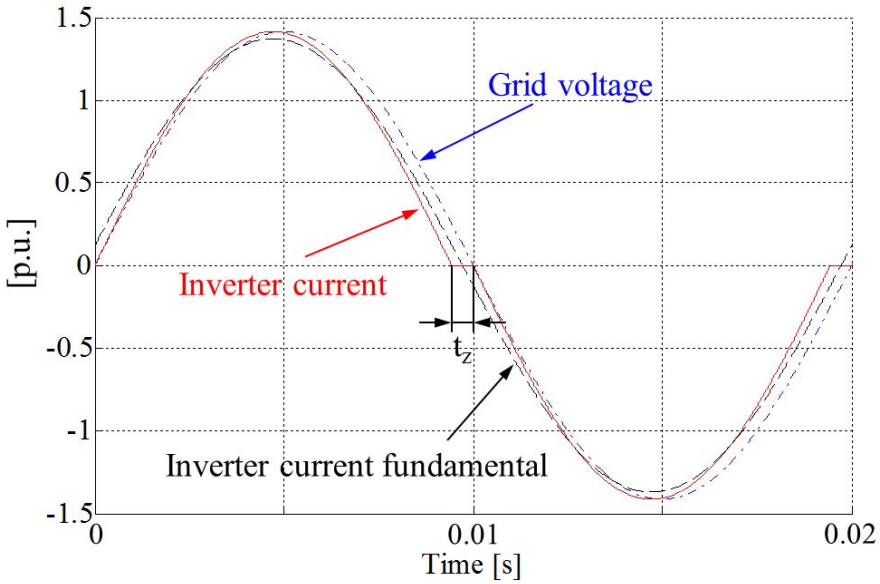

Figure 9.3: Inverter output current waveform using Sandia frequency shift anti-islanding method.

constant DER generation.

Here, the DERs SFS active anti-islanding protection is included in the unintentional islanding NDZ analysis. When the SFS is activated, the inverter injected current presents a slightly distorted waveform in order to drift the frequency outside the protection limits. As reported in Fig 9.3, the implementation of the SFS method is based on the use of a zero-current segment per semi-cycle for a time t_z, defined by:

$$t_z = \frac{1}{2}[(1/f) - (1/(f + \delta f))], \tag{9.1}$$

where f is the measured grid voltage frequency and δf is the difference between f and the actual frequency during the positive semi-cycle. In this implementation $\delta f = 1.5$ during grid-connected condition [48] [101].

The ratio between t_z and half of the grid voltage period T_v is referred as the chopping fraction cf, defined by:

$$cf = \frac{2 \cdot t_z}{T_v} = 2 \cdot f \cdot t_z. \tag{9.2}$$

The SFS introduces a positive feedback to increase the cf and t_z in order to destabilize the unintentional islanded system increasing the deviation of the frequency from the nominal value [101]. The chopping factor as a function of the voltage measured frequency

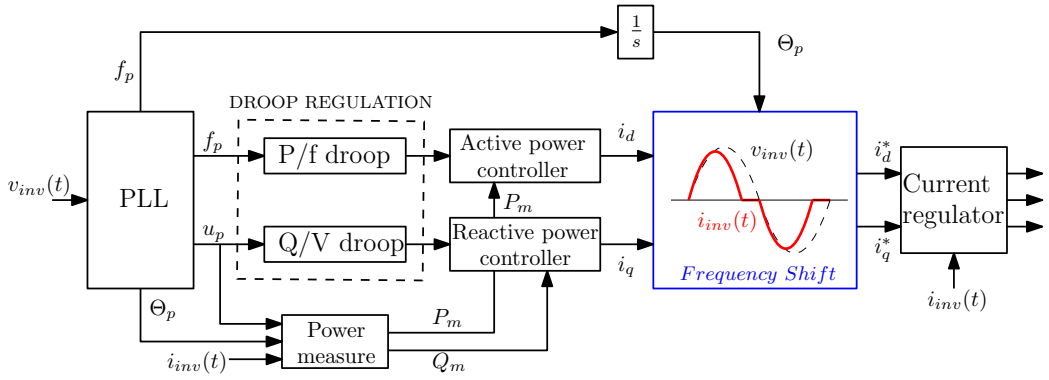

Figure 9.4: Inverter control scheme with active and reactive power loops based on the P/f and Q/V droop regulation and the SFS active anti islanding method.

is given by:

$$cf = cf_0 + k(f - f_0), \tag{9.3}$$

where cf_0 is the nominal chopping factor during the grid-connection , i.e. grid connected, and k is a gain factor which accelerates the frequency deviation in islanding operations; in this work we consider $cf_0 = 0.03$ and $k = 0.064$ in order to detect the islanding condition according the IEEE standard [39].

When islanding occurs in presence of a parallel RLC loading condition and a DER constant generated power, the SFS control algorithm increases the frequency of the output current as a consequence to maintain a constant chopping fraction. Therefore, the voltage follows the frequency variation, drifting outside the protection thresholds and the islanding condition can be detected [39].

The model of the DER inverter presented is compliant with the droop regulations P/f and Q/V required by the standard [57]. The inverter is equipped with an inner current loop ($\sim 1kHz$) and external active and reactive regulation loops in order to provide the correct power references imposed by the P/f and the Q/V functions. The inverter synchronization system with the grid voltage has been implemented using SRF-PLL (Synchronous reference frame - phase locked loop) system.

9.2 Inverter Regulation Speed Response

For the sake of investigation, the possibility to change the active and the reactive power regulation speed response has been considered demonstrating the importance of the speed regulation in terms of NDZ in presence of active anti-islanding protection. This implementation is relevant for the upcoming grid codes and standards requirements, because it shows the important role of the speed response of the inverter. As matter of facts, the lately introduced grid code requires an inverter regulation which is fast as technical feasible in order to support the power system stability. However, the following results show how this requirement plays negative role in terms of unintentional islanding risk allowing the presence of the protection NDZ even when an active anti-islanding method activated.

Two speed responses for active and reactive regulation have been selected to perform the analysis:

1. *"Slow regulation"*: $\tau_P = 2s$, $\tau_Q = 10s$,
2. *"Fast regulation"*: $\tau_P = 0.5s$, $\tau_Q = 1.1s$,

where τ_P and τ_Q are the settling time of active and reactive power regulations on a 1 p.u. step variation of the power set-point values, calculated in grid connected conditions.

The τ_P, τ_Q of the *"Slow regulation"* have been selected because they represent the maximum limit conditions imposed by standard [57]. Meanwhile, the *"Fast regulation"* is an arbitrary faster regulation.

The active SFS anti-islanding protection has been implemented in the current loop of the inverter control scheme, as shown in Fig. 9.4. The SFS chopping factor, reported in (9.3), modifies the angle θ_P of the PLL system. This implementation is based on the zero-current segment per semi-cycle introduced in the dq current components, which allows the frequency shift and the detection of the islanding operation in the test-bench conditions required by IEEE standard [39].

9.3 Case Study: Droop function and SFS Interfaced With a Real Protection System in HIL Simulations

The possible interactions between P/f and Q/V droop regulating functions and the SFS active anti-islanding detection method are analyzed using four case studies:

Case I) *"Slow regulation"* droop functions and SFS disabled;

Case II) *"Slow regulation"* droop functions and SFS enabled;

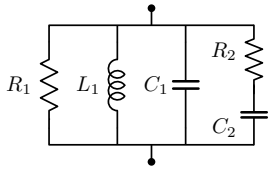

Figure 9.5: Load used for the HIL simulation setup.

Case III) *"Fast regulation"* droop functions and SFS disabled;

Case IV) *"Fast regulation"* droop functions and SFS enabled.

Thus, the importance of the power regulation speed response is addressed comparing the test case I with case III and case II with case IV. The analysis has been carried out with hardware in the loop (HIL) simulations, where an employed setup comprises the real time simulator OP4500 by OPAL-RT, a signal amplifier in and a commercial IPS.

The model of PV-based DER unit is implemented with active and reactive power control logics, based on the regulating droop functions stated by the standards, and on an embedded three-phase SRF-PLL synchronization system [20, 57]. The models presented have been validated comparing to lab-scale tests, using the same configurations and control schemes. Thus, it proposes an investigation on a suitable platform to analyze the active anti-islanding protection system and the DER control actions interfaced with a real IPS.

The general analysis, presented in this chapter, is suitable for a generic local load with active and reactive power dependencies on voltage amplitude and frequency $P_L(f, u)$ and $Q_L(f, u)$. In this work, we consider a local load that consists of a set of passive components, as shown in Fig. 9.5.

The load is represented by a parallel-connected RLC in parallel with a series-connected RC, as described in chapter 6.

9.4 Simulation Results

The HIL tests report important results in the investigation of the droop regulating functions role in presence of the active anti-islanding SFS protection. Results of Fig. 9.6 shows that the combination of P/f and Q/V regulations and control speed response may cancel the effect of the SFS protection.

The comparison among of results reported in Fig. 9.6a and 9.6b shows that the active anti-islanding protection efficiency in the islanding detection in case of *"Slow regulation"* of the inverter control system. In case I of Fig. 9.6a, the droop regulation allows the inverter to change its power references. Therefore, it is possible to create a matching of

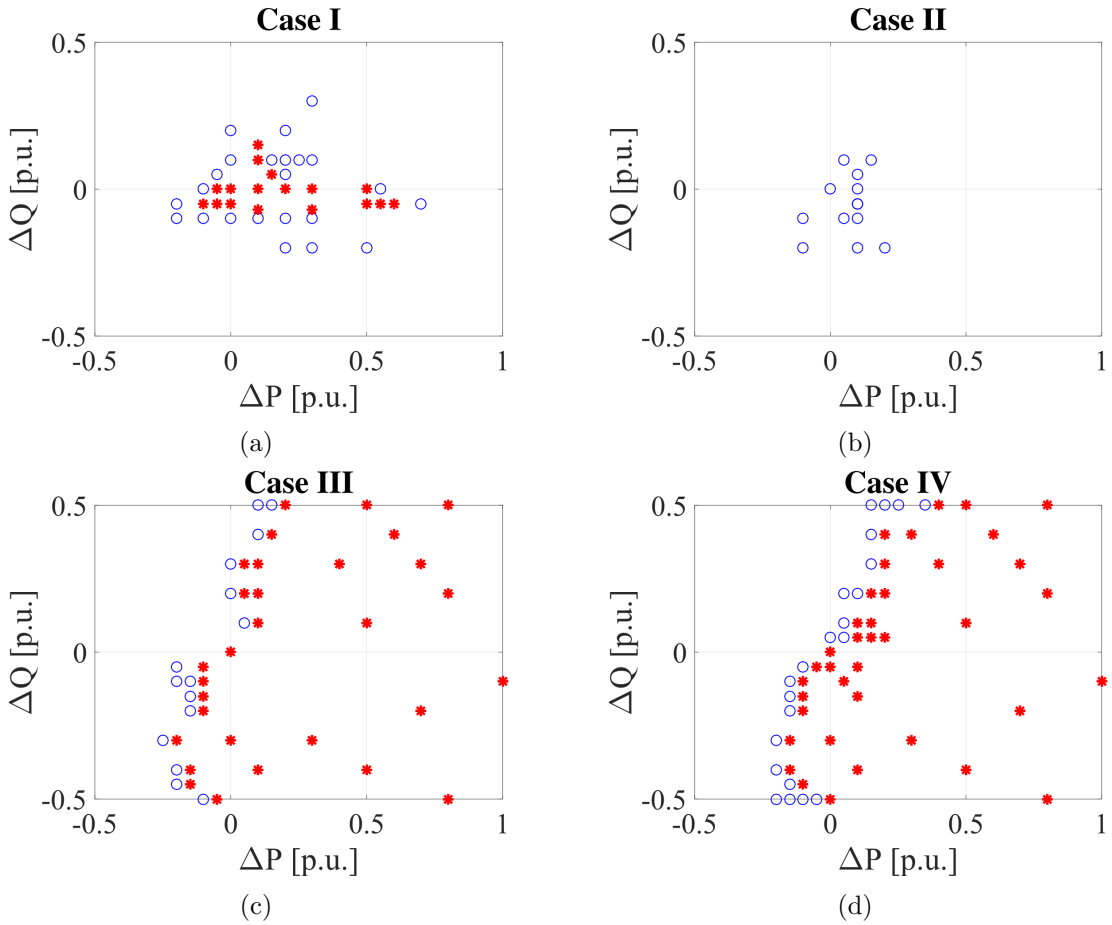

Figure 9.6: NDZ cases in which the " $*$ " symbols represent an permanent unintentional islanding condition, while the " $\circ$ " symbols represent the intervention of the IPS. (a) NDZ with *"Slow regulation"* droop functions and SFS disabled; (b) NDZ with *"Slow regulation"* droop functions and SFS enabled; (c) NDZ with *"Fast regulation"* droop functions and SFS disabled; (d) NDZ with *"Fast regulation"* droop functions and SFS enabled.

power generated and absorbed by the load without the tripping of the IPS. Using the droop regulations as grid supporting functions, the NDZ of the IPS is compromised with multiple cases of unintentional islanding operations, depending on the speed response of the inverter control power loops as shown comparing results of Fig. 9.6a to Fig. 9.6d.

From the case of sensible NDZ size of Fig. 9.6a, the activation of the SFS ensures a frequency deviation, which allows the intervention of IPS, preventing any permanent unintentional islanding operation. This is due to the difference between the control speed regulation of the inner current loop and the external power loops, which allows the SFS action before the intervention of the P/f and Q/V functions.

The main focus is related to the important result reported in Fig. 9.6d, in which SFS

active anti-islanding protection and the droop regulations have been activated and, in particular, the speed response of the power control are set as *"Fast regulation"*.

In this conditions, the combination of the P/f and Q/V functions and *"Fast regulation"* cancels the SFS function of detecting the islanding condition forcing a frequency drift. To explain this behavior, we considered the fundamental component of the distorted inverter output current which leads the voltage (if unity power factor) by the angle Φ_{SFS} [24], given by:

$$\Phi_{SFS} = -\frac{\pi}{2}[cf_0 + k(f - f_0)]. \tag{9.4}$$

Therefore, the SFS protection changes the current angle Φ_{SFS} depending on the frequency value. The change of Φ_{SFS} due to frequency variations causes active and reactive power deviations, which are compensated by the *"Fast regulation"* droop functions. Therefore, the NDZ size reported in Fig. 9.6d is slightly changed from the case III in Fig. 9.6c, where the SFS is deactivated. Only few tests have changed their status from islanded to detected.

As shown in Fig. 9.7, the introduction of the SFS in the inverter control scheme may not be the solution in unintentional islanding detection in presence of *"Fast regulation"* droop functions. This figure shows the islanding transients of a particular power unbalance condition: $\Delta P = 0.05$ p.u. and $\Delta Q = -0.1$ p.u. It also reports the signal $Start_{IPS}$, which is the feedback signal of the real IPS of the HIL setup. The $Start_{IPS}$ is set to zero if the IPS does not detect the voltage amplitude and frequency out of the standard limits. At the instant that one threshold triggered, the IPS generates a sinusoidal $Start_{IPS}$ signal (50 Hz), and, after the required tripping time the protection, will disconnect the inverter.

In Fig. 9.7a, the islanding is detected by the IPS due to an under voltage transient and the DER is disconnected. Besides, in Fig. 9.7b, the same initial conditions ($\Delta P - \Delta Q$) are applied, but the phase shift introduced by the SFS is compensated by the *"Fast regulation"* droop functions allowing the islanding operation and the IPS does not have the possibility to disconnect the inverter.

Therefore, the positive feedback introduced by the implemented anti-islanding algorithm is compensated by the *"Fast regulation"* of the droop functions, which have been conceived to support the grid stability.

The leaking of regulation and standardization on the active protection methods do not help the unintentional islanding detection. Therefore, a coordination between the regulation droop functions P/f and Q/V and protection system is needed.

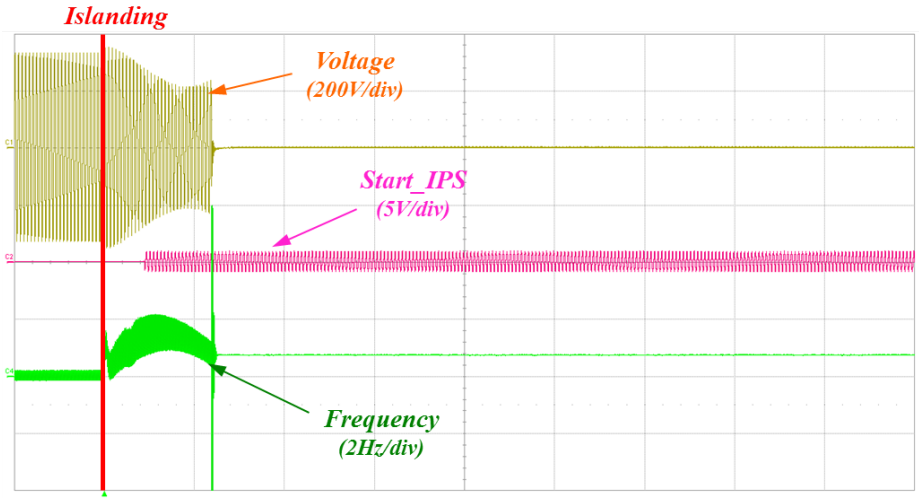

(a) Case II: *"Slow regulation"* with SFS

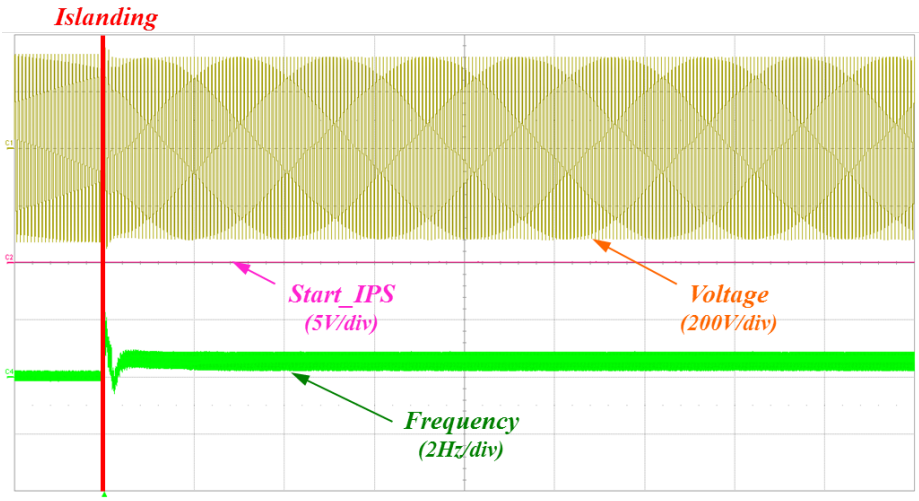

(b) Case IV: *"Fast regulation"* with SFS

Figure 9.7: Role of the speed response of the inverter power regulations combined with the SFS anti-islanding protection in the HIL test $\Delta P = 0.05$ and $\Delta Q = -0.1$. (a) *"Slow regulation"* of the droop functions P/f and Q/V and SFS enabled; (b) *"Fast regulation"* of the droop functions P/f and Q/V and SFS enabled. ($Voltage$ = 200 V/div, $Start_{IPS}$ = 5 V/div, $Frequency_{PLL}$ = 2 Hz/div, time = 500 ms/div).

9.5 Conclusions

The results presented describe the complex scenario of the increasing penetration of DER units and as consequence the unintentional islanding probability. Indeed, the active AI algorithm implemented is not always sufficient to detect the islanding conditions and the inverter is not disconnected by the IPS.

A critical aspect in the unintentional islanding detection is a coordination between the speed regulation of the droop functions and the active AID protection system. The

reason of this analysis is to emphasize the importance of a standardization of protection and regulation functions, in particular with the speed response of the P/f and Q/V droop functions. The speed of active and reactive power regulation seems to be a key factor on the sizing of the unintentional islanding NDZ in general, with or without the active SFS protection.

Therefore, the results offer a view of a possible scenario that needs new certification procedure and connection rules for upcoming guidelines and standards.

Chapter 10

Multiple Inverter Case

The following analysis addresses on the possible interaction between two distributed renewable resources (DERs). This chapter addresses the role of the power regulation speed in a more complex scenario respect to the previous chapters. Two inverters are considered in order to better understand some basic phenomena in the distribution electrical network, where many different DER are connected. Each distributed generator affects network behavior and dynamics depending on the specific control algorithms designed by manufacturers. Thus, DERs influence in different way the distribution network, due to the diversity of manufacturers implementations. Moreover, the adoption of active anti-islanding (AI) techniques is not always mandatory and not all the inverters may be equipped with such techniques.

The single phase equivalent diagram of the test case is reported in Fig. 10.1, where two low voltage three-phase PV inverters are connected at the same PCC bus in parallel to a local load and the main grid.

In this investigation, a local load described in chapter 6, has been considered with reference to Tab. 6.1. It is a parallel connection of a resistor R_1, an inductor L_1, a capacitor C_1 and a resistive-capacitive series (R_2 and C_2), and it introduces power dependencies $P_L(f, u)$ and $Q_L(f, u)$ similar to the ones of residential loads. The load selection is also due

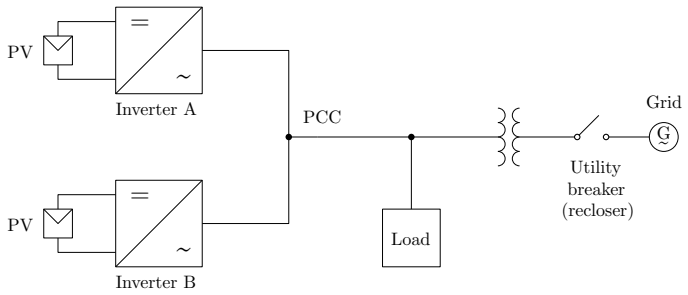

Figure 10.1: Unintentional islanding operation on a basic LV system composed by two PV units, one local load and the main grid.

to HIL simulations purpose, because it replicates the hardware experimental laboratory setup. Therefore, since being the hardware experimental load a composition of such passive components, the same load condition is replicated in the HIL test case model (shown in Fig. 10.1) in order to deal with unintentional islanding operations with dynamic and steady-state behavior equal to the experimental setup.

10.1 Different Power Regulation Speed

This section describes the case study presented in Fig. 10.1, where two low voltage three phase inverters are connected to the distribution network. The different share of the two inverters' generated power plays a relevant role on the sizing of the protection NDZ. Inverter A and B adopt the same control scheme described in chapter 5.2.

They are required to regulate the output power using both the droop functions P/f and Q/V, as stated by the Italian standard [57]. The anti-islanding method is based only on the passive over/under frequency (OUF) and over/under voltage (OUV) protections of the IPS. However, the two inverters, power control closed-loops have been designed with different bandwidths in order to analyze the role of the power regulation speed considering a distribution network where different DER with different control speed implementation are connected.

The reason of this investigation is that the speed response is not considered to be a problem in the standard anti-islanding requirements. The grid code requires DERs to perform as fast as technical feasible the droop power regulations and also the Italian standard do not consider the possible negative effects during unintentional islanding. Only a maximum settling time ir required for the regulation. Thus, how fast the inverter action will be depends solely on the manufacturer.

This analysis proposes two different regulation power speeds, as described in chapter 9:

- *Inverter A*: the so called *slow regulation*, which performs the P/f and Q/V droop functions within the maximum allowed settling time stated by the Italian standard ($\tau_P = 2s$, $\tau_Q = 10s$) [57];
- *Inverter B*: the so called *fast regulation*, arbitrarily faster than the *Inverter A* ($\tau_P = 0.5s$, $\tau_Q = 1.1s$);

where τ_P and τ_Q are the settling time of active and reactive power regulations on a set-point step variation in grid connected conditions. The tests have been carried out with the same load conditions and varying the share of generated power of each inverter, as reported in Tab. 10.1. Five cases have been analyzed so that different levels of grid diffusion of inverter type B (*fast regulation*) can be investigated.

Table 10.1: Two inverter test-case: share of total power generated.

	Active power share [%]				
	Case I	Case II	Case III	Case IV	Case V
Inverter A	100	90	65	30	0
Inverter B	0	10	35	70	100

The Case I and V represent the two opposite scenarios: 1) (Case I) all the generation on the distribution network is based on inverters with power regulation speed adjusted at the maximum settling time accepted by the standard [57]; 2) (Case II) all the DER inverters are designed fast as possible [19, 20, 59].

Important results are presented in Fig. 10.2 reporting the main role of the regulation speed, in case of an increase share of total power generated by the Inverter B with the fastest regulation. Unintentional islanding NDZ is highly influenced by the presence of inverter B (designed with *fast regulation* of the droop function P/f and Q/V). Moreover, in particular in case III the 35% of generation is based on the inverter B and the NDZ is about twice the size compared to Case I.

Finally, results reported in Fig. 10.2 are congruent with the experimental results in chapter 6, which describes how increasing the power regulation speed maximizes the NDZ. Here the same effect is obtained increasing the amount of generated power with *fast regulation* droop functions.

10.2 Different Regulation Speed with the Active Anti Islanding Method

The role of the active AI methods, based on the Sandia frequency shift (SFS) has been presented in chapter 9, and the results indicate that the SFS method could be beneficial for reducing the unintentional islanding issue. As a matter of fact, the specific case of adopting this anti-islanding algorithm combined with the design of a "slow "inverter control presents a null NDZ, meaning that any permanent unintentional islanding operations are detected. Reasonably, the combination of SFS method with *slow regulation* drop functions (P/f and Q/V) can be assumed as an efficient method to prevent islanding events. Hence, the following analysis is based on two different inverter control implementations:

- *Inverter A*: power closed-loop designed with *slow regulation* ($\tau_P = 2s$, $\tau_Q = 10s$ [57]) combined with SFS anti-islanding method;

- *Inverter B*: power closed-loop designed with *fast regulation* ($\tau_P = 0.5s$, $\tau_Q = 1.1s$) without active anti-islanding functions;

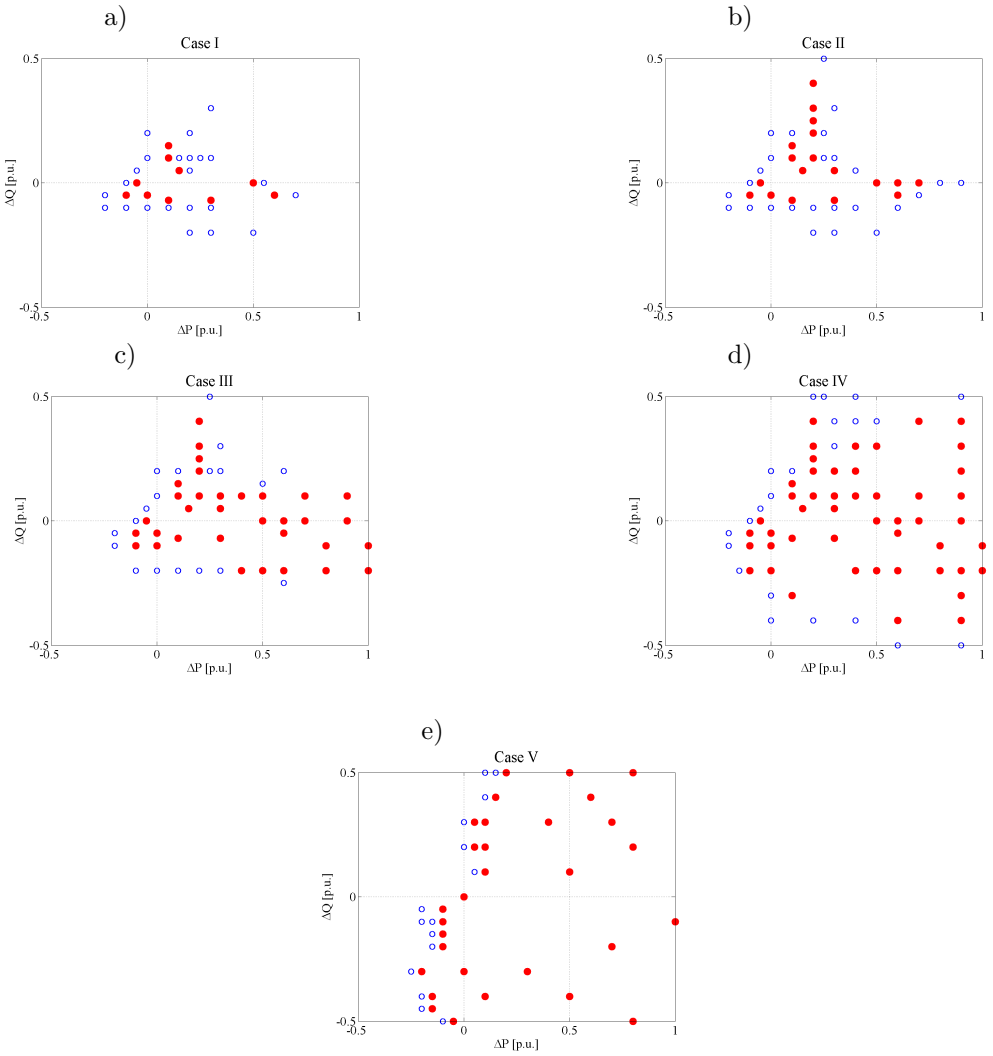

Figure 10.2: Non detection zone of the two inverter case: Inverter A (power regulation $\tau_P = 2s$, $\tau_Q = 10s$) and Inverter B (power regulation $\tau_P = 0.5s$, $\tau_Q = 1.1s$); active power share of the inverter B a) 0% b) 10 c) 35% d) 70% e) 100%.

where τ_P and τ_Q are the settling time of active and reactive power regulations. In this scenario the possible iterations between *fast regulation* and active anti-islanding protection are addressed changing the sharing of the total power generated between inverter A and B, as shown in Tab. 10.2.

This analysis concerns to the complex case of DERs integration in a distribution network of several inverters with different dynamic and AI methods. The Fig. 10.3a shows how the SFS with a *slow regulation* basically eliminates the NDZ, whereas making the 25% of the generation from the inverter B, the NDZ increases (10.3c), and adding more *fast regulation* power the NDZ reaches the same limits of a system without the active SFS methods, as presented in chapter 9.

Table 10.2: Two inverter test-case: share of total power generated

	Active power share [%]						
	Case I	Case II	Case III	Case IV	Case V	Case VI	Case VII
Inverter A	100	90	75	50	35	20	0
Inverter B	0	10	25	50	65	80	100

10.3 Conclusions

The fast droop regulations required in some grid codes may play a detrimental role in terms of unintentional islanding, even in presence of active anti-islanding protections. The amount of *fast regulation* droop functions P/f and Q/V needed to a NDZ relevant size, is less than the 30%. Therefore, high level of speed regulation may compensate the active AI methods.

These results highlight the lack of coordination on the standards requirements. More precisely, the main player in the unintentional islanding is the power regulation speed, which should be taken in consideration in the upcoming grid codes and standards in order to avoid unexpected compensation of anti-islanding methods.

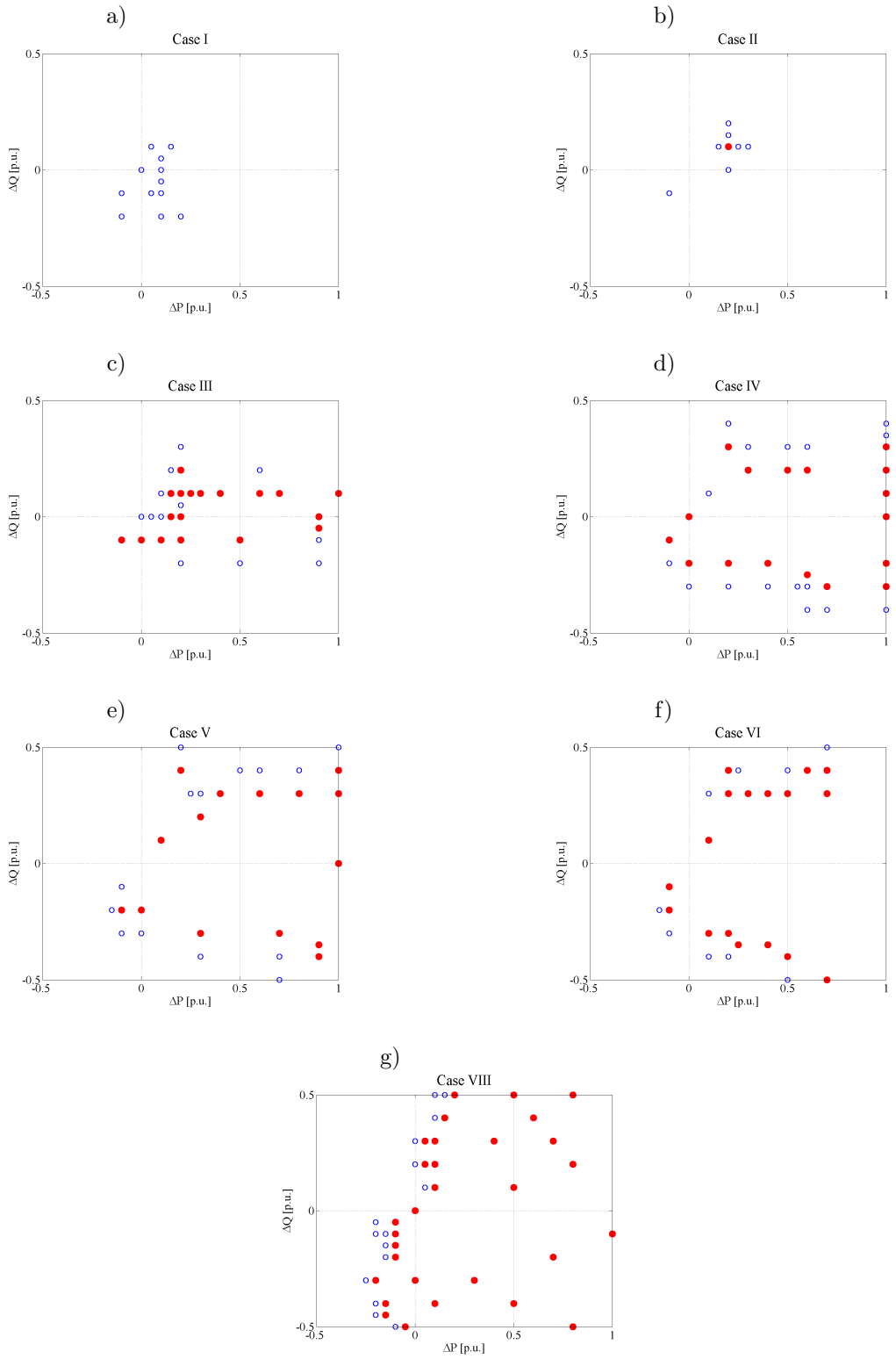

Figure 10.3: Non detection zone of the two inverter case: Inverter A (power regulation $\tau_P = 2s$, $\tau_Q = 10s$ and SFS activated) and Inverter B (power regulation $\tau_P = 0.5s$, $\tau_Q = 1.1s$); active power share of the inverter B a) 0% b) 10 c) 25% d) 50% e) 65% f) 80% g) 100%.

Chapter 11

Conclusions

The diffusion of renewable distributed energy resources (DERs), such as photovoltaic and wind energy sources, is continuously increasing and changing the structure and operation of the Medium and Low Voltage (MV and LV) distribution networks. Several factors, as technological advances, social changes and policy goals, are driving a transformation from centralized systems to more-complex systems that comprise a growing number of decentralized generating units. Residential environments have experienced one of the most relevant growth of distributed-generation power systems. Most of low-power DER units consist of power electronic converters with limited number of sensors and communication capabilities, increasing the complexity of the network management and operation for the Distribution System Operator (DSO).

This complex scenario has also influenced the latest grid code requirements for DER units. In fact, European standards state the reference technical rules for the DER connection in order to ensure the power quality and stability of distribution and transmission electric systems. Standards state DER requirements for grid connection under normal and transient conditions of the electric system. Moreover, many standard bodies require that distributed generators have to play an active role in the system stability by participating to the ancillary services of active and reactive power regulation. More precisely, many standard bodies require that DER units provide active and reactive power (P/f and Q/V) regulation characteristics. Another relevant modification is the wider frequency range that is allowed during normal operation of DER units, from the traditional thresholds (49.7 Hz and 50.3 Hz) to the less stringent values (47.5 Hz and 51.5 Hz), and at the same time, permissive voltage levels are in a range of $\pm$ 15 % of the rated voltage.

The proliferation of such systems combined with the new technical rules has led to an increasing concern about the problem of unintentional islanding on distribution networks, defined as a portion of the utility system containing both loads and DER units that remains energized while it is disconnected from the main grid. Islanding, even for very

short time, is undesirable, as the voltage on the islanded portion can drift respect to the one of the main grid, with a risk of damage in the electric equipment during the automatic grid reconnection. Therefore, islanding detection methods are essential in the design of the inverter control strategy, with the role of recognizing the islanding conditions and disconnecting the islanded DER unit.

The unintentional islanding issue has been addressed in several studies and publications over the last decades. However, the literature research is lacking of considering the lately introduced European standards and technical specifications for DERs. This thesis describes the novel aspects of how requirements and ancillary services influence the unintentional islanding operations. Moreover, the presented study highlights new relevant factors on this topic, such as the role of the loads characteristics, the influence of the frequency measure and the inverter regulation speed.

Several analytical, numerical and experimental tools have been adopted in order to comprehensively study the different aspects of the unintentional islanding issue. This has been analyzed via small-signal modeling, simulations, experimental validations and hardware in the loop (HIL) simulations.

The main results of this PhD thesis describe the complex scenario of the increasing penetration of DER units and the conclusions highlight several factors influencing the non detection zone (NDZ) of the anti-islanding protection system.

The NDZ describes the unbalance conditions between DERs and local loads ($\Delta P - \Delta Q$ area) when unintentional islanding can occur, which depend by the load and source characteristics. In particular, the different dynamic response of the loads highly influences the behavior of the phenomena. Thus further investigations on the dynamic characterization of loads (active and reactive variation function of voltage amplitude and frequency, inertia, etc.) should be carried out in order to achieve sufficient level of details. The presented analysis of the NDZ is general and it can be applied to generic local loads, whose active and reactive power dependencies are known. This approach differs from the majority of literature works, which promote the NDZ analysis on a resonant parallel connected RLC load, considered the worst case in terms of islanding detection, but it does not represent the behavior of distribution networks loads. Therefore, different effects are expected with real loads, especially when the inverter regulating functions are activated. With regards to generators, different generator capabilities strongly influence the system behavior. The work has reported an analytic approach in order to draw the NDZ $\Delta P - \Delta Q$ areas of permanent unintentional islanding, which has been confirmed by experimental verifications on a lab-scale prototype. The proposed investigation shows that the risk of permanent unintentional islanding increases introducing P/f or Q/V droop regulations to the control of DERs and that the $\Delta P - \Delta Q$ area widens more including both the P/f and Q/V droop

regulations, rather than only one of them. Thus, the non-simultaneous operation of P/f and Q/V seems to be a possible effective approach to reduce the NDZ, for example disabling the Q/V function under over-frequency operation conditions. Hence, in setting or revising future grid code standards for distribution grids with large penetration of renewable energy sources, understanding of the stabilizing effects of droop control in islanded operation is of paramount importance in order to provide insights on design criteria for the DER connections and on settings of P/f and Q/V droop functions parameters. From Distribution System Operators (DSOs) perspective, this type of analysis would represent a powerful planning criteria to evaluate DER connections to distribution networks and to identify proper settings and activation delays (even complete deactivation) of P/f and Q/V droop functions and, possibly, other regulation laws.

The work has also proposed an assessment of the $\Delta P - \Delta Q$ area where temporary unintentional islanding can occur, i.e. below the 600 ms for automatic re-closure procedures. Moreover, the speed of response of the P/f and Q/V droop functions imposed by standards to DER generators enlarges the $\Delta P - \Delta Q$ area: faster time responses potentially increase the risk of temporary islanding.

In a scenario with large diffusion of single-phase DERs, the single-phase PLL (Phase locked loop) important role sustaining islanding conditions compared with a typical three-phase PLL, has been investigated. The investigation was focused on the single-phase SRF-PLL (Synchronous reference frame - phase locked loop) with orthogonal component calculated by a fixed filter at nominal condition (e.g. 50 Hz), which is still a popular solution adopted by manufacturers. However, different single-phase PLL models may leads to two different conclusions, clearly indicating that future investigations of the role of PLL algorithms would be useful to follow up the presented analysis. Since the size of the $\Delta P - \Delta Q$ NDZ results not negligible.

None of the previous literature works have investigated the effect of combining the droop functions and the active anti-islanding methods on the physical interface protection system (IPS) during unintentional islanded conditions. In this work, an active frequency shift anti-islanding method is considered, which is the most widely used in the DER inverter interfaced systems in order to interrupt unintentional islanding operations. Thus, the Sandia frequency shift (SFS) active protection algorithm has been implemented in the embedded inverter control system. Results show that the active anti-islanding algorithm implemented is not always sufficient to detect the islanding conditions and the inverter is not disconnected by the IPS. A crucial aspect in the unintentional islanding detection is a coordination between the speed regulation of the droop functions and the active protection system. In fact, using as fast as technically feasible power regulations the active anti-

islanding method considered in this study, can be compensated and thus failing to detect the unintentional islanding operations. The reason of this analysis is to emphasize the importance of a standardization of protection and regulation functions, in particular with the speed response of the P/f and Q/V droop functions. The speed of active and reactive power regulation seems to be a key factor on the sizing of the unintentional islanding NDZ in general, with or without the active SFS protection.

Such standardization would be of paramount importance to ensure the necessary coordination between IPS, the active anti-islanding method and of P/f and Q/V DER inverter functions and, in general terms, to enable the Distributor System Operator (DSO) to predict how the large diffusion of DERs in the distribution grids would affect the unintentional islanding and other transient phenomena.

11.1 List of publications

The research activity discussed in the previous chapters led to several international conference publications and journal papers, as listed below.

Journal papers

J.1 R. Sgarbossa, S. Lissandron, P. Mattavelli, R. Turri and A. Cerretti, "Analysis of $\Delta P - \Delta Q$ Area of Uncontrolled Islanding in Low-Voltage Grids With PV Generators," in IEEE Transactions on Industry Applications, vol. 52, no. 3, pp. 2387-2396, May-June 2016.

Conference papers

C.1 R. Sgarbossa, S. Lissandron, P. Mattavelli, R. Turri, A. Cerretti," Analysis of Unintentional Islanding in low-voltage grids with PV generators" IEEE COMPEL'14, June 2014, Santander.

C.2 F. Amadei, A. Cerretti, M. Coppo, P. Mattavelli, R. Sgarbossa, R. Turri, "Temporary islanding operations of MV/LV active distribution networks under fault conditions" 2014 Power Engineering Conference (UPEC), September 2014.

C.3 R. Sgarbossa, S. Lissandron, P. Mattavelli, R. Turri, A. Cerretti," Analysis of $\Delta P - \Delta Q$ area of uncontrolled islanding in low voltage grids with PV generators " IEEE Energy Conversion Congress and Exposition (ECCE), September 2014, Pittsburg (USA), pp. 5667- 5674.

C.4 A. Cerretti, L. D'Orazio,C. Pezzato, G. Sapienza, G. Valvo, N. Cammalleri, P. Mattavelli, R. Sgarbossa, R. Turri, E. De Berardinis, "Uncontrolled islanding operations

of MV/LV active distribution networks," in PowerTech, 2015 IEEE Eindhoven , vol., no., pp.1-6, June 29 2015-July 2 2015.

C.5 P. Mattavelli, R. Sgarbossa, R. Turri, G. Sapienza, G. Valvo, C. Pezzato, A. Cerretti, E. Berardinis, " Generators and loads models to investigate uncontrolled islanding on active distribution networks", CIRED, 2015 23rd International Conference and exhibition on Electricity Distribution , June 2015.

C.6 S. Lissandron, R. Sgarbossa, L. Dalla Santa, P. Mattavelli, R. Turri, A. Cerretti, "Impact of non-simultaneous P/f and Q/V grid code requirements on PV inverters on unintentional islanding operation in distribution network," in Power Electronics for Distributed Generation Systems (PEDG), 2015 IEEE 6th International Symposium on , vol., no., pp.1-7, 22-25 June 2015.

C.7 R. Sgarbossa, L. Dalla Santa, P. Mattavelli, A. Petucco, F. Cavazzana, A. Cerretti "Phase-Locked Loop Effect on Non-Detection Zone of Unintentional Islanding" in 17th Conference on Power Electronics and Applications, EPE'15-ECCE Europe, Geneva, 8th to 10th September 2015.

C.8 S. Lissandron, R. Sgarbossa, L. Dalla Santa, P. Mattavelli, R. Turri, A. Cerretti,"$\Delta P-\Delta Q$ Area Assessment of Temporary Unintentional Islanding with P/f and Q/V Droop Controlled PV Generators in Distribution Networks" IEEE Energy Conversion Congress and Exposition (ECCE), September 2015, Montreal (CDN).

C.9 L. Cocchi, A. Cerretti, E. Deberardinis, F. Bignucolo, A. Savio, R. Sgarbossa, "Influence of average power factor management on active distribution networks" CIRED, 2015 23rd International Conference and exhibition on Electricity Distribution, Lione, June 2015, Paper 634.

C.10 A. Savio, F. Bignucolo, R. Sgarbossa, P. Mattavelli, A. Cerretti and R. Turri, "A Novel Measurement-based Procedure for Load Dynamic Equivalent Identification", 1st Int. Forum on Research and Technologies for Society and Industry (RTSI), Torino, 16-18 Sep. 2015.

C.11 R. Sgarbossa, L. Dalla Santa , P. Mattavelli, R. Turri, A. Cerretti , "Analysis of interface protection system with Distributed Energy Resources compliant with the most recent grid codes: the Unintentional Islanding case" PES General Meeting, Boston, 16-21 July 2016.

C.12 R. Sgarbossa, L. Dalla Santa , P. Mattavelli, R. Turri, A. Cerretti , "Effects of P/f and Q/V Regulations on Anti-islanding Detection Methods in Distribution Networks " ISGT Europe, Ljubljana, 2016.

Bibliography

[1] U.S. Energy Information Administration, *International Energy Outlook 2016*, May 11, 2016.

[2] T. Randall, "Fossil fuels just lost the race against renewables," *Bloomberg*, April 14, 2015.

[3] Angus McCrone, Ulf Moslener, Francoise d'Estais, Eric Usher and Christine Grüning, *Global Trends in Renewable Energy Investment 2016*. FS-UNEP Collaborating Center for Climate and Sustainable Energy Finance, March, 2016.

[4] International Energy Agency, *Key World Energy Trends. Excerpt from: World energy balances*, 2016.

[5] REN21 Renewable Energy Policy Network for the 21st Century, *Renewables 2016 Global Status Report*, 2016.

[6] T. SpA, "Dati statistici sull'energia elettrica in italia," in *Dati statistici*, 2015.

[7] I. E. Agency, *Medium-Term Renewable Energy Market Report 2015*, 2015.

[8] E. Martinot, "Grid integration of renewable energy: flexibility, innovation, experience," *Annual Review of Environment and Resources 2016*, February , 2016.

[9] Mackay Miller , Eric Martinot , Sadie Cox , Bethany Speer , Owen Zinaman , Sam Booth , Romain Zissler , Jaquelin Cochran , S.K. Soonee , Pierre Audinet , Luis Munuera , and Doug Arent, "Status report on power system transformation: A 21st century power partnership report," *National Renewable Energy Laborator NREL*, May , 2015.

[10] H. K. Trabish, "Primer: The now and future impacts of energy storage," *Utility Dive*, October 20, 2015.

[11] International Hydropower Association, *Briefing: 2016 Key Trends in Hydropower*, March 2016.

[12] F. Consulting, "Global wind market update—demand and supply 2015," 2016.

[13] E. Estebanez, V. Moreno, A. Pigazo, M. Liserre, and A. Dell'Aquila, "Performance evaluation of active islanding-detection algorithms in distributed-generation photovoltaic systems: Two inverters case," *IEEE Transactions on Industrial Electronics*, vol. 58, no. 4, pp. 1185–1193, April 2011.

[14] F. Blaabjerg, R. Teodorescu, Z. Chen, and M. Liserre, "Power converters and control of renewable energy systems," *in Proc. ICPE*, October 2004.

[15] J. S. Lai, "Power conditioning circuit topologies," *Industrial Electronics Magazine, IEEE*, vol. 3, no. 2, pp. 24–34, June 2009.

[16] M. Ropp, K. Aaker, J. Haigh, and N. Sabbah, "Using power line carrier communications to prevent islanding [of pv power systems]," in *Photovoltaic Specialists Conference, 2000. Conference Record of the Twenty-Eighth IEEE*, 2000, pp. 1675–1678.

[17] P. Villenueve, "Concerns generated by islanding [electric power generation]," *Power and Energy Magazine, IEEE*, vol. 2, no. 3, pp. 49–53, May 2004.

[18] T. Tatishvili, "Energy union: Advancing the integration of european energy markets," *The Financial*, June 8, 2015.

[19] ENTSO, "Entso-e network code for requirements for grid connection applicable to all generators," March 2013.

[20] pr TS 50549-1, "Requirements for the connection of generators above 16 a per phase - part 1: Connection to the lv distribution system (clc tc 8x)."

[21] R. Teodorescu, M. Liserre, and P. Rodr?guez, *Introduction.* Wiley-IEEE Press, 2011.

[22] Z. Ye, A. Kolwalkar, Y. Zhang, P. Du, and R. Walling, "Evaluation of anti-islanding schemes based on nondetection zone concept," *IEEE Transactions on Power Electronics*, vol. 19, no. 5, pp. 1171–1176, Sept 2004.

[23] R. Brundlinger and B. Bletterie, "Unintentional islanding in distribution grids with a high penetration of inverter-based DG: Probability for islanding and protection methods," in *2005 IEEE Russia Power Tech*, June 2005, pp. 1–7.

[24] L. A. C. Lopes and Y. Zhang, "Islanding detection assessment of multi-inverter systems with active frequency drifting methods," *IEEE Transactions on Power Delivery*, vol. 23, no. 1, pp. 480–486, Jan. 2008.

[25] R. Sgarbossa, S. Lissandron, P. Mattavelli, R. Turri, and A. Cerretti, "Analysis of ΔP - ΔQ area of uncontrolled islanding in low voltage grids with pv generators," *IEEE Transactions on Industry Applications*, vol. PP, no. 99, pp. 1–1, 2016.

[26] S. Lissandron, R. Sgarbossa, L. Dalla Santa, P. Mattavelli, R. Turri, and A. Cerretti, "Impact of non-simultaneous P/f and Q/V grid code requirements on pv inverters on unintentional islanding operation in distribution network," in *2015 IEEE 6th International Symposium on Power Electronics for Distributed Generation Systems (PEDG)*, June 2015, pp. 1–7.

[27] R. Sgarbossa, S. Lissandron, P. Mattavelli, R. Turri, and A. Cerretti, "Analysis of ΔP - ΔQ area of uncontrolled islanding in low voltage grids with pv generators," in *Energy Conversion Congress and Exposition (ECCE), 2014 IEEE*, Sept 2014, pp. 5667–5674.

[28] R. Sgarbossa, L. D. Santa, P. Mattavelli, A. Petucco, F. Cavazzana, and A. Cerretti, "Phase-locked loop effect on non-detection zone of unintentional islanding," in *2015 17th European Conference on Power Electronics and Applications (EPE'15 ECCE-Europe)*, Sept 2015, pp. 1–10.

[29] S. Lissandron, R. Sgarbossa, L. Dalla Santa, P. Mattavelli, R. Turri, and A. Cerretti, "ΔP - ΔQ area assessment of temporary unintentional islanding with p/f and q/v droop controlled pv generators in distribution networks," in *IEEE Energy Conversion Congress and Exposition (ECCE)*, Sept 2015, pp. 1968–1975.

[30] A. Cerretti, L. D'Orazio, C. Pezzato, G. Sapienza, G. Valvo, N. Cammalleri, P. Mattavelli, R. Sgarbossa, R. Turri, and E. D. Berardinis, "Uncontrolled islanding operations of mv/lv active distribution networks," in *PowerTech, 2015 IEEE Eindhoven*, June 2015, pp. 1–6.

[31] F. Amadei, A. Cerretti, M. Coppo, P. Mattavelli, R. Sgarbossa, and R. Turri, "Temporary islanding operations of mv/lv active distribution networks under fault conditions," in *2014 Power Engineering Conference (UPEC)*, September 2014, pp. 1–7.

[32] R. Sgarbossa, P. Mattavelli, L. D. Santa, R. Turri, and A. Cerretti, "Effects of p/f and q/v regulations on anti-islanding detection methods in distribution networks," in *IEEE PES Innovative Smart Grid Technologies, Europe (Ljubljana)*, October 2016, pp. 1–6.

[33] R. Sgarbossa, L. D. Santa, P. Mattavelli, R. Turri, and A. Cerretti, "Analysis of interface protection system with distributed energy resources compliant with the

most recent grid codes: the unintentional islanding case," in *2016 IEEE PESGeneral meeting, Paving te way for grid modernization*, July 2016, pp. 1–6.

[34] R. Sgarbossa, S. Lissandron, P. Mattavelli, R. Turri, and A. Cerretti, "Analysis of unintentional islanding in low-voltage grids with pv generators," in *IEEE COMPEL14*, June 2014, pp. 1–7.

[35] P. Mattavelli, R. Sgarbossa, R. Turri, G. Sapienza, G. Valvo, C. Pezzato, A. Cerretti, , and E. D. Berardinis, "Generators and loads models to investigate uncontrolled islanding on active distribution networks," in *23rd International Conference on Electricity Distribution, CIRED*, June 2015, pp. 1–5.

[36] I. Balaguer, H.-G. Kim, F. Peng, and E. Ortiz, "Survey of photovoltaic power systems islanding detection methods," in *2008 IECON 34th Annual Conference of IEEE Industrial Electronics*, Nov. 2008, pp. 2247–2252.

[37] R. Kunte and W. Gao, "Comparison and review of islanding detection techniques for distributed energy resources," in *2008. NAPS '08. 40th North American Power Symposium*, 2008, pp. 1–8.

[38] F. J. Pazos, "Operational experience and field tests on islanding events caused by large photovoltaic plants," in *Proceedings of the 21st International Conference on Electricity Distribution (CIRED'11)*, 2011.

[39] "Ieee standard conformance test procedures for equipment interconnecting distributed resources with electric power systems," *IEEE Std 1547.1a-2015 (Amendment to IEEE Std 1547.1-2005)*, pp. 1–27, May 2015.

[40] "Test Procedure of Islanding PreventionMeasures for Utility-Interconnected Photovoltaic Inverters," Standard, 2005.

[41] M. Ropp, D. Larson, S. Meendering, D. McMahon, J. Ginn, J. Stevens, W. Bower, S. Gonzalez, K. Fennell, and L. Brusseau, "Discussion of a power line carrier communications-based anti-islanding scheme using a commercial automatic meter reading system," in *2006 IEEE 4th World Conference on Photovoltaic Energy Conference*, vol. 2, May 2006, pp. 2351–2354.

[42] F. De Mango, M. Liserre, and A. Aquila, "Overview of anti-islanding algorithms for pv systems. part ii: Activemethods," in *Power Electronics and Motion Control Conference, 2006. EPE-PEMC 2006. 12th International*, Aug 2006, pp. 1884–1889.

[43] O. Raipala, A. Maäkinen, S. Repo, and P. Jaärventausta, "The effect of different control modes and mixed types of dg on the non-detection zones of islanding

detection," in *Integration of Renewables into the Distribution Grid, CIRED 2012 Workshop*, May 2012, pp. 1–4.

[44] W. Bower and M. Ropp, "Evaluation of islanding detection methods for photovoltaic utility-interactive power systems," *Energy Conversion, IEEE Transactions on*, vol. Tech. Rep. IEA-PVPS, Dec 2002.

[45] J. Jeong and H. Kim, "Active anti-islanding method for pv system using reactive power control," *Electronics Letters*, vol. 42, no. 17, pp. 1004–1005, August 2006.

[46] L. Lopes and H. Sun, "Performance assessment of active frequency drifting islanding detection methods," *Energy Conversion, IEEE Transactions on*, vol. 21, no. 1, pp. 171–180, March 2006.

[47] IEEE Task Force, "Load representation for dynamic performance analysis [of power systems]," *IEEE Transactions on Power Systems*, vol. 8, no. 2, pp. 472–482, May 1993.

[48] H. H. Zeineldin and M. M. A. Salama, "Impact of load frequency dependence on the ndz and performance of the sfs islanding detection method," *IEEE Transactions on Industrial Electronics*, vol. 58, no. 1, pp. 139–146, Jan 2011.

[49] T. E. Grebe, "Application of distribution system capacitor banks and their impact on power quality," in *Rural Electric Power Conference, 1995. Papers Presented at the 39th Annual Conference*, Apr 1995, pp. C3/1–C3/6.

[50] Ropp, M. E., Begovic, M. and Rohatgi, A., "Analysis and performance assessment of the active frequency drift method of islanding prevention," *IEEE Transactions onEnergy Conversion*, vol. 14, no. 3, pp. 810–816, Sept 1999.

[51] G. A. Kern, "Sunsine300, utility interactive ac module anti-islanding test results," in *Photovoltaic Specialists Conference, 1997., Conference Record of the Twenty-Sixth IEEE*, Sep 1997, pp. 1265–1268.

[52] I. Varjasi, A. Balogh, and S. Halasz, "Sensorless control of a grid-connected pv converter," in *Power Electronics and Motion Control Conference, 2006. EPE-PEMC 2006. 12th International*, Aug 2006, pp. 901–906.

[53] Choe, G. H., Kim, H. S., Kim, H.G., Choi, Y. H. andKim, J. C., "The characteristic analysis of grid frequency variation under islanding mode for utility interactive pv system with reactive power variation scheme for anti-islanding," in *Power Electronics Specialists Conference, 2006. PESC '06. 37th IEEE*, June 2006, pp. 1–5.

[54] M. Salman, N. Kapsokavathis, X. Zhang, D. Walters, and X. Tang, "Method and apparatus for monitoring an electrical energy storage device," Jun. 26 2008, uS Patent App. 11/736,151. [Online]. Available: https://www.google.ch/patents/US20080150457

[55] L. Asiminoaei, R. Teodorescu, F. Blaabjerg, and U. Borup, "A digital controlled pv-inverter with grid impedance estimation for ens detection," *IEEE Transactions on Power Electronics*, vol. 20, no. 6, pp. 1480–1490, Nov 2005.

[56] M. Ciobotaru, R. Teodorescu, and F. bjerg, "On-line grid impedance estimation based on harmonic injection for grid-connected pv inverter," in *2007 IEEE International Symposium on Industrial Electronics*, June 2007, pp. 2437–2442.

[57] CEI Comitato Elettrotecnico Italiano, "Standard-CEI 0-21, reference technical rules for the connection of active and passive users to the lv electrical utilities," 2011-12, standards.

[58] CEI Comitato Elettrotecnico Italiano, "Standard-CEI 0-16, reference technical rules for the connection of active and passive consumers to the hv and mv electrical networks of distribution company," Tech. Rep., 2011-12, standards.

[59] pr TS 50549-2, "Requirements for the connection of generators above 16 a per phase - part 2: Connection to the mv distribution system (clc tc 8x)."

[60] K. Tomiyama, S. Ueoka, T. Takano, I. Iyoda, K. Matsuno, K. Temma, and J. J. Paserba, "Modeling of load during and after system faults based on actual field data," in *Power Engineering Society General Meeting, 2003, IEEE*, vol. 3, July 2003, p. 1391 Vol. 3.

[61] J. R. Ribeiro and F. J. Lange, "A new aggregation method for determining composite load characteristics," *IEEE Transactions on Power Apparatus and Systems*, vol. PAS-101, no. 8, pp. 2869–2875, Aug 1982.

[62] Y. Baghzouz and C. Quist, "Determination of static load models from ltc and capacitor switching tests," in *Power Engineering Society Summer Meeting, 2000. IEEE*, vol. 1, 2000, pp. 389–394 vol. 1.

[63] T. Frantz, T. Gentile, S. Ihara, N. Simons, and M. Waldron, "Load behavior observed in lilco and rg amp;e systems," *IEEE Power Engineering Review*, vol. PER-4, no. 4, pp. 37–38, April 1984.

[64] K. Yamashita, M. Asada, and K. Yoshimura, "A development of dynamic load model parameter derivation method," in *2009 IEEE Power Energy Society General Meeting*, July 2009, pp. 1–8.

[65] K. Tomiyama, S. Ueoka, T. Takano, I. Iyoda, K. Matsuno, K. Temma, and J. J. Paserba, "Modeling of load during and after system faults based on actual field data," in *Power Engineering Society General Meeting, 2003, IEEE*, vol. 3, July 2003, p. 1391 Vol. 3.

[66] F. Blaabjerg, Z. Chen, and S. B. Kjaer, "Power electronics as efficient interface in dispersed power generation systems," *IEEE Transactions on Power Electronics*, vol. 19, no. 5, pp. 1184–1194, Sept 2004.

[67] M. Calais, J. Myrzik, T. Spooner, and V. G. Agelidis, "Inverters for single-phase grid connected photovoltaic systems-an overview," in *Power Electronics Specialists Conference, 2002. pesc 02. 2002 IEEE 33rd Annual*, vol. 4, June 2002, pp. 1995–2000.

[68] S. B. Kjaer, J. K. Pedersen, and F. Blaabjerg, "A review of single-phase grid-connected inverters for photovoltaic modules," *IEEE Transactions on Industry Applications*, vol. 41, no. 5, pp. 1292–1306, Sept 2005.

[69] Y. Xue, L. Chang, S. B. Kjaer, J. Bordonau, and T. Shimizu, "Topologies of single-phase inverters for small distributed power generators: an overview," *IEEE Transactions on Power Electronics*, vol. 19, no. 5, pp. 1305–1314, Sept 2004.

[70] M. Saitou and T. Shimizu, "Generalized theory of instantaneous active and reactive powers in single-phase circuits based on hilbert transform," in *2002 IEEE 33rd Annual Power Electronics Specialists Conference*, vol. 3, 2002, pp. 1419–1424 vol.3.

[71] T. Thacker, R. Wang, D. Dong, R. Burgos, F. Wang, and D. Boroyevich, "Phase-locked loops using state variable feedback for single-phase converter systems," in *APEC 2009, Twenty-Fourth Annual IEEE Applied Power Electronics Conference and Exposition, 2009.*, Feb 2009, pp. 864–870.

[72] S. M. Silva, B. M. Lopes, B. J. C. Filho, R. P. Campana, and W. C. Bosventura, "Performance evaluation of pll algorithms for single-phase grid-connected systems," in *39th IAS Annual Meeting. Conference Record of the 2004 IEEE Industry Applications Conference, 2004.*, vol. 4, Oct 2004, pp. 2259–2263 vol.4.

[73] R. M. S. Filho, P. F. Seixas, P. C. Cortizo, L. A. B. Torres, and A. F. Souza, "Comparison of three single-phase pll algorithms for ups applications," *IEEE Transactions on Industrial Electronics*, vol. 55, no. 8, pp. 2923–2932, Aug 2008.

[74] S. Shinnaka, "A robust single-phase pll system with stable and fast tracking," *IEEE Transactions on Industry Applications*, vol. 44, no. 2, pp. 624–633, March 2008.

[75] F. M. Gardner, *Phase Lock Techniques*. Wiley, 1979.

[76] J. Park and F. Maloberti, "Fractional-n pll with 90/spl deg/ phase shift lock and active switched-capacitor loop filter," in *Proceedings of the IEEE 2005 Custom Integrated Circuits Conference, 2005.*, Sept 2005, pp. 329–332.

[77] J. R. C. Piqueira, A. Z. Caligares, and L. H. A. Monteiro, "Considering double frequency terms from phase detectors in synchronous master-slave networks," in *2006 Proceeding of the Thirty-Eighth Southeastern Symposium on System Theory*, March 2006, pp. 453–456.

[78] F. Cadoux and G. Gross, "Integration of vehicles with rechargeable batteries into distribution networks," *Smart Grids*, pp. 243–261, 2013.

[79] Y. Degeilh, F. Cadoux, N. Navid, and G. Gross, "Economic assessment of the explicit representation of ramping requirements on conventional generators in systems with integrated intermittent resources," in *2012 IEEE Power and Energy Society General Meeting*. IEEE, 2012, pp. 1–5.

[80] H. Zeineldin, E. El-Saadany, and M. Salama, "Impact of DG interface control on islanding detection and nondetection zones," *IEEE Transactions on Power Delivery*, vol. 21, no. 3, pp. 1515–1523, July 2006.

[81] D. Salles, W. Freitas, J. Vieira, and B. Venkatesh, "A practical method for non-detection zone estimation of passive anti-islanding schemes applied to synchronous distributed generators," *IEEE Transactions on Power Delivery*, 2014.

[82] H. Zeineldin and M. Salama, "Impact of load frequency dependence on the NDZ and performance of the SFS islanding detection method," *IEEE Transactions on Industrial Electronics*, vol. 58, no. 1, pp. 139–146, Jan 2011.

[83] J. Bruschi, F. Cadoux, B. Raison, Y. Bésanger, and S. Grenard, "Impact of new european grid codes requirements on anti-islanding protections: a case study," in *23rd International Conference and Exhibition on Electricity Distribution (CIRED 2015)*, June 2015.

[84] D. Reigosa, F. Briz, C. Charro, P. Garcia, and J. Guerrero, "Active islanding detection using high-frequency signal injection," *IEEE Transactions on Industry Applications*, vol. 48, no. 5, pp. 1588–1597, Sept 2012.

[85] M. Cespedes and J. Sun, "Renewable energy systems instability involving grid-parallel inverters," in *Applied Power Electronics Conference and Exposition, 2009. APEC 2009. Twenty-Fourth Annual IEEE*, Feb 2009, pp. 1971–1977.

[86] D. Dong, J. Li, D. Boroyevich, P. Mattavelli, I. Cvetkovic, and Y. Xue, "Frequency behavior and its stability of grid-interface converter in distributed generation systems," in *2012 Twenty-Seventh Annual IEEE Applied Power Electronics Conference and Exposition (APEC)*, Feb 2012, pp. 1887–1893.

[87] F. Blaabjerg, R. Teodorescu, M. Liserre, and A. V. Timbus, "Overview of control and grid synchronization for distributed power generation systems," *IEEE Transactions on Industrial Electronics*, vol. 53, no. 5, pp. 1398–1409, Oct 2006.

[88] A. Timbus, M. Liserre, R. Teodorescu, and F. Blaabjerg, "Synchronization methods for three phase distributed power generation systems - an overview and evaluation," in *2005 IEEE 36th Power Electronics Specialists Conference*, June 2005, pp. 2474–2481.

[89] S. K. Chung, "Phase-locked loop for grid-connected three-phase power conversion systems," *IEEE Proceedings - Electric Power Applications*, vol. 147, no. 3, pp. 213–219, May 2000.

[90] P. Rodriguez, J. Pou, J. Bergas, J. I. Candela, R. P. Burgos, and D. Boroyevich, "Decoupled double synchronous reference frame pll for power converters control," *IEEE Transactions on Power Electronics*, vol. 22, no. 2, pp. 584–592, March 2007.

[91] P. Rodriguez, A. Luna, I. Candela, R. Teodorescu, and F. Blaabjerg, "Grid synchronization of power converters using multiple second order generalized integrators," in *Industrial Electronics, 2008. IECON 2008. 34th Annual Conference of IEEE*, Nov 2008, pp. 755–760.

[92] S. A. O. da Silva, R. Novochadlo, and R. A. Modesto, "Single-phase pll structure using modified p-q theory for utility connected systems," in *2008 IEEE Power Electronics Specialists Conference*, June 2008, pp. 4706–4711.

[93] H. K. Yada and M. S. R. Murthy, "A new topology and control strategy for extraction of reference current using single phase sogi-pll for three-phase four-wire shunt active power filter," in *Power Electronics, Drives and Energy Systems (PEDES), 2014 IEEE International Conference on*, Dec 2014, pp. 1–6.

[94] M. Karimi-Ghartemani and M. R. Iravani, "A method for synchronization of power electronic converters in polluted and variable-frequency environments," *IEEE Transactions on Power Systems*, vol. 19, no. 3, pp. 1263–1270, Aug 2004.

[95] P. Rodriguez, A. Luna, M. Ciobotaru, R. Teodorescu, and F. Blaabjerg, "Advanced grid synchronization system for power converters under unbalanced and distorted operating conditions," in *IECON 2006 - 32nd Annual Conference on IEEE Industrial Electronics*, Nov 2006, pp. 5173–5178.

[96] I. Carugati, P. Donato, S. Maestri, D. Carrica, and M. Benedetti, "Frequency adaptive pll for polluted single-phase grids," *IEEE Transactions on Power Electronics*, vol. 27, no. 5, pp. 2396–2404, May 2012.

[97] P. Rodriguez, R. Teodorescu, R. Candela, I. Timbus, M. Liserre, and F. Blaabjerg, "New positive-sequence voltage detector for grid synchronization of power converters under faulty grid conditions," in *Power Electronics Specialists Conference, 2006. PESC '06. 37th IEEE*, June 2006, pp. 1–7.

[98] R. Walling and N. Miller, "Distributed generation islanding-implications on power system dynamic performance," in *2002 IEEE Power Engineering Society Summer Meeting*, vol. 1, July 2002, pp. 92–96.

[99] A. Cerretti, G. Scrosati, and L. Consiglio, "Upgrade of ENEL MV network automation to improve performances in presence of faults and to deal DG," in *CIRED 2011*, June 6th-9th - Frankfur 2011.

[100] F. D. Mango, M. Liserre, A. Dell'Aquila, and A. Pigazo, "Overview of anti-islanding algorithms for pv systems. part I: Passive methods," in *12th International Power Electronics and Motion Control Conference EPE-PEMC*, Aug 2006, pp. 1878–1883.

[101] M. Ropp, M. Begovic, A. Rohatgi, G. A. Kern, S. Bonn, R.H., and S. Gonzalez, "Determining the relative effectiveness of islanding detection methods using phase criteria and nondetection zones," *IEEE Transactions on Energy Conversion*, vol. 15, no. 3, pp. 290–296, Sep 2000.